UCRL-18263
Cy. 2

University of California

Ernest O. Lawrence Radiation Laboratory

TWO-WEEK LOAN COPY

This is a Library Circulating Copy which may be borrowed for two weeks. For a personal retention copy, call Tech. Info. Division, Ext. 5545

AN INVESTIGATION OF THE (^{3}He,t) AND (^{3}He,^{3}He') REACTIONS ON 1p SHELL NUCLEI

Gordon Charles Ball
(Ph.D. Thesis)

May 1968

RECEIVED
LAWRENCE
RADIATION LABORATORY
JUL 1 1968
LIBRARY AND
DOCUMENTS SECTION

Berkeley, California

UCRL-18263
Cy. 2

DISCLAIMER

This document was prepared as an account of work sponsored by the United States Government. While this document is believed to contain correct information, neither the United States Government nor any agency thereof, nor the Regents of the University of California, nor any of their employees, makes any warranty, express or implied, or assumes any legal responsibility for the accuracy, completeness, or usefulness of any information, apparatus, product, or process disclosed, or represents that its use would not infringe privately owned rights. Reference herein to any specific commercial product, process, or service by its trade name, trademark, manufacturer, or otherwise, does not necessarily constitute or imply its endorsement, recommendation, or favoring by the United States Government or any agency thereof, or the Regents of the University of California. The views and opinions of authors expressed herein do not necessarily state or reflect those of the United States Government or any agency thereof or the Regents of the University of California.

UCRL-18263

UNIVERSITY OF CALIFORNIA

Lawrence Radiation Laboratory
Berkeley, California

AEC Contract No. W-7405-eng-48

AN INVESTIGATION OF THE (^{3}He,t) AND (^{3}He,^{3}He') REACTIONS ON 1p SHELL NUCLEI

Gordon Charles Ball
(Ph.D. Thesis)

May 1968

AN INVESTIGATION OF THE (^{3}He,t) AND (^{3}He,^{3}He') REACTIONS ON 1p SHELL NUCLEI

Gordon Charles Ball

UNIVERSITY OF CALIFORNIA

Lawrence Radiation Laboratory
Berkeley, California

AEC Contract No. W-7405-eng-48

July 1968

ERRATA

Page	Line	As it is	Should read
11	1	$\lvert L - S\rvert \leq L \leq L + S$	$\lvert L - S\rvert \leq J \leq L + S$
110	column 9	omit the number 1.5	
118	3	$\exp-(\alpha r_{12})/\alpha r_{12}$	$\exp(-\alpha r_{12})/\alpha r_{12}$

AN INVESTIGATION OF THE (^{3}He,t) AND (^{3}He,^{3}He') REACTIONS ON 1p SHELL NUCLEI

Contents

Abstract v

I. Introduction 1

II. Theory 4

A. Introduction 4

B. Microscopic Model 6

1. General Discussion 6

2. Selection Rules 10

3. Target-Nucleus Spectroscopic Factors 11

4. A Critical Analysis of the Assumptions of a Simple Microscopic Description 12

III. Experimental Procedures 14

A. Cyclotron and External Beam Facilities 14

B. Detectors and Electronics 16

C. Targets 19

1. Gas Targets 19

2. Solid Targets 19

IV. Experimental Results and Discussion 22

A. The ^{12}C(^{3}He,t)^{12}N and ^{12}C(^{3}He,^{3}He')^{12}C Reactions . . 22

B. The ^{13}C(^{3}He,t)^{13}N and ^{13}C(^{3}He,^{3}He')^{13}C Reactions . . 49

C. The ^{14}C(^{3}He,t)^{14}N Reaction 49

D. The ^{14}N(^{3}He,t)^{14}O Reaction 49

E. The ^{14}N(^{3}He,^{3}He')^{14}N Reaction 50

F. The ^{15}N(^{3}He,t)^{15}O and ^{15}N(^{3}He,^{3}He')^{15}N Reactions . . 50

V. A Microscopic Description of the (^{3}He,t) and (^{3}He,^{3}He') Reactions 51

A. Theoretical Calculations 52

1. Optical Model Parameters 52

2. Nuclear Structure Factors 58

3. Bound-state Wave Functions, Binding Energies and Radial Form Factors 69

4. Range Effects of a Yukawa Interaction 73

5. Nonlocal Corrections 76

B. Comparison with Experiment 77

1. The (^{3}He,t) p1/2,p3/2→ p1/2 Dominant L = 0 Transitions 77

2. The (^{3}He,^{3}He') p3/2→ p1/2 ($T_f = T_i$) Transitions 84

3. The (^{3}He,t) p3/2→ p1/2 Dominant L = 2 Transitions 91

4. The (^{3}He,^{3}He') p1/2→ d5/2 Transitions 96

5. The (^{3}He,t) p1/2→ d5/2 Transitions 100

6. The (^{3}He,^{3}He') p1/2→ s1/2 Transitions 104

7. The (^{3}He,t) p1/2→ s1/2 Transitions 106

C. The (^{3}He,^{3}He') and (α,α') Reactions on 1p Shell Nuclei 106

D. The ^{12}C(p,p')^{12}C and ^{12}C(^{3}He,^{3}He')^{12}C Reactions . . 114

E. A Comparison of the Effective and Free Nucleon-Nucleon Interactions 117

VI. The (^{3}He,t) and (^{3}He,^{3}He') Reactions Populating Analog Final States 120

A. T = 3/2 Levels in Mass 9, 13 and 15 121

B. The ^{14}N(^{3}He,t)^{14}O (g.s.,0+) ^{14}N(^{3}He,^{3}He')^{14}N (2.31 MeV, 0+) and ^{14}C(^{3}He,t)^{14}N (g.s.,1+) Reactions 123

C. T = 1 Levels in ^{12}C and ^{12}N 123

1. The 1.20 and 1.65 MeV Levels in ^{12}N 129

2. The 2.43 and 3.50 MeV Levels in ^{12}N 129

3. The 3.10 MeV Level in ^{12}N 131

4. The 4.24 MeV Level in ^{12}N 131

VII. Conclusions 132

Acknowledgements 135

References 137

AN INVESTIGATION OF THE (^{3}He,t) AND (^{3}He,^{3}He') REACTIONS ON 1p SHELL NUCLEI

Gordon Charles Ball

Lawrence Radiation Laboratory
University of California
Berkeley, California

May 1968

ABSTRACT

The (^{3}He,t) and (^{3}He,^{3}He') reactions on ^{9}Be, ^{12}C, ^{13}C, ^{14}C [(^{3}He,t) reaction only], ^{14}N and ^{15}N have been investigated at ^{3}He energies of 39.9, 49.8, 39.6, 44.8, 44.6 and 39.8 MeV, respectively. Angular distributions were obtained for all prominent states up to excitations of 20 MeV. A microscopic analysis of these data has been carried out using a local two-body interaction with an arbitrary spin-isospin exchange mixture. Spectroscopic factors were calculated using intermediate-coupling wave functions for p shell states while simple j-j configurations were assumed for the levels which were populated by promoting a p nucleon to the s-d shell. A Yukawa interaction with a range of α^{-1} = 1.2 F was found to give the best results. The strength of the effective nucleon-nucleon interaction required to fit these data is in good agreement with recent (p,p'), (p,n) and (^{3}He,t) calculations on light nuclei. In particular, dominant L = 0 transitions observed in the (^{3}He,t) reaction gave values for the isospin $V_{ST} = V_{01}$ and spin-isospin V_{11} dependent terms (converted to an effective nucleon-nucleon interaction at α^{-1} = 1.0 F) of 20.6 and 16.5 MeV, respectively, while the strengths required to fit (^{3}He,t) L = 2,3 transitions were generally enhanced. For inelastic transitions, the average strengths obtained for V_{00}, assuming a Serber exchange mixture, varied from 47.2 to 67.3 MeV depending upon the L transfer involved. A comparison of the (^{3}He,t) and (^{3}He,^{3}He') reactions populating analog final states (where $T_f = T_i + 1$) is also presented. In general, these transitions were weakly populated; however, it was possible to observe the lowest T = 3/2 levels in the mirror nuclei ^{9}B - ^{9}Be and ^{13}N - ^{13}C and several T = 1 levels in ^{12}N - ^{12}C.

I. INTRODUCTION

There has been a growing interest recently in the applications of a microscopic description to the inelastic and charge-exchange scattering of various projectiles by nuclei.[1-14] Utilizing the available experimental data from the (p,n) and (p,p') reactions, several attempts have been made to determine an effective nucleon-nucleon interaction in terms of a simple local potential with an arbitrary spin-isospin exchange mixture.[6-12] In particular, the population of ground and excited isobaric analog states in the (p,n) reaction provide a direct measurement of the isospin $V_{ST} = V_{01}$ and spin-isospin V_{11} terms in the effective two-body interaction while the levels which are strongly populated in inelastic scattering are generally sensitive to the spin independent terms. So far, the (p,n) reaction has been reasonably successful in determining the strengths of isospin dependent terms;[8,10-12] however, the inelastic transitions generally give values for V_{00} which are enhanced due to collective or core polarization effects not accounted for by the wave functions of the initial and final states.[3,6-9]

One of the main purposes of this thesis was to extend the concepts of a microscopic description to an analysis of the (^{3}He,t) and (^{3}He,^{3}He') reactions on several 1p shell nuclei, particularly, ^{9}Be, ^{12}C, ^{13}C, ^{14}C, ^{14}N and ^{15}N. These experiments were carried out at ^{3}He energies of 40-50 MeV and therefore the population of well known levels up to an excitation energy of 15-20 MeV could be investigated simultaneously in both reactions.

Some experimental studies of the (^{3}He,t)[13-16] and (^{3}He,^{3}He')[17] reactions on light and medium weight nuclei have been reported previously. However, microscopic analyses of these data have been generally limited to an investigation of the ground isobaric analog transitions observed in the (^{3}He,t) reaction on several light nuclei, particularly, ^{17}O, ^{18}O, ^{27}Al, ^{30}Si, ^{39}K, and ^{48}Ti at $E_{^3He}$ = 18-25 MeV.[13,14]

In principle, an investigation of the (^{3}He,t) and (^{3}He,^{3}He') reactions on 1p shell nuclei has several advantages which make it attractive for a microscopic analysis. First of all, many of the levels which are strongly populated in these reactions correspond to transitions which mainly involve the promotion of a single nucleon (i.e., almost pure single-

particle transitions).[18] Secondly, the shapes and relative magnitudes of the angular distributions arising from single-particle transitions appear to fall into groups which depend not only on the orbital angular momentum transfer but also on the specific shell-model transition involved.[18] This effect has been very useful in utilizing the (^{3}He,t) reaction as a spectroscopic tool.[16] In particular, it was possible in these experiments to make spin and parity assignments for all levels observed in ^{14}O below 8 MeV.[18]

Finally, intermediate-coupling wave functions are available which have already been successful in predicting many nuclear properties for 1p shell states.[19] Although these wave functions are unable to predict the observed E2 transition rates without including an effective charge for the neutron,[20] the collective enhancement required is much less than that for heavier nuclei. As a result, the ability of a microscopic description to predict the shapes and relative magnitudes of the angular distributions for well-known p shell transitions should provide a sensitive test of the applicability of a simple local potential for the inelastic and charge-exchange scattering of complex projectiles. Although the effective nucleon-nucleon interaction obtained for complex projectiles may be different from that for nucleon projectiles, there is no strong evidence that it is greatly different.

In the present analysis, DWBA calculations have been performed using the microscopic description developed by Madsen.[5] Spectroscopic factors were calculated using the wave functions of Cohen and Kurath[19,21] for p shell states while simple j-j configurations were assumed for the levels which were populated by promoting a p nucleon to the s-d shell. The effective interaction was assumed to be a local Yukawa potential with an arbitrary spin-isospin exchange mixture. The strength of the effective nucleon-nucleon interaction required to fit these data is discussed in detail and also compared with the results obtained from recent (p,p'), (p,n)[6-12] and (^{3}He,t)[13,14] calculations.

Of additional interest in these experiments was the comparison of the (^{3}He,t) and (^{3}He,^{3}He') reactions populating analog final states where $T_f = T_i + 1$. Assuming the charge independence of nuclear forces, the angular distributions for these transitions should be identical after phase-

space and isospin-coupling corrections are made. In general, these transitions were weakly populated; however, it was possible to observe the lowest $T = 3/2$ levels in mass 9 and 13 and several $T = 1$ levels in mass 12. As a result, a correspondence was established between seven excited $T = 1$ levels in ^{12}C and ^{12}N.

II. THEORY

A. Introduction

The inelastic or charge-exchange scattering of various projectiles by nuclei can be described using either a collective or microscopic model. Both of these descriptions generally utilize the distorted-wave Born-approximation (DWBA) expression for the transition amplitude given by:[22]

$$T = \int \chi_f^{(-)*}(\underset{\sim}{k}_f,\underset{\sim}{R}')\langle\Psi_f(\xi)|\overline{V}(\underset{\sim}{R}',\xi)|\Psi_i(\xi)\rangle\, \chi_i^{(+)}(\underset{\sim}{k}_i,\underset{\sim}{R}')d\underset{\sim}{R}' \quad , \qquad (1)$$

where $\underset{\sim}{R}'$ is a vector between the center of mass of the projectile and the center of mass of the target and ξ describes all of the nuclear coordinates. The $\chi_i^{(+)}$ and $\chi_f^{(-)}$ are distorted waves which describe the elastic scattering in the entrance and exit channels while the remaining factor represents the matrix element of the effective interaction taken over all nuclear coordinates of the initial and final states.

Until recently, the collective model was extensively used to describe inelastic scattering since it was known that the states which are strongly excited by inelastic scattering are also strongly coupled to the ground state by the electromagnetic field.[23] This approach consisted of generalizing the optical model potential to include non-spherical shapes. The nuclear matrix element, Eq. (1), was then replaced by the radial derivative of the optical potential which gave rise to the elastic scattering.[24] The resulting cross sections are proportional to the deformation parameters β_L for each multipole. Although the macroscopic description has been successfully applied to strongly excited states which can be characterized as collective in nature, the information which is obtained concerning nuclear structure is limited and in general the model is not applicable to weakly excited levels.

Charge-exchange reactions have also been described in terms of an optical potential model in which the ground isobaric analog (quasi-elastic) transition results from an isospin or symmetry term in the optical potential.[25-27] By analogy, the radial derivative of this symmetry term gives rise to quasi-inelastic transitions.[27] While the strength of the symmetry term required to fit the quasi-elastic transitions is close to that found in an analysis of elastic scattering data,[26,27] the cross sections for quasi-inelastic transitions are generally underestimated.[27,28]

If a microscopic description is used, the nuclear wave functions Ψ_i and Ψ_f, Eq. (1), are expressed in terms of the motions of the individual target and projectile nucleons while the effective interaction is represented by a sum of two-body interactions between the projectile and target nucleons. In principle, this model is capable of describing all inelastic and charge-exchange transitions and also offers a means for testing nuclear wave functions providing the effective interaction is known.

For incident protons or neutrons at sufficiently high energies ($\geq$ 100 MeV) the impulse approximation is valid and the effective interaction can be replaced by the free nucleon-nucleon scattering amplitude.[1,29] However, at lower energies, multiple scattering becomes more important and in addition the nucleon-nucleon scattering is modified by the presence of other target nucleons; therefore, the effective interaction is expected to be very complex. For simplicity, the effective interaction is generally restricted to be real, local and only dependent upon the distance between the projectile and target nucleons; however, an arbitrary spin-isospin exchange mixture is included. Hopefully, a consistent set of parameters are obtainable for the effective interaction providing the nucleon wave functions are well known.

One final restriction usually imposed in a microscopic description is to neglect the contributions from exchange processes in which the projectile nucleon (nucleons) is captured while a target nucleon (nucleons) is ejected; these effects will be discussed further later.

B. The Microscopic Model

1. General Discussion

Several theoretical formalisms convenient for discussion and calculation have been reported recently, based on a microscopic description of the inelastic and charge-exchange scattering of various projectiles from nuclei.[3-5] The formalism developed by Madsen[5] has been used in the present work to carry out a microscopic analysis of the (^{3}He,t) and (^{3}He,^{3}He') reactions on 1p shell nuclei.

The effective interaction, Eq. (1), can be expressed in terms of a sum of projectile-nucleon interactions

$$\overline{V}(\underset{\sim}{R}',\xi) = \sum_{i=1}^{A} \overline{V}(\underset{\sim}{R}',\underset{\sim}{r}_i) \quad , \tag{2}$$

where $\underset{\sim}{r}_i$ is the space coordinate of the ith target nucleon and A is the mass of the target nucleus. If the wave functions for the projectile are assumed to be entirely s states (a reasonable approximation for all complex projectiles up to α particles), then the projectile wave functions can be factored into a part depending on space coordinates and a part depending on spin-isospin coordinates. As a result, the interaction, Eq. (2), can be expressed in terms of the effective nucleon-nucleon interaction

$$\overline{V}(\underset{\sim}{R}',\underset{\sim}{r}_i) = \int d\xi' f^2(\xi')\, V(\underset{\sim}{r}_p' - \underset{\sim}{r}_i) \quad , \tag{3}$$

where $\underset{\sim}{r}_p'$ is the space coordinate of a nucleon in the projectile and $f(\xi')$ is the internal wave function of the projectile. The effective nucleon-nucleon interaction has the form

$$V(\underset{\sim}{r}_p' - \underset{\sim}{r}_i) = \left[V_{00} + V_{10}\, \underset{\sim}{\sigma}_p \cdot \underset{\sim}{\sigma}_i + \underset{\sim}{\tau}_p \cdot \underset{\sim}{\tau}_i (V_{01} + V_{11}\, \underset{\sim}{\sigma}_p \cdot \underset{\sim}{\sigma}_i) \right] g(\underset{\sim}{r}_p' - \underset{\sim}{r}_i), \tag{4}$$

where the strengths V_{ST} (for spin S and isospin T transfer) are expressed in MeV while the radial dependence $g(\underset{\sim}{r}_p' - \underset{\sim}{r}_i)$ is limited to functional forms which yield analytic expressions for the multipole expansion. In particular, the Gaussian

$$g(r) = \exp(-\beta r^2) \tag{5a}$$

and the Yukawa

$$g(r) = \exp(-\alpha r)/\alpha r \tag{5b}$$

are two suitable finite range forms. In order to compare the strengths V_{ST} for potentials of different ranges and different strengths, Johnson et al.[7] suggest using the volume integral of the potential

$$A_{ST} = V_{ST} \int g(r)\, dr \quad , \tag{6}$$

where

$$\begin{aligned} A_{ST} &= V_{ST} \times (\pi/\beta)^{3/2} \quad : \text{ Gaussian} \\ A_{ST} &= V_{ST} \times (4\pi/\alpha^3) \quad : \text{ Yukawa} \quad . \end{aligned} \tag{7}$$

In order to compute the effective projectile-nucleon interaction, Eq. (3), the internal wave functions of the ^{3}He and triton projectiles are normally assumed to be Gaussian. If the nucleon-nucleon interaction, Eq. (4), is also chosen to be a Gaussian, then the resulting expression for $\bar{V}(\underset{\sim}{R}', \underset{\sim}{r}_i)$ is a Gaussian with a longer range and lower depth but the same volume integral, Eq. (7), as the nucleon-nucleon interaction.[5]

In the present analysis of the (^{3}He,t) and (^{3}He,^{3}He') reactions, $g(r)$ was chosen to be a Yukawa. As a result, the expression obtained for the effective projectile-nucleon interaction, Eq. (3), is very complex. Wesolowski et al.[14] have shown, however, that for large values of $(\underset{\sim}{R}' - \underset{\sim}{r}_i)$ this complicated expression can be approximated by a Yukawa with the same range α^{-1} but normalized strengths $\bar{V}_{ST}$ given by:

$$\bar{V}_{ST} = V_{ST} \exp(\alpha^2/18\gamma^2) \quad , \tag{8}$$

where γ is proportional to the size parameter or average size parameters for the Gaussian wave functions of the ^{3}He and/or t projectiles (i.e., γ = 0.318 and 0.291 for the (^{3}He,t) and (^{3}He,^{3}He') reactions, respectively).[5]

At a range of $\alpha^{-1} = 1.0$ F the simple Yukawa and the exact expression are almost identical for $|\underset{\sim}{R}' - \underset{\sim}{r}_i| \geq 3$ F and only deviate strongly at distances less than two fermis (i.e. ≈20% at 2.0 F).[14] Since complex projectiles are strongly absorbed inside the nuclear surface, the simple Yukawa interaction is expected to be reasonably correct but not as accurate for light nuclei which have much smaller radii. In particular, when DWBA calculations were performed for the (^{3}He,t) and (^{3}He,^{3}He') reactions on 1p shell nuclei, the computed angular distributions were only insensitive to lower radial cutoffs ≤ 1.5 F. However, a comparison of the absolute strengths obtained in these experiments with those obtained in an analysis of the (p,p') and (p,n) reactions should provide a test of the validity of this approximation. The expression for the differential cross section can be written as a coherent sum of single particle transition amplitudes $F_{LM}^{j_1 j_2}(\hat{k}_f)$:

$$\frac{d\sigma}{d\Omega} = \left(\frac{2\mu}{4\pi\hbar^2}\right)^2 \frac{k_f}{k_i} \frac{1}{(2J'+1)(2J_i+1)} \sum_{JSLM} (2J+1)(2S+1)$$

$$\times \left| \sum_{j_1 j_2 T} D_{j_1 j_2}(JSLT)\, \bar{V}_{ST}\, F_{LM}^{j_1 j_2}(\hat{k}_f)(2L+1)^{-1/2} \right|^2 , \qquad (9)$$

where

$$F_{LM}^{j_1 j_2}(\hat{k}_f) = \left\langle \chi_f^{(-)*}(\underset{\sim}{k}_f \underset{\sim}{R}') \middle| Y_L^M(\hat{R}')\, g_L^{j_1 j_2}(R') \middle| \chi_i^{(+)}(\underset{\sim}{k}_i, \underset{\sim}{R}') \right\rangle ,$$

$$g_L^{j_1 j_2}(R') = \int \mathcal{R}_{j_2 \ell_2}(r_i)\, \bar{g}_L(R', r_i)\, \mathcal{R}_{j_1 \ell_1}(r_i) r_i^2 dr_i ,$$

and

$$
\begin{aligned}
D_{j_1 j_2}(JSLT) = {} & 4(2j_1+1)^{1/2}\,(2j_2+1)^{1/2}\,\langle \ell_2 \| Y_L \| \ell_1 \rangle \\
& \times \begin{pmatrix} j_1 & \frac{1}{2} & \ell_1 \\ j_2 & \frac{1}{2} & \ell_2 \\ J & S & L \end{pmatrix} \Big[\mathcal{S}(JJ_iJ_f;1T_iT_f;j_1j_2)\,\mathcal{S}'(SJ';1T') \\
& \times C'(T'T'1;P_i'-P_f')\,C(T_iT_f1;P_i-P_f)(-1)^{T'+T_i-P_i-P_f'} \\
& \times \delta_{P_i'-P_f',P_f-P_i}\,\delta_{T,1} + \mathcal{S}(JJ_iJ_f;0T_iT_f;j_1j_2) \\
& \times \mathcal{S}'(SJ';0T')\,\delta_{P_i'P_f'}\,\delta_{P_iP_f}(2T_i+1)^{-1/2}(2T'+1)^{-1/2}\,\delta_{T,0} \Big] .
\end{aligned}
\tag{10}
$$

In the above expressions the subscripts i and f label initial and final states; primes indicate projectile coordinates and quantum numbers; J, L, S, and T denote total, orbital, spin, and isospin transfer; the quantum numbers labeled P represent z components of isospin; and ℓ_1, j_1 and ℓ_2, j_2 represent the orbital and total angular momenta of the target nucleon in its initial and final states. The radial form factors $g_L^{j_1 j_2}(R')$ are dependent upon radial wave functions $\mathcal{R}_{jl}$ of the bound particle in its initial and final state while the nuclear structure information is contained in the quantity $D_{j_1 j_2}$ where $\mathcal{S}$,C and $\mathcal{S}'$,C' represent target and projectile spectroscopic factors and isospin Clebsch-Gordan coefficients, respectively.

As was mentioned previously, the levels which are strongly populated in the (^{3}He,t) and (^{3}He,^{3}He') reactions on 1p shell nuclei correspond either to p shell hole states or levels which have the configuration $s^4p^{A-5}s$ or $s^4p^{A-5}d$. Since simple j-j configurations will be assumed for the levels which are formed by promoting a p nucleon to the s-d shell, only one single-particle transition $j_1 \rightarrow j_2$ contributes to the cross section. If intermediate-coupling wave functions are used for p shell states, then several different single-particle transitions (all with $l_1=l_2=1$) contribute.

However, if the single-particle transition amplitudes $F_{LM}^{j_1 j_2}$ are relatively insensitive to the binding energies of the target nucleon in its initial and final states, then it is only necessary to calculate $F_{LM}^{j_1 j_2}$ for the dominant single-particle transition predicted in the j-j limit. The validity of this approximation will be discussed later (see Sec. VA-3).

Since in the present analysis $F_{LM}^{j_1 j_2}$ was computed for only one single-particle transition $j_1 \rightarrow j_2$, the expression for the differential cross section, Eq. (9), could be written as:

$$\frac{d\sigma}{d\Omega} = \sum_{JSL} \sigma(j_1 j_2 L\theta) \left| \sum_{T} \frac{G(JSLT)}{\sqrt{\pi}} \bar{V}_{ST} \right|^2 , \tag{11}$$

where

$$\sigma(j_1 j_2 L\theta) = \left(\frac{2\mu}{4\pi\hbar^2}\right)^2 \frac{k_f}{k_i} \sum_{M} \left| F_{LM}^{j_1 j_2}(\hat{k}_f)(2L+1)^{-1/2} \right|^2 \tag{12}$$

and the nuclear structure factor G(JSLT) is given by:

$$\begin{aligned} G(JSLT) &= \left[\frac{\pi(2J+1)(2S+1)}{(2J'+1)(2J_i+1)}\right]^{1/2} \sum_{j_1 j_2} D_{j_1 j_2}(JSLT) , \quad \text{for} \quad \ell_1 = \ell_2 \\ &= \left[\frac{\pi(2J+1)(2S+1)}{(2J'+1)(2J_i+1)}\right]^{1/2} D_{j_1 j_2}(JSLT) , \quad \text{for} \quad \ell_1 \neq \ell_2 . \end{aligned} \tag{13}$$

2. Selection Rules

The microscopic formalism which has been described in the previous section implies several restrictions on the various quantum numbers:

$$|J_f - J_i| \leq J \leq J_i + J_f \tag{14a}$$

$$|j_2 - j_1| \leq J \leq j_1 + j_2 \tag{14b}$$

$$0 \leq S \leq 1 \tag{14c}$$

$$|l_2 - l_1| \leq L \leq l_1 + l_2 \tag{14d}$$

$$|L - S| \leq L \leq L + S \tag{14e}$$

$$|T_f - T_i| \leq T \leq T_f + T_i \tag{14f}$$

$$|P_i' - P_f'| \leq T \leq 1 \tag{14g}$$

while the conservation of parity gives

$$\pi_f \, \pi_i = (-)^{\ell_1 + \ell_2} = (-)^L \quad . \tag{15}$$

It is interesting to compare the restrictions on the isospin transfer T as they apply to the (^{3}He,t) and (^{3}He,^{3}He') reactions. First of all, for a (^{3}He,t) transition, T must be equal to one (14g) and therefore this reaction is only dependent upon the isospin V_{01} and spin-isospin V_{11} terms in the effective interaction, Eq. (4). Secondly, for a (^{3}He,^{3}He') reaction where $T_i = T_f = 0$, T must be equal to zero (14f) and only the V_{00} and V_{10} terms contribute to the cross section, whereas if $T_i = T_f \neq 0$, then $T = 0, 1$ and all four terms can contribute. Finally, if $T_f = T_i \pm 1$ then only the isospin-dependent terms are allowed (14f) for both the (^{3}He,t) and (^{3}He,^{3}He') reactions.

3. Target - Nucleus Spectroscopic Factors

The target - nucleus spectroscopic factors $\mathcal{S}(JJ_iJ_f;TT_iT_f;j_1j_2)$ can be calculated from wave functions in a coordinate representation using the following relationship:

$$\mathcal{S}(JJ_iJ_f;TT_iT_f;j_1j_2) = A(2J_i+1)(2J_f+1)(2T_i+1)(2T_f+1)$$
$$\times \sum_{J''T''\gamma} W_J(J_iJ''Jj_2;j_1J_f)\; W_T(T_iT''T\tfrac{1}{2};\tfrac{1}{2}T_f)$$
$$\times F_i(J_i(j_1J''),\; T(\tfrac{1}{2}T''),\gamma)\; F_f(J_f(j_2J''),\; T_f(\tfrac{1}{2}T''),\gamma) \tag{16}$$

where A is the number of particles included in the wave function of the target nucleus and W_J, W_T are standard Racah coefficients. The quantities F_i and F_f are coefficients of fractional parentage defined by the equations

$$\Phi^{M_i P_i}_{J_i T_i} = \sum_{J''T''j_1\gamma} F_i(J_i(j_1 J''),\ T_i(\tfrac{1}{2}T''),\gamma)\ \psi(J_i M_i(j_1 J''),\ T_i P_i(\tfrac{1}{2}T''),\gamma) \qquad (17)$$

for F_i and an analogous expression for F_f, where J'' and T'' are the spin and isobaric spin of the parent state and γ represents all other quantum numbers (if any) required to characterize the parent state.

4. A Critical Analysis of the Assumptions of a Simple Microscopic Description

Several of the simplifying assumptions and possible inadequacies of a simple microscopic description deserve further comment. First of all, the mechanism is assumed to be direct so that contributions from exchange and multiple excitation processes are neglected. It is expected that multiple excitation should be relatively unimportant for levels which have simple shell-model configurations unless some selection rule or accidental cancellation of a nuclear matrix element inhibits the direct process.[8] However, a comparison of the (^{3}He,^{3}He') and (α,α') cross sections for transitions restricted to be S = 1 indicates that while the contributions from multiple excitation may be small they are not negligible for these transitions. (See Sec. VB-2).

Exchange terms result both from antisymmetrization between projectile and target nucleons and from exchange forces in the effective interaction; in general the overlap integrals are complicated and difficult to compute, particularly for complex projectiles. The few calculations which have been reported for nucleon projectiles[30-33] indicate that the contributions from exchange integrals are small for L = 0 transitions,[31,33] though for higher L transfers these terms become more important[31-33] and in certain cases the direct and exchange contributions can be of comparable

magnitude.[32] What the situation would be for the (^{3}He,^{3}He') and (^{3}He,t) reactions to be considered here is not known. It is evident that more theoretical analyses are necessary before the real importance of exchange effects is fully understood.

Another important approximation concerns the use of a simple local interaction which does not vary with energy and also neglects spin-orbit and tensor forces which are known to contribute to the interaction between free nucleons.[34] The validity of this assumption can only be determined by a comparison with experiment; so far the evidence indicates that this approach can be reasonably successful.[6-12]

Finally, one of the most important criteria for the success of a microscopic description is the availability of reliable shell-model wave functions which accurately describe the properties of the initial and final states. In particular, if the wave functions are unable to predict the observed electromagnetic transition rates (E2 and E3 especially) then the effective interaction required to fit the corresponding inelastic scattering data will be enhanced. Fortunately, accurate wave functions are available for 1p shell states which have been successful in predicting several nuclear properties including M1 transition rates and Gamow-Teller beta decays.[19] Furthermore, the effective charges required to predict the observed E2 transition rates only enhance the E2 matrix elements by factors of 1.5-2.0.[20] As a result, the contributions from collective or "core polarization" effects should be smaller for these transitions than those observed for heavier nuclei.

Recently, Satchler proposed using a simple core polarization model in order to account for the inadequacies (i.e., neglected configurations) in the nuclear wave functions.[8,9] This treatment of core polarization effects is analogous to the use of an effective charge for electromagnetic transitions. As a result, the core-coupling parameters for this model can be obtained from the effective charges required to predict the observed electromagnetic transition rates. In the present analysis of the (^{3}He,t) and (^{3}He,^{3}He') reactions the contributions from core polarization effects have been neglected. The results of this approximation for 1p shell nuclei will be discussed further later.

III. EXPERIMENTAL PROCEDURES

A. Cyclotron and External Beam Facilities

These experiments were carried out using 40-50 MeV ^{3}He beams from the Berkeley 88" cyclotron in conjunction with the external beam facilities shown in Fig. 1. Only a brief description of the experimental equipment will be given in this report since detailed discussions have been presented elsewhere.[35,36]

The beam is focused and analyzed using a series of four quadrupole magnets, one bending magnet and an analyzing slit. Variable beam intensities between .01 and 1.0 μA were obtained with an energy resolution of ≈0.14%; typical beam spots were 80 mils wide by 110 mils high. Beam currents were measured using a Faraday cup and an integrating electrometer while the energy of the beam was determined using a series of remotely controlled foil wheels containing aluminum absorbers of various thicknesses.

Particles were detected using two independently moveable counter telescopes located an an angle of 10 deg. above and below the median plane. The solid angle subtended by these detectors was defined using rectangular tantalum collimators .085" wide by .200" high located ≈19" from the center of the scattering chamber. When gas targets were used, an additional set of collimators .085" wide were placed 4" from the center of the scattering chamber. The angular resolution of this system can be measured by obtaining the width of the peak observed in the p(^{3}He,^{3}He)p reaction. This reaction has such a high cross section that it was observed in the ^{3}He spectra from all solid targets. Typical values (FWHM) of 0.32 and 0.85 degrees were obtained depending upon whether a solid or gas target was used in a given experiment. The larger value obtained for gas targets is due primarily to multiple scattering in the entrance and exit windows.

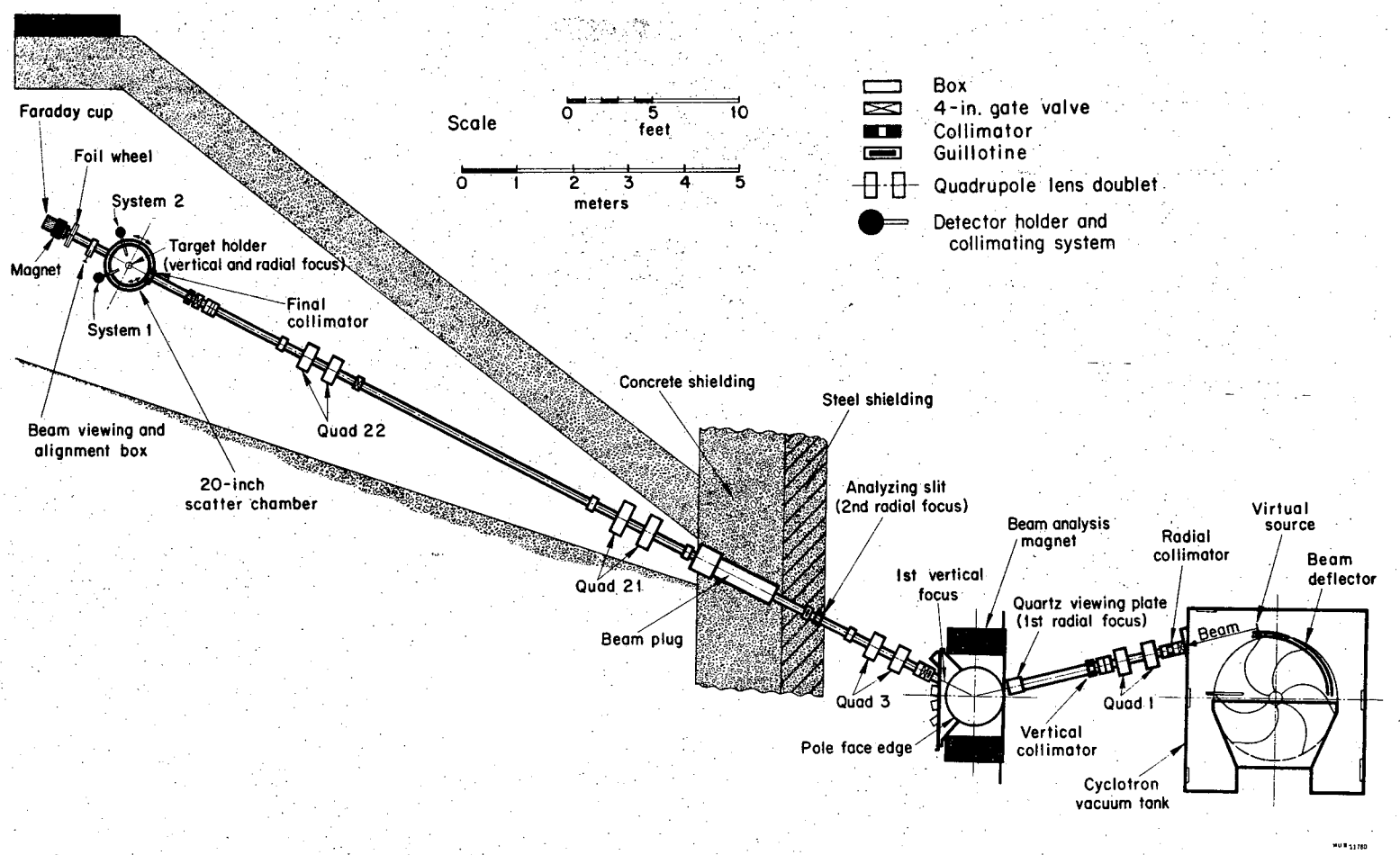

Fig. 1. Schematic diagram of the 88" cyclotron and the external beam facilities used in these experiments.

B. Detectors and Electronics

The two counter telescopes mentioned previously each consisted of an 8.5 or 11.8 mil phosphorus-diffused silicon ΔE detector, a 120 mil lithium-drifted silicon E detector and a 20 mil lithium-drifted silicon E_{rej} detector;[37] the last was used to eliminate the energy signals from long range particles which passed through the first two detectors. In some experiments it was necessary to rotate the E detectors to an angle of 30 deg. in order to stop the high energy tritons.

A block diagram of the electronics is shown in Fig. 2. Energy signals from the ΔE, E, and E_{rej} detectors were connected to fast-rise, charge-sensitive preamplifiers which then fed linear amplifiers with delay-line shaping networks.[37] The energy signals from the ΔE and E amplifiers which satisfied the necessary slow-coincidence requirements were sent to a Goulding-Landis particle identifier.[38] This identifier utilizes the empirical range-energy relationship $R = aE^{1.73}$ producing an output signal which is proportional to T/a, where T is the thickness of ΔE detector and a is a contant which depends upon the particle type. A typical particle identifier spectrum observed in these experiments is shown in Fig. 3.

Two four channel routers were used to set gates around the triton, ^{3}He and α peaks, and also the deuteron-triton valley. (This last region was monitored in order to record any possible leak-through of tritons. In general this leak-through only amounted to ≈1-2%; however, in the $^{13}C(^3He,t)^{13}N$ reaction a malfunction in the particle identifier system resulted in a leak-through of ≈25% for high-energy ground state tritons.) In this manner four energy spectra were recorded simultaneously from each system using a nuclear data 4096-channel pulse height analyzer and a PDP-5 computer (used in conjunction with an eight-channel pulse multiplexer and a 4096-channel analogue-to-digital converter) both operating in a 4×1024 channel mode. Typical energy resolutions (FWHM) for tritons and ^{3}He particles were 150 or 190 keV and 175 or 210 keV, respectively, depending upon whether a solid or gas target was used in the experiment.

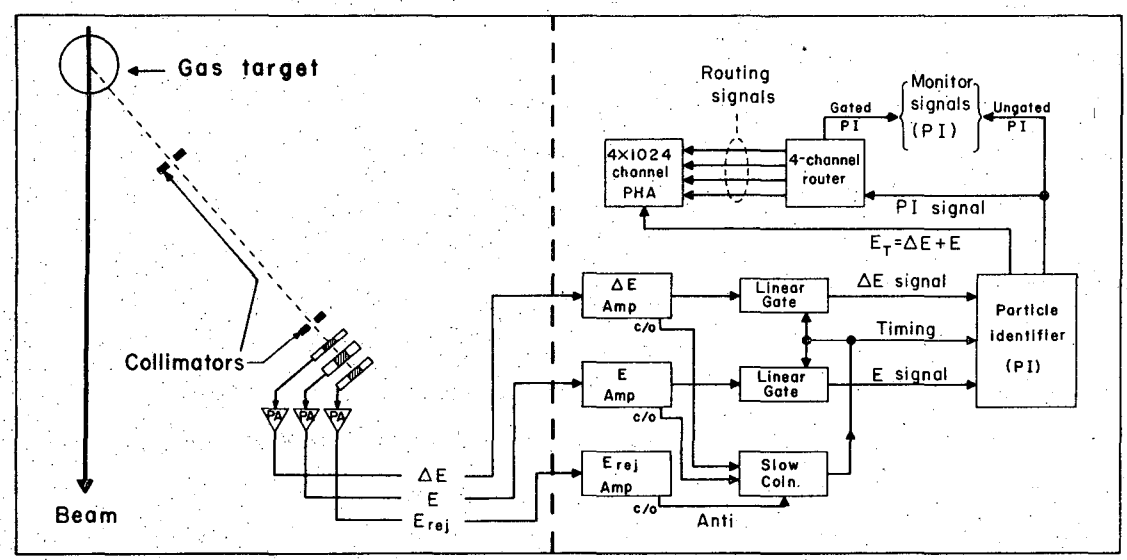

Fig. 2. A block diagram of the electronics used in these experiments.

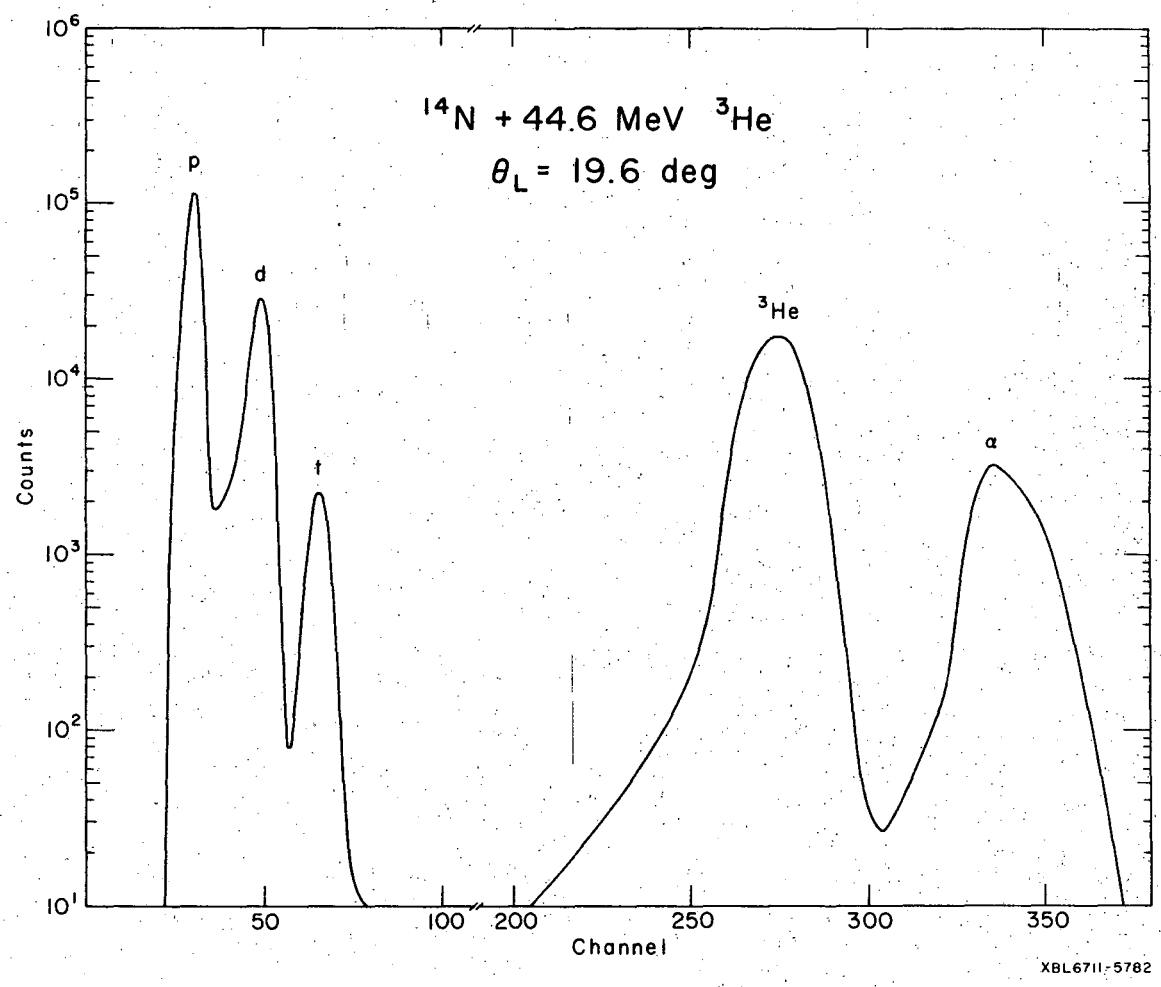

Fig. 3. A typical particle identifier spectrum.

A 120 mil lithium-drifted silicon detector located in the median plane at an angle of 27.5 deg was used to monitor the beam energy and also to detect any changes in the composition of the target. This was of particular importance when ^{13}C in the form of methane was used as a target.

C. Targets

1. Gas Targets

A 7.66 cm diameter gas cell with a window of Havar foil .00025 cm thick[39] was used to contain isotopically pure (> 98%) ^{15}N, ^{14}N, and 93% pure ^{13}C in the form of methane. Gas pressures on the order of 25 to 30 cm Hg were used, and a mercury displacement pump was available for the recovery of rare gases.

2. Solid Targets

A ^{14}C target was obtained from Brookhaven National Laboratory; it was prepared by depositing ^{14}C onto a 2 mg/cm^2 gold backing. This target contained large amounts of ^{12}C and ^{16}O and the exact ^{14}C target thickness was unknown. In order to obtain absolute cross sections, the $^{14}C(^3He,\alpha)^{13}C$ and $^{13}C(\alpha,^3He)^{14}C$ reactions were carried out at 44.8 and 64.5 MeV, respectively. Since the momentum of the incoming ^3He(outgoing α) particle from the $(^3He,\alpha)$ reaction is the same as the momentum of the outgoing ^3He (incoming α) particle from the $(\alpha,^3He)$ reaction, time reversal invariance implies a detailed balance between these two nuclear reactions. As a result, the ground state differential cross sections should satisfy the equation[40]

$$\left(\frac{d\sigma}{d\Omega}\right)_{^3He,\alpha} = \frac{(2J_\alpha+1)(2J_{^{13}C}+1)}{(2J_{^3He}+1)(2J_{^{14}C}+1)} \cdot \frac{k_\alpha^2}{k_{^3He}^2} \cdot \left(\frac{d\sigma}{d\Omega}\right)_{\alpha,^3He}$$

$$= 1.645 \left(\frac{d\sigma}{d\Omega}\right)_{\alpha,^3He} , \qquad (18)$$

where k_α and $k_{^3He}$ are the momenta of the α and ^3He particles, respectively. The angular distributions which were obtained from these two reactions are shown in Fig. 4. Since the cross section for the $(\alpha,^3He)$ reaction was accurately measured it was possible to determine the cross section for the $(^3He,\alpha)$ reaction to ± 15%.

^{12}C targets were prepared from a "Dag" solution consisting of colloidal graphite in alcohol and acetone. The details of this experimental procedure are well known and have been reported elsewhere.[41]

A solid adenine ($C_5H_5N_5$) target, which was used in the $^{14}N(^3He,t)^{14}O$ and $^{14}N(^3He,^3He')^{14}N$ reactions, was made by evaporating ≈1.1 mg/cm^2 of adenine onto a 150 μgm/cm^2 carbon backing. No detectable decomposition of the target was observed over a period of 48 hr at beam intensities of 0.1 to 0.4 μA.

A self-supporting ^9Be target 650 μgm/cm^2 thick was also obtained by evaporation. This target was found to contain small amounts of ^{12}C and ^{16}O impurities.

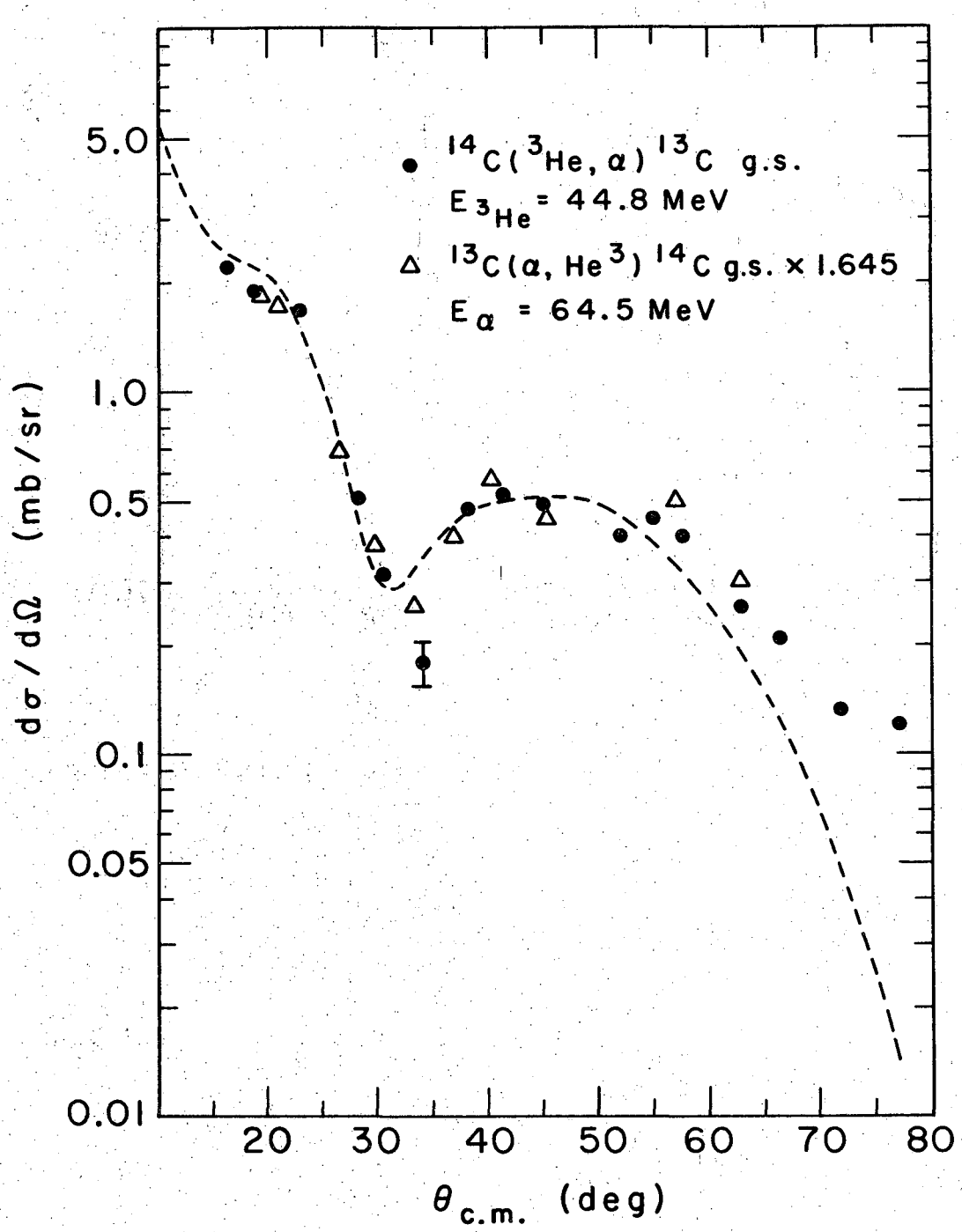

XBL6711-5770

Fig. 4. Angular distributions from the $^{14}C(^{3}He,\alpha)^{13}C$(g.s.) and $^{13}C(\alpha,^{3}He)^{14}C$ (g.s.) reactions at $E_{^3He}$ = 44.8 and E_α = 64.5 MeV, respectively. The $(^{3}He,\alpha)$ distribution has been normalized to the measured $(\alpha,^{3}He)$ distribution; the latter was multiplied by the factor 1.645 required for a detailed balance between these two reactions.

IV. EXPERIMENTAL RESULTS AND DISCUSSION

The (^{3}He,t) and (^{3}He,^{3}He') reactions were investigated for several 1p shell nuclei—in particular, ^{12}C, ^{13}C, ^{14}C[(^{3}He,t) reaction only], ^{14}N and ^{15}N, at ^{3}He energies of 49.8, 39.6, 44.8, 44.6 and 39.8 MeV, respectively. Typical energy spectra are shown in Figs. 5-11.

A summary of the levels observed in these experiments and a comparison with previous data[42-62] is presented in Tables I-VI; the results will be discussed individually later. Excitation energies were determined using the peak channels and energies of well known levels. The analysis was carried out both with the computer program LORNA[63] and by hand.

In general, angular distributions between 15 and 80 degrees in the center of mass were obtained for all prominent levels and are presented in Figs. 12-23. All absolute cross sections are accurate to ± 10% with the exception of the ^{14}C(^{3}He,t)^{14}N reaction where the absolute cross sections are accurate to ± 15% due to an uncertainty in the ^{14}C target thickness (see Sec. III-C). In all cases lines have been drawn through the experimental points to guide the eye.

A. The ^{12}C(^{3}He,t)^{12}N and ^{12}C(^{3}He,^{3}He')^{12}C Reactions

The energy spectra shown in Figs. 5 and 6 for the ^{12}C(^{3}He,t)^{12}N and ^{12}C(^{3}He,^{3}He') ^{12}C reactions indicate that several T = 1 levels can be readily observed in ^{12}C which have a corresponding analog state in ^{12}N. Assuming the charge independence of nuclear forces, the angular distributions for (^{3}He,t) and (^{3}He,^{3}He') reactions populating analog final states ($T_f = T_i \pm 1$) should be identical after phase-space and isospin-coupling corrections are made. Utilizing the known information concerning the spins and parities of T = 1 levels in ^{12}C, it was possible to make several assignments in ^{12}N. These results will be discussed in detail in Sec. VI.

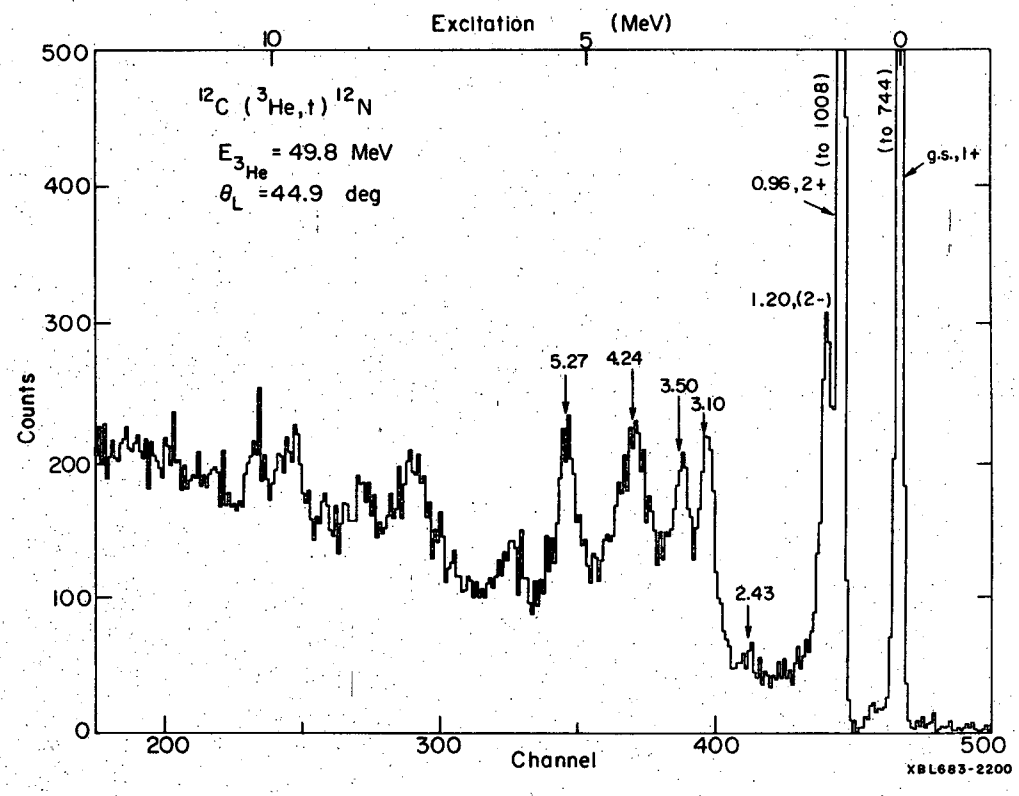

Fig. 5. Energy spectrum of the $^{12}C(^{3}He,t)^{12}N$ reaction at a ^{3}He energy of 49.8 MeV.

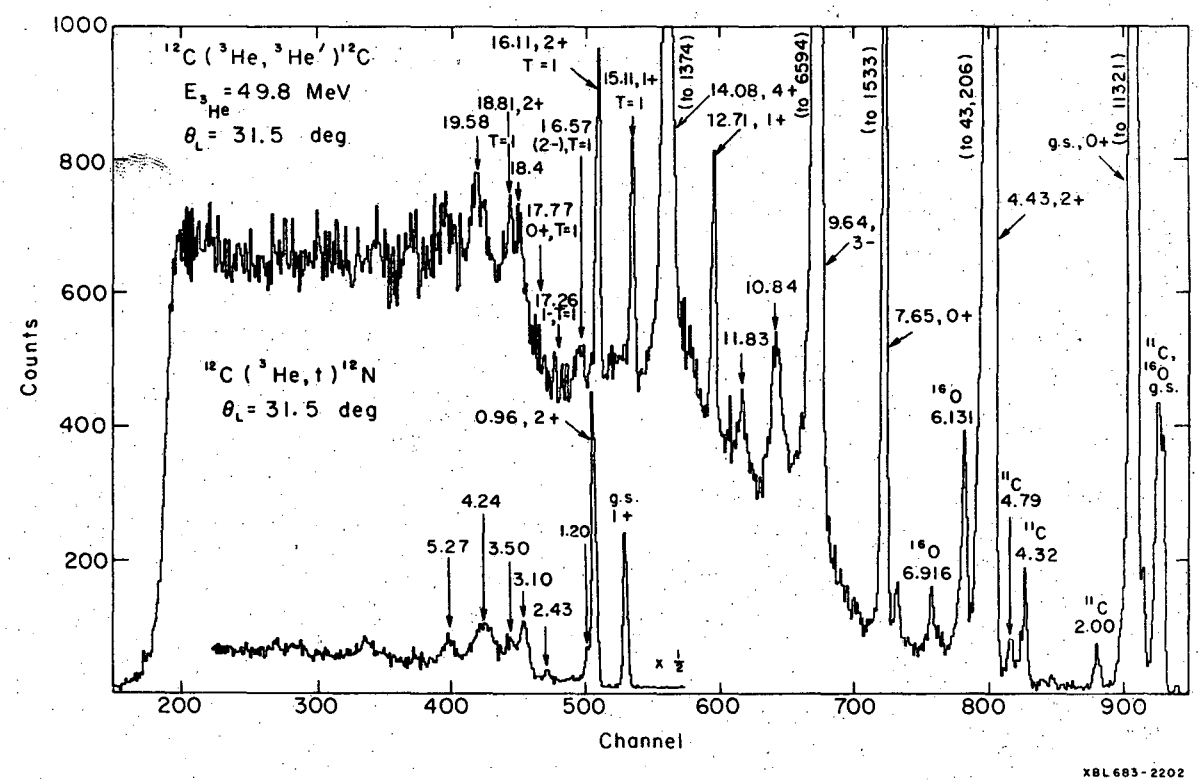

Fig. 5. Energy spectra of the $^{12}C(^3He,t)^{12}N$ and $^{12}C(^3He,^3He')^{12}C$ reactions at a scattering angle of 31.5 deg. The ^{12}N spectrum has been adjusted to align the T = 1 analog states populated in both reactions. The peaks corresponding to the 0.0, 2.00, 4.32, and 4.79 MeV levels of ^{11}C represent an α contamination in the ^3He spectrum of ≈5%.

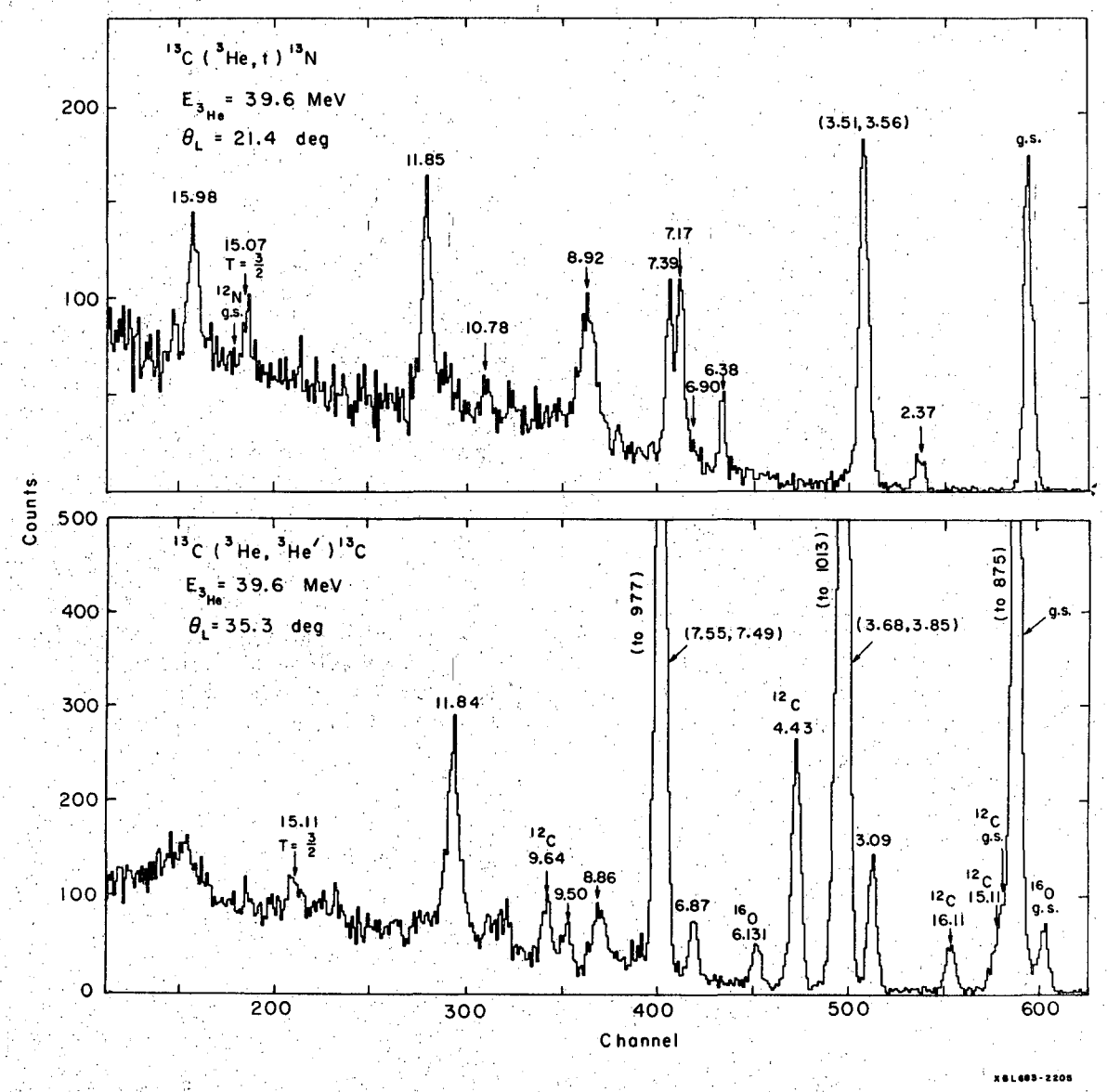

Fig. 7. Energy spectra of the $^{13}C(^3He,t)^{13}N$ and $^{13}C(^3He,^3He')^{13}C$ reactions at a ^3He energy of 39.6 MeV. The spectra were recorded on separate analyzers with different gains. The peaks corresponding to the 15.11 and 16.11 MeV levels of ^{12}C represent an α contamination in the ^3He spectrum of ≈6%.

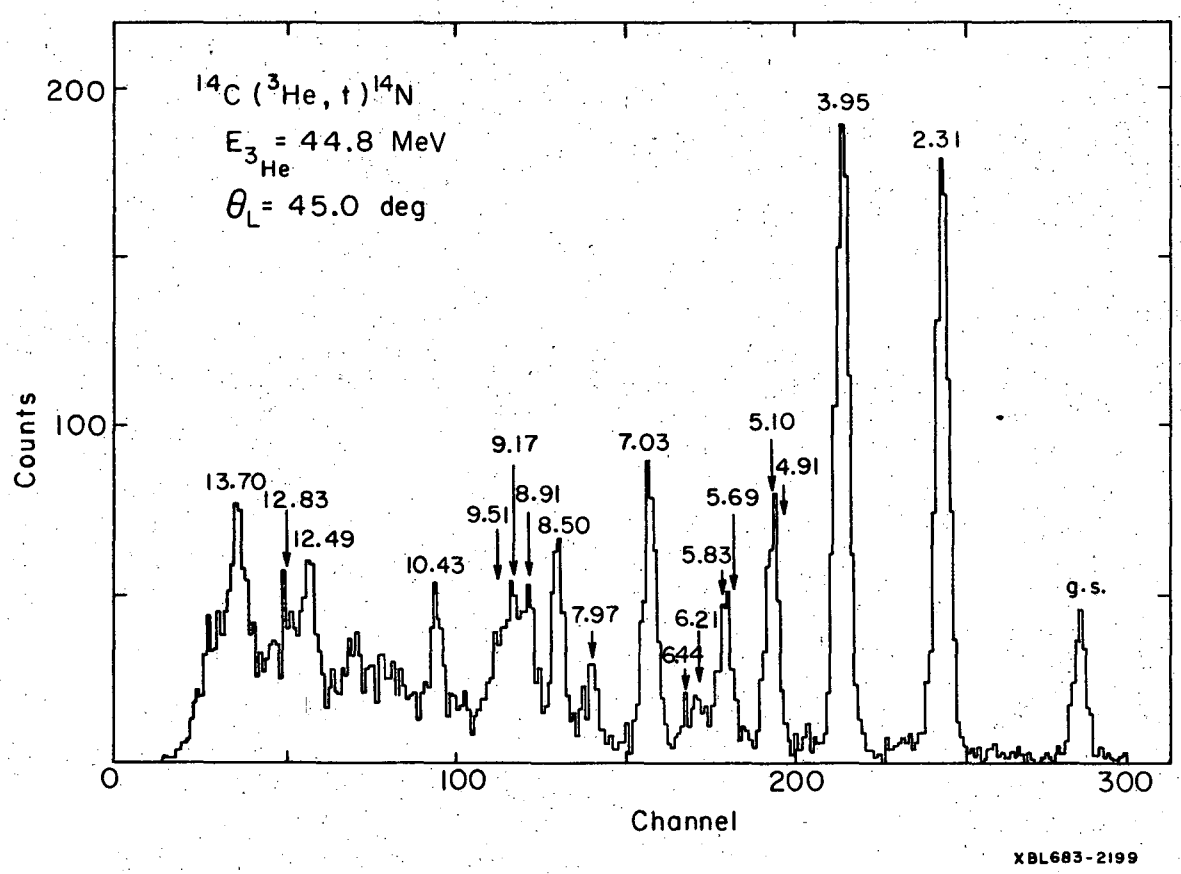

Fig. 8. Energy spectrum of the $^{14}C(^{3}He,t)^{14}N$ reaction at a ^{3}He energy of 44.8 MeV.

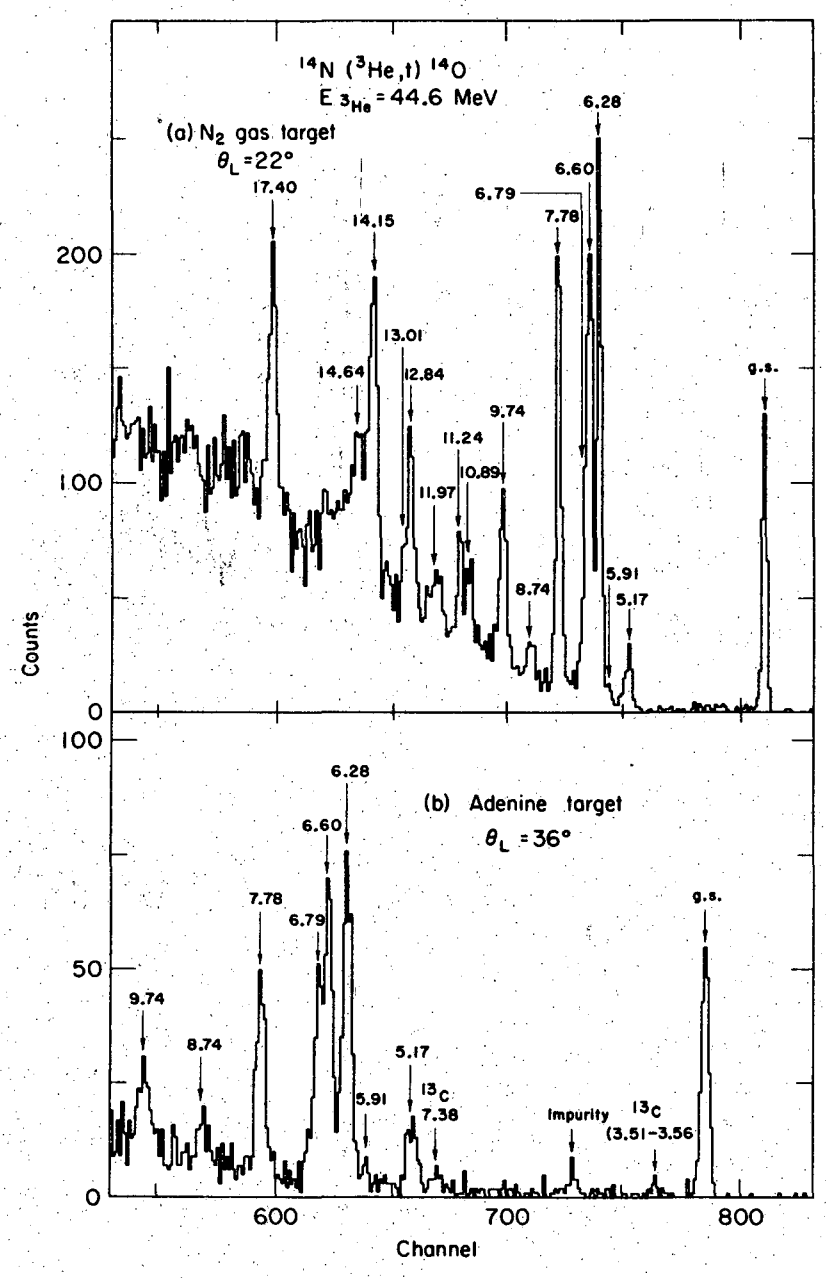

Fig. 9. Energy spectra of the $^{14}N(^{3}He,t)^{14}O$ reaction at a ^{3}He energy of 44.6 MeV using a) a N_2 gas target and b) a solid adenine target.

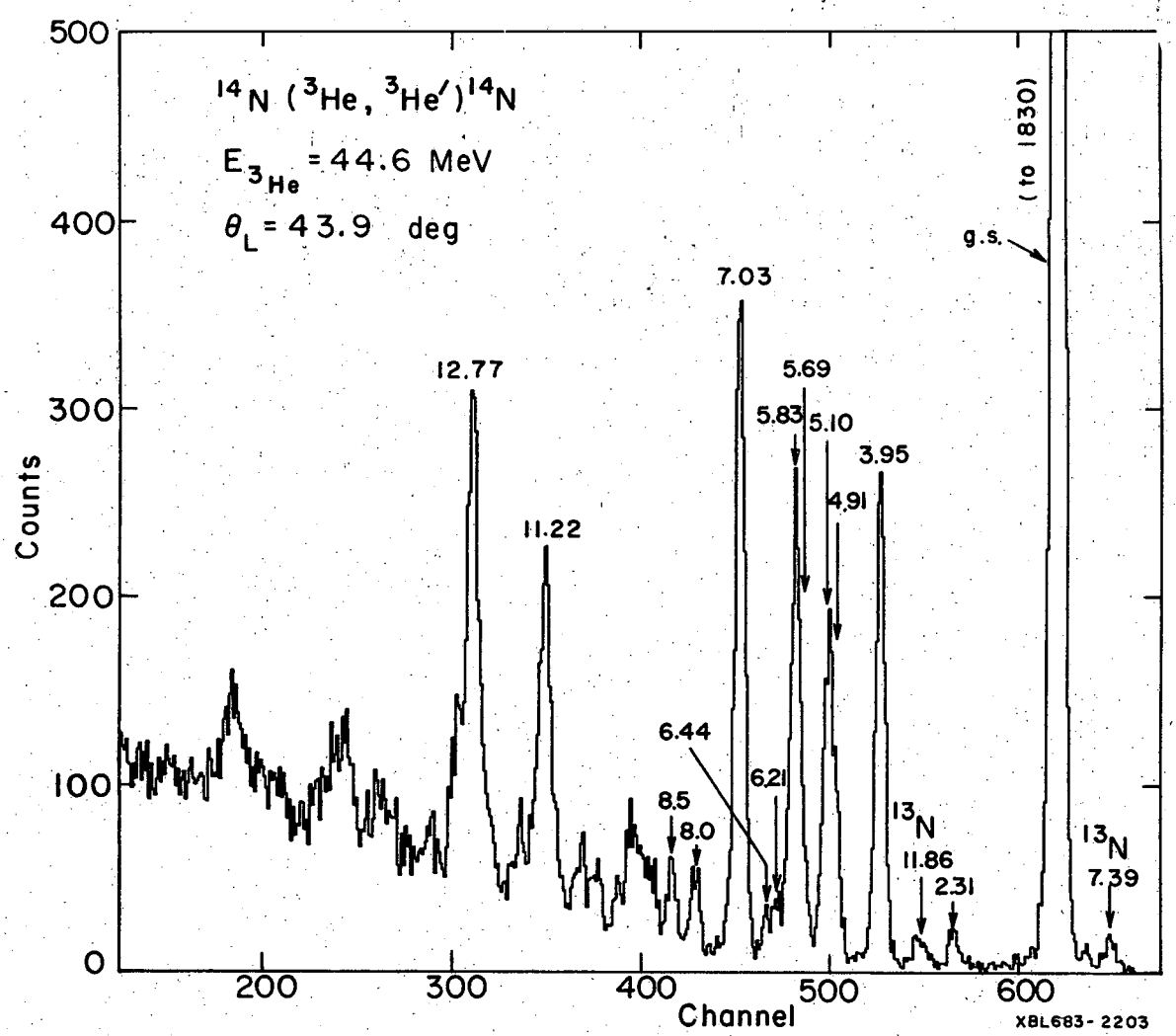

Fig. 10. Energy spectrum of the $^{14}N(^{3}He,^{3}He')^{14}N$ reaction at a ^{3}He energy of 44.6 MeV. The peaks corresponding to the 7.39 and 11.86 MeV levels in ^{13}N represent an α contamination in the ^{3}He spectrum of $\approx$3%.

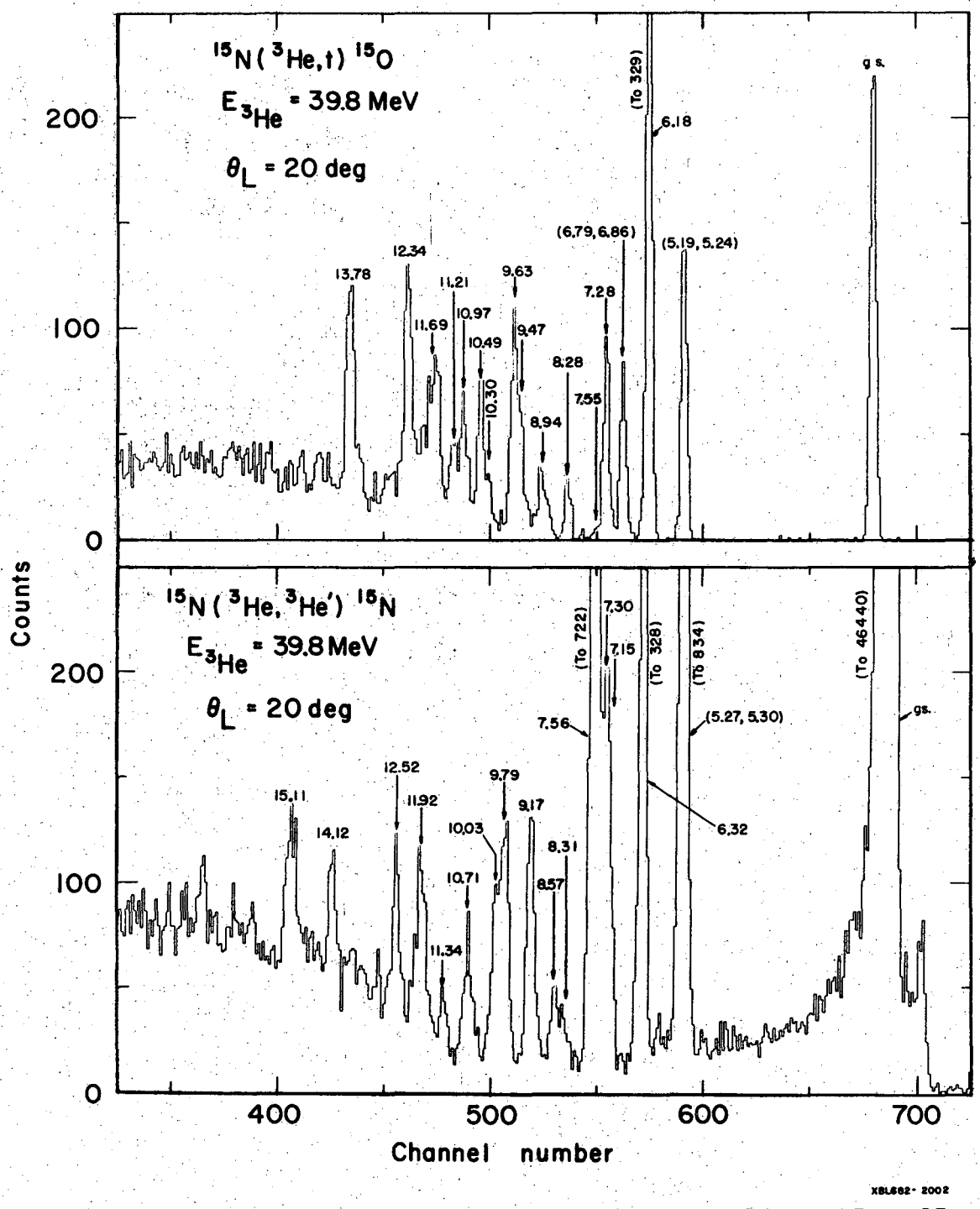

Fig. 11. Energy spectra of the $^{15}N(^3He,t)^{15}O$ and $^{15}N(^3He,^3He')^{15}N$ reactions at a ^3He energy of 39.8 MeV. The ^{15}O spectrum has been adjusted to align the mirror levels populated in both reactions.

Table I. Energy levels observed in ^{12}N

$^{12}C(^{3}He,t)^{12}N$ (Present Work) Energy (MeV ± keV)	J^{π}	(Previous Data)[a] Energy (MeV ± keV)	J^{π}	Dominant[a] Shell-Model Configuration
0	1+	0	1+	$(p\ 3/2)^{7}_{3/2}\ p\ 1/2$
0.96 ± 20	2+[b]	0.969 ± 7		$(p\ 3/2)^{7}_{3/2}\ p\ 1/2$
1.20 ± 30	(2-)[b]	1.198 ± 9		$p^{7}s$
Not observed		1.65 ± 80		$p^{7}s$
Not observed		(2.0 ± 100)		
2.43 ± 40[c]		2.35 ± 80		p^{8} [b]
3.10 ± 30		3.15 ± 80		
3.50 ± 40[c]		3.55 ± 80		p^{8} [b]
4.24 ± 50[d]				
5.27 ± 40				

[a]See Ref. 42 and 43.

[b]Assignments made in present work.

[c]Angular distributions were not obtained for these levels.

[d]Broad level or group of levels.

Table II. Energy levels observed in the $^{12}C(^{3}He,^{3}He')^{12}C$ reaction.

Energy (MeV ± keV)[a]	$J^{\pi};T$[b]	Dominant[b] Shell-Model Configurations
0.0	0+;0	$(p\ 3/2)^{8}_{0} + (p\ 3/2)^{6}_{0}\ (p\ 1/2)^{2}_{0}$
4.43	2+;0	$(p\ 3/2)^{7}_{3/2}\ p\ 1/2$
7.65	0+;0	$p^{8} + p^{6}(s,d)$
9.64	3-;0	$p^{7}d$
10.84[c]	1-;0	$p^{7}(s;d)$
11.83[c]	2-;0	$p^{7}(s;d)$
12.71	1+;0	$(p\ 3/2)^{7}_{3/2}\ p\ 1/2$
14.08	4+;0	p^{8}
15.11	1+;1	$(p\ 3/2)^{7}_{3/2}\ p\ 1/2$
16.11	2+;1	$(p\ 3/2)^{7}_{3/2}\ p\ 1/2$
16.57	2-;1	$p^{7}s$
(17.26)[d]	1-;1	$p^{7}s$
(17.77)[d]	0+;1	p^{8}
18.40 ± 60[c]	(;1)[e]	
18.81[c]	2+;1	p^{8}
(19.2)[d]	1-,2-;1	
19.58 ± 60[f]	(;1)[e]	

[a]Energy levels without error bars were well known previously (see Refs. 43-46).
[b]See Refs. 19, 43-49.
[c]Angular distributions were not obtained for these levels.
[d]These levels were not observed in the $(^{3}He,^{3}He')$ reaction.
[e]Tentative assignments made in present work.
[f]Broad level or group of levels.

Table III. Energy levels observed in ^{13}C and ^{13}N.

^{13}C			^{13}N			
$^{13}C(^{3}He, {}^{3}He')^{13}C$ (Present Work) Energy (MeV ± keV)	Previous Data[a] Energy (MeV ± keV)	J^{π}	$^{13}C(^{3}He, t)^{13}N$ (Present Work) Energy (MeV ± keV)	Previous Data[a] Energy (MeV ± keV)	J^{π}	Dominant[a] Shell-Model Configuration
0.0	0.0	1/2-	0.0	0.0	1/2-	$(p\ 3/2)^{8}_{0}\ p\ 1/2$
3.09	3.086 ± 3	1/2+	2.37	2.366 ± 2	1/2+	$(p\ 3/2)^{8}_{0}\ s\ 1/2$
3.68	3.681 ± 3	3/2-	3.53 ± 30	3.510 ± 2	3/2-	$(p\ 3/2)^{7}_{3/2}\ (p\ 1/2)^{2}_{0}$
3.85	3.852 ± 3	5/2+		3.547 ± 6	5/2+	$(p\ 3/2)^{8}_{0}\ d\ 5/2$
6.87	6.866 ± 7	5/2+	6.38	6.382	5/2+	$p^{8}\ s$
7.55 ± 30	7.490 ± 15	7/2+	7.17	7.166 ± 8	7/2+	$p^{8}\ d$
	7.550 ± 15	5/2-	7.39	7.385 ± 8	5/2-	$(p\ 3/2)^{7}_{3/2}\ (p\ 1/2)^{2}_{1}$
8.86 ± 30	8.86 ± 20	1/2-	8.92 ± 40	8.90 ± 40	1/2-	$(p\ 3/2)^{7}_{3/2}\ (p\ 1/2)^{2}_{1}$
9.50 ± 30[b]	9.503 ± 15	(3/2-)	c	9.48	3/2-	
c	11.078 ± 20	(1/2-)	10.78 ± 40[b]	10.80 ± 30	1/2-	p^{9}
11.84 ± 30	11.80 ± 30	3/2-	11.85 ± 40	11.87 ± 30	3/2-	$(p\ 3/2)^{7}_{3/2}\ (p\ 1/2)^{2}_{1}$
15.11[b]	15.113 ± 5	3/2-, T=3/2	15.07	15.068 ± 8	3/2-, T=3/2	$(p\ 3/2)^{7}_{3/2}\ (p\ 1/2)^{2}_{0}$
			15.98 ± 50[b]	15.96 ± 50		

[a]See Refs. 35, 44, 45, 49-52.

[b]Angular distributions were not obtained for these levels.

[c]These levels were weakly populated (see Fig. 7).

Table IV. Energy levels observed in ^{14}N.

Present Work: $^{14}N(^{3}He, ^{3}He')^{14}N$ Energy[a] (MeV ± keV)	Present Work: $^{14}C(^{3}He, t)^{14}N$ Energy[a] (MeV ± keV)	Previous Data[b] Energy (MeV)	Previous Data[b] J^{π}, T	Dominant[b] Shell-Model Configurations
0.0	0.0	0.0	1+,0	$(p\ 1/2)^2$
2.31	2.31	2.311	0+,1	$(p\ 1/2)^2$
3.95	3.95	3.945	1+,0	$(p\ 3/2,\ p\ 1/2)^{-1}$
4.91	4.91[c]	4.910	0-,0	(p 1/2, s 1/2)
5.10	5.10	5.104	2-,0	(p 1/2, d 5/2)
5.69	5.69	5.685	1-,0	(p 1/2, s 1/2)
5.83	5.83	5.832	3-,0	(p 1/2, d 5/2)
6.21[c]	6.21[c]	6.21	1+,0	$(s\ 1/2)^2$
6.44[c]	6.44[c]	6.44	3+,0	(s 1/2, d 5/2)
7.03	7.03	7.029	2+,0	$(p\ 3/2,\ p\ 1/2)^{-1}$
8.0 ± 50[c]	7.97 ± 40[c]	7.97	2-,0	(p 1/2, d 3/2)
		8.060	1-,1	(p 1/2, s 1/2)
8.5 ± 50[c]	8.50 ± 40	8.489	4-,0	$(p\ 3/2)^{-1}(p\ 1/2)^2(d\ 5/2)$
		8.617	0+,1	$(s\ 1/2)^2$
		8.71	0-,1	(p 1/2, s 1/2)
		8.906	3-,1	(p 1/2, d 5/2)
		8.963	5+,0	$(d\ 5/2)^2$
	d	8.979	2+,0	(s 1/2, d 5/2)
		9.129	2-,0	$(p\ 3/2)^{-1}(p\ 1/2)^2(s;\ d)$
		9.17	2+,1	$(p\ 3/2,\ p\ 1/2)^{-1}+(s,\ d)$
d		9.388	2-,0	
		9.508	2-,1	(p 1/2, d 5/2)
		9.702	1+,0	
		10.096	(1+),0	
		10.213	1+,(0)	(s, d)
	10.43	10.431	2+,1	$(p\ 3/2,\ p\ 1/2)^{-1}+(s,\ d)$
		10.55	(1-),	
		10.85	(4+),0	(d 3/2, d 5/2)+(p 1/2, f 7/2)

Table IV. Continued.

Present Work $^{14}N(^{3}He, ^{3}He')^{14}N$ Energy[a] (MeV ± keV)	$^{14}C(^{3}He, t)^{14}N$ Energy[a] (MeV ± keV)	Previous Data[b] Energy (MeV)	J^{π},T	Dominant[b] Shell-Model Configurations
		11.06	1+,0	
11.22 ± 40[e]		11.23	(3-),1	
		11.299	2-,0	
		12.41	4-,0	
	12.49 ± 40[c]	12.52	(2+,1)[f]	$(p\ 3/2,\ p\ 1/2)^{-1}+(s,\ d)^{f}$
		12.61	3+,	
		12.69	3-,	
12.77 ± 40[e]	12.83 ± 50[c]	12.80	4+,	
		12.83	4-,0	
	13.70 ± 40	13.72	1+,1	$(p\ 3/2,\ p\ 1/2)^{-1}$

[a]Energy levels without error bars were well known previously.

[b]See Refs. 18, 44, 45, 49, 51, 53-56.

[c]Angular distributions were not obtained for these levels.

[d]Several unresolved levels were populated in these regions (compare Figs. 8, 10).

[e]Strong levels were also observed in the $^{14}N(\alpha, \alpha')^{14}N$ reaction[62] at 11.3 and 12.9 MeV.

[f]Tentative assignment (See Ref. 49).

Table V. Energy levels observed in ^{14}O.

$^{14}N(^{3}He,t)^{14}O$ (Present Work)		Values from Lauritsen et al.[a]		Dominant Shell-Model Configuration[b]
Energy (MeV ± keV)	J^{π} [b]	Energy (MeV ± keV)	J^{π}	
0	0+	0	0+	$(p\ 1/2)^2$
5.17 ± 40	(1-)			(p 1/2,s 1/2)
5.91 ± 40[c]	(0+)	5.91 ± 12		$(s\ 1/2)^2$
6.28 ± 30	(3-)	6.30 ± 30		(p 1/2,d 5/2)
6.60 ± 30	2+	6.59 ± 12		$(p\ 3/2,p\ 1/2)^{-1}+(s,d)$
6.79 ± 30	(2-)			(p 1/2,d 5/2)
7.78 ± 30	2+	~7.5		$(p\ 3/2,p\ 1/2)^{-1}+(s,d)$
8.74 ± 60[c]				
9.74 ± 30	(2+)	~9.3		$(p\ 3/2,\ p1/2)^{-1}+(s,d)$
10.89 ± 50				
11.24 ± 50				
11.97[c,d]				
12.84 ± 50[c]				
13.01 ± 50[c]				
14.15 ± 40				
14.64 ± 60[c]				
17.40 ± 60				

[a]See Ref. 45.

[b]Assignments made in present work (see also Ref. 18).

[c]Angular distributions were not obtained for these levels.

[d]Several levels are populated in this region.

Table VI. Energy levels observed in ^{15}N and ^{15}O.

$^{15}N(^{3}He, {}^{3}He')^{15}N$ (Present Work) Energy (MeV ± keV)	Previous Data[a] Energy[b] (MeV ± keV)	J^{π}	$^{15}N(^{3}He, t)^{15}O$ (Present Work) Energy (MeV ± keV)	Previous Data[a] Energy[b] (MeV ± keV)	J^{π}	Dominant Shell-Model Configuration[c]
0.0	0.0	1/2-	0.0	0.0	1/2-	$p\ 1/2^{-1}$
5.28 ± 30	5.27	5/2+	5.24 ± 30	5.24	5/2(+)	$(p\ 1/2)^2_0\ d\ 5/2$
	5.30	1/2+		5.19	1/2+	$(p\ 1/2)^2_0\ s\ 1/2$
6.32	6.32	3/2-	6.18	6.18	3/2(-)	$p\ 3/2^{-1}$
7.15	7.15	5/2+	6.84 ± 40	6.86	5/2+	$(p\ 1/2)^2_1\ d\ 5/2$
7.30	7.30	3/2+		6.79	3/2+	$(p\ 1/2)^2_1\ s\ 1/2$
7.56	7.56	7/2+	7.28	7.28	7/2(+)	$(p\ 1/2)^2_1\ d\ 5/2$
8.31	8.31	1/2+,(3/2+)	7.55	7.55	1/2+	$(p\ 1/2)^2_1\ s\ 1/2$
8.57	8.57	3/2+	8.28	8.28	3/2+	$(p\ 1/2)^2_1\ d\ 5/2$
	9.05	1/2+,(3/2+)		8.75	1/2+	
9.17 ± 30	9.16	3/2(-),(5/2)	8.94 ± 40	8.98	3/2-	
	9.22	3/2,(1/2)		8.92	3/2(+)	
9.79 ± 40	9.76	5/2-	9.47 ± 50	9.485	5/2-	
	9.83	7/2(-)		9.49 ± 40	3/2+	
10.03 ± 40	9.93	1/2+,3/2+	9.63 ± 40	9.61	3/2-	
	10.07	3/2+		9.67	(7/2,9/2)-	
	10.45	3/2,5/2,7/2	10.30 ± 40	10.28		
	10.54	5/2	10.49 ± 40	10.46		
10.71 ± 40	10.70	3/2+	10.97 ± 50	10.94	≥ 3/2	
	10.80	3/2		11.02		
11.34 ± 40	d		11.21 ± 60	d		
11.92 ± 40			11.69 ± 40			
12.52 ± 40			12.34 ± 40			
14.12 ± 40			13.78 ± 40			
15.11 ± 40						

[a] See Refs. 44, 45, 57-61.

[b] Energy levels without error bars were well known previously.

[c] See Refs. 57, 59-61.

[d] Several levels have been reported above 11 MeV in both ^{15}N and ^{15}O (see Refs. 44, 45).

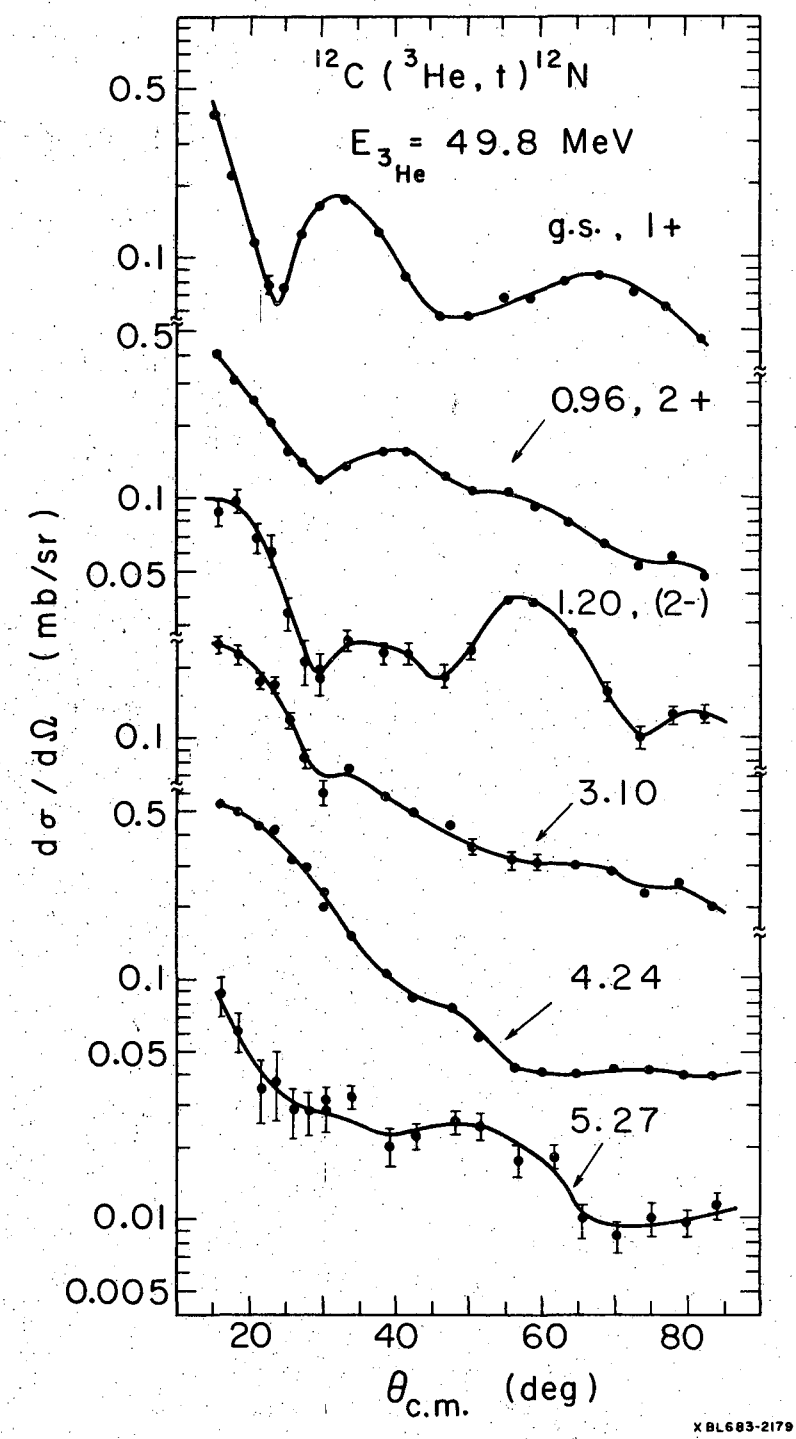

Fig. 12. Angular distributions from the $^{12}C(^{3}He,t)^{12}N$ reaction. When no error bars are shown the statistical errors are $\leq$ 7%. Curves have been drawn through the experimental points to guide the eye.

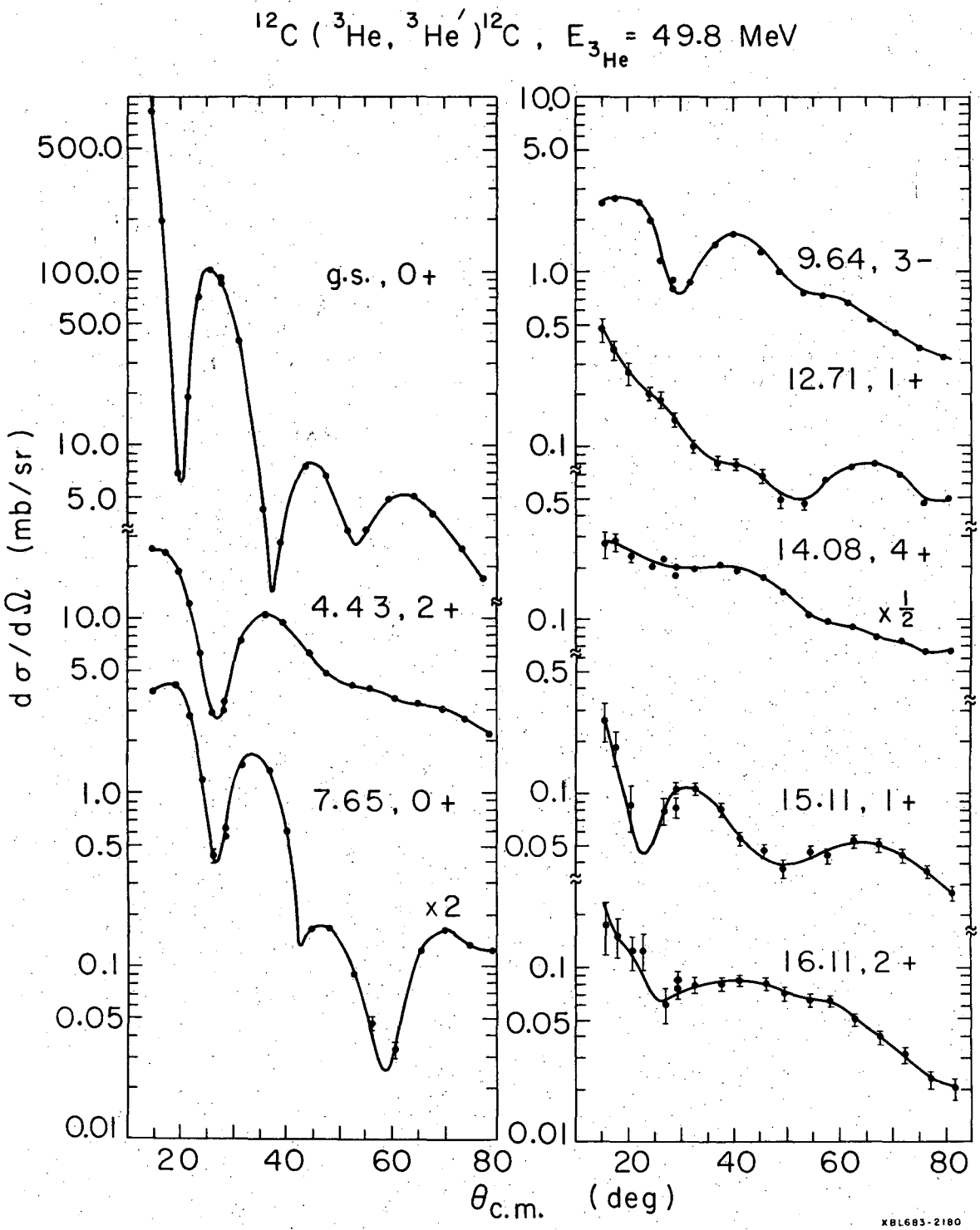

Fig. 13. Angular distributions from the $^{12}C(^{3}He,^{3}He')^{12}C$ reaction. The curves have no theoretical significance.

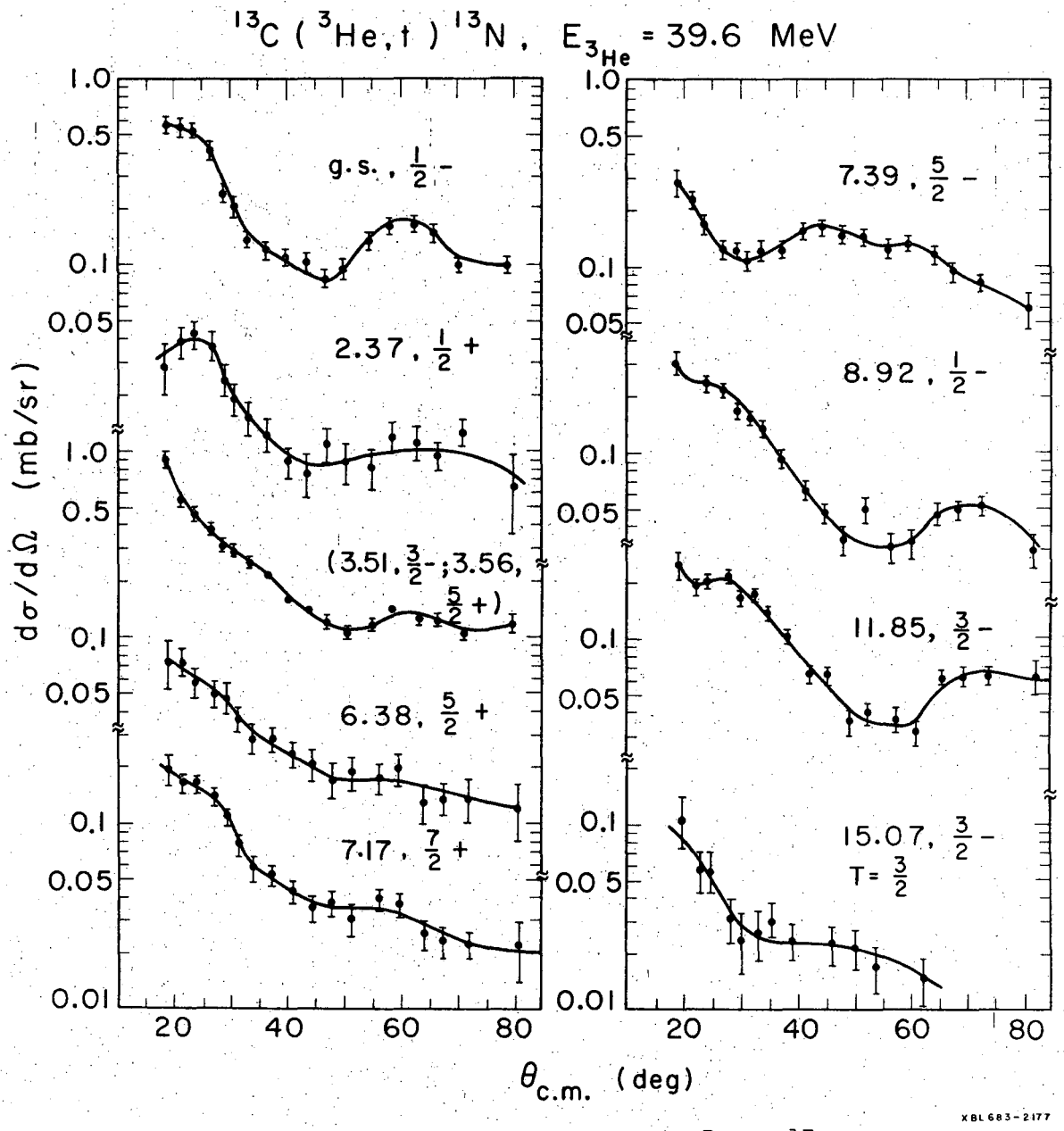

Fig. 14. Angular distributions from the $^{13}C(^{3}He,t)^{13}N$ reaction. The curves have no theoretical significance.

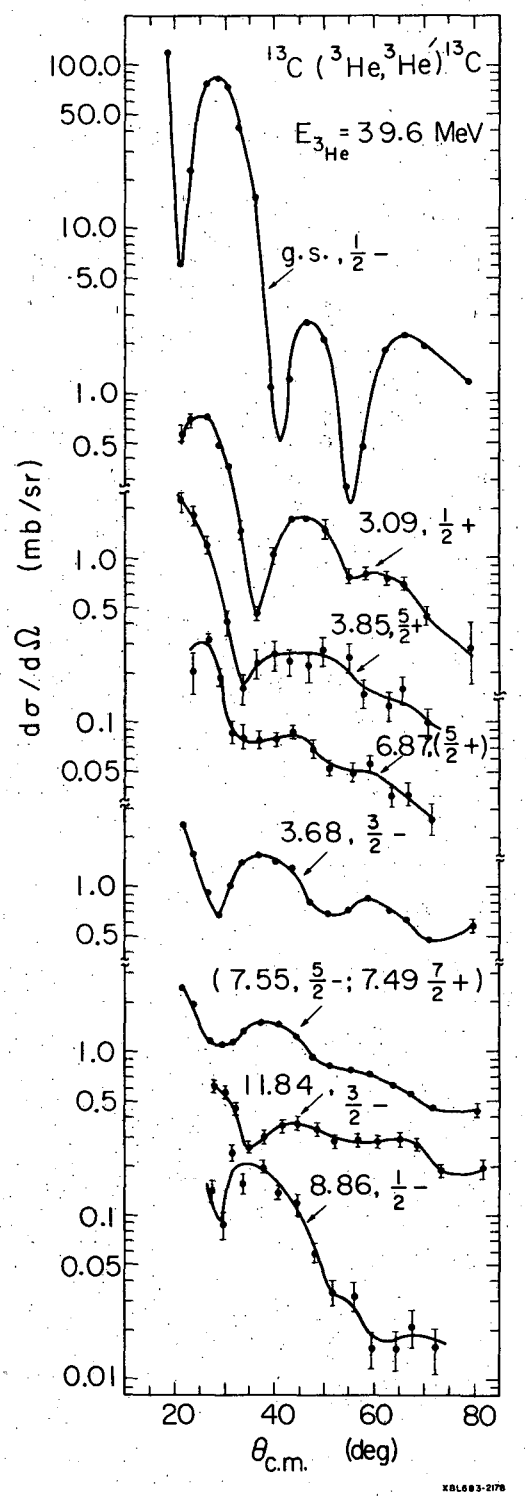

Fig. 15. Angular distributions from the $^{13}C(^3He,^3He')^{13}C$ reaction. The curves have no theoretical significance.

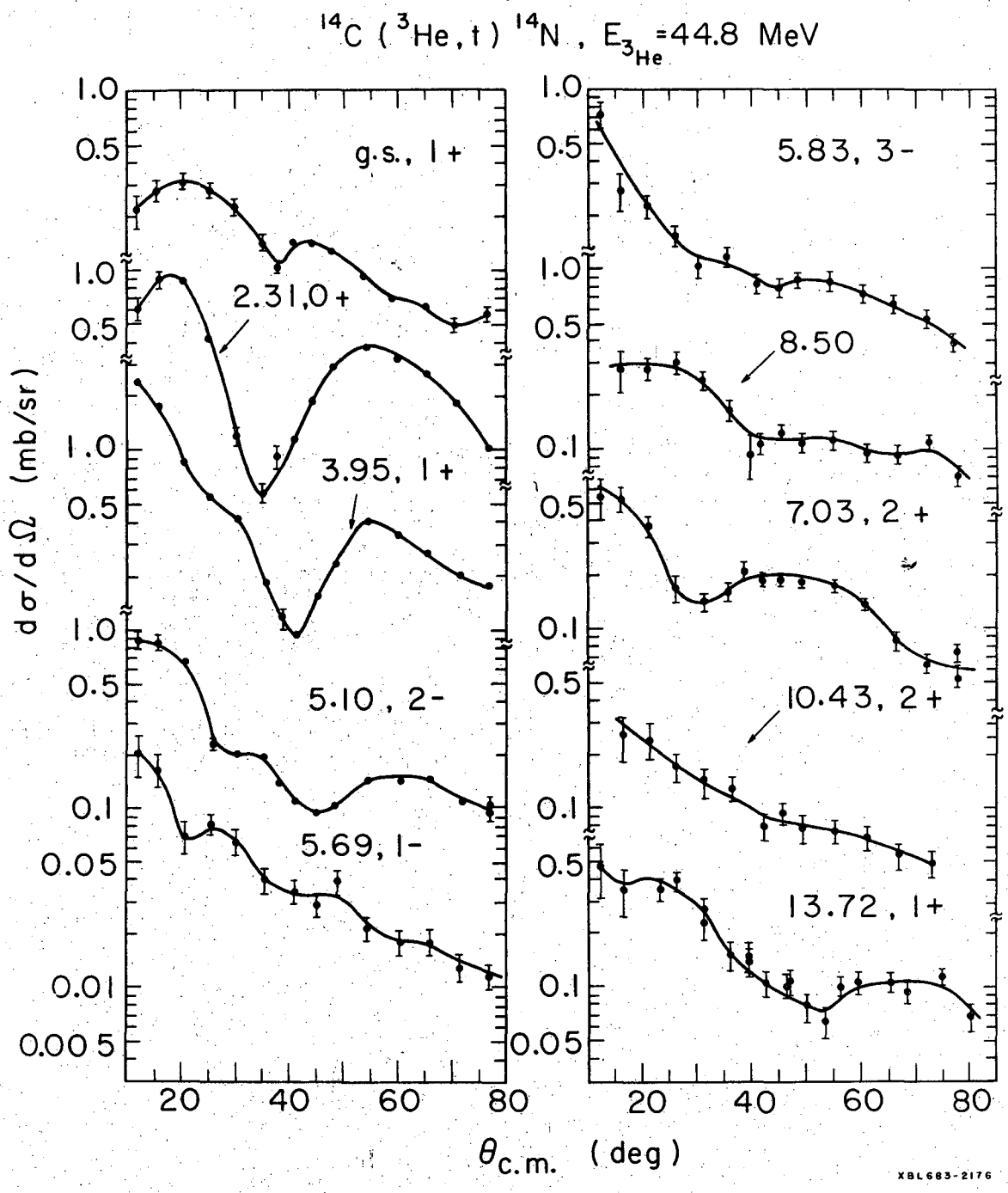

Fig. 16. Angular distributions from the $^{14}C(^{3}He,t)^{14}N$ reaction. The curves have no theoretical significance.

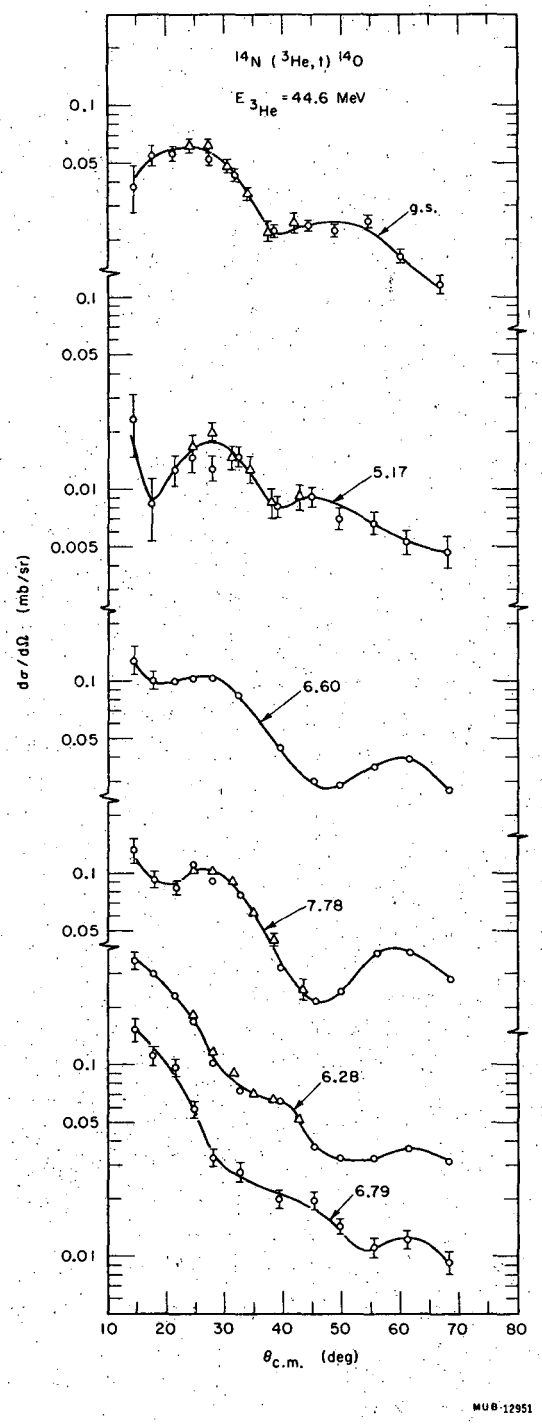

Fig. 17. Angular distributions from the $^{14}N(^{3}He,t)^{14}O$ reaction. Points obtained from the gas target data are shown as triangles, while the solid adenine target data are indicated by circles. The curves have no theoretical significance.

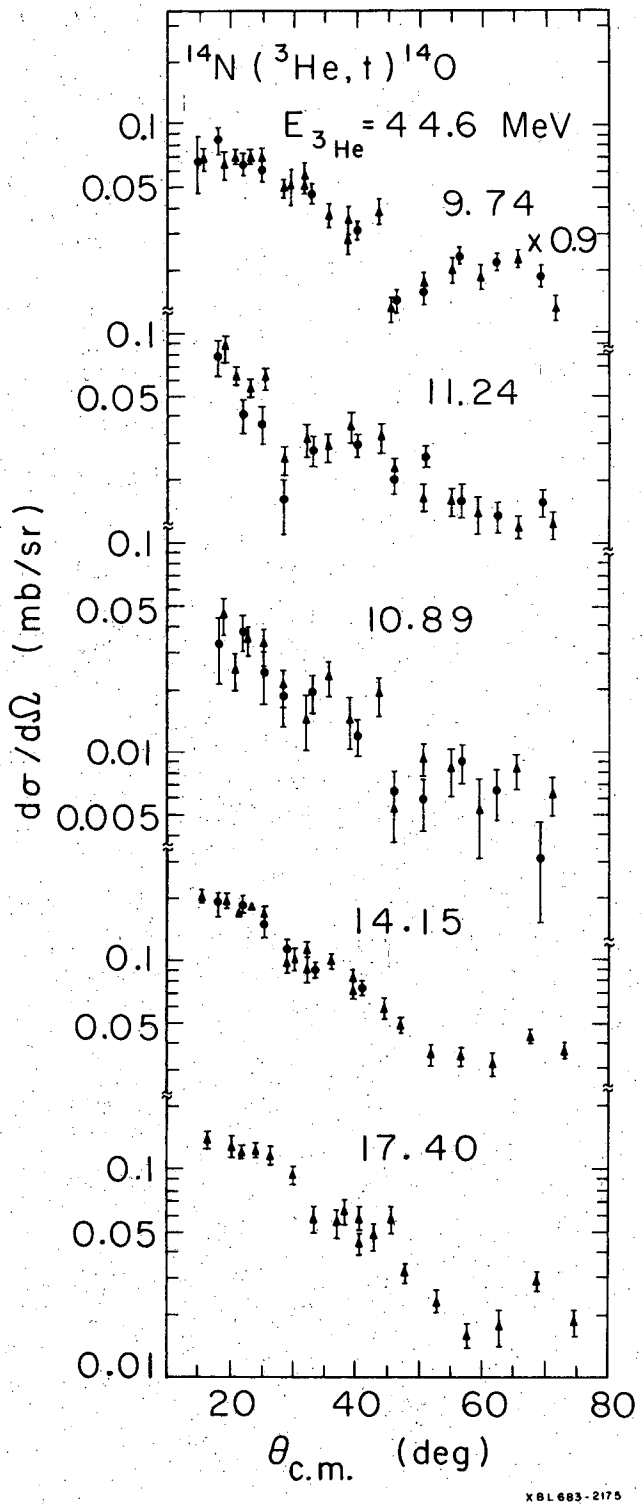

Fig. 18. Angular distributions from the $^{14}N(^{3}He,t)^{14}O$ reaction. Points obtained from the gas target data are shown as triangles, while the solid adenine target data are indicated by circles.

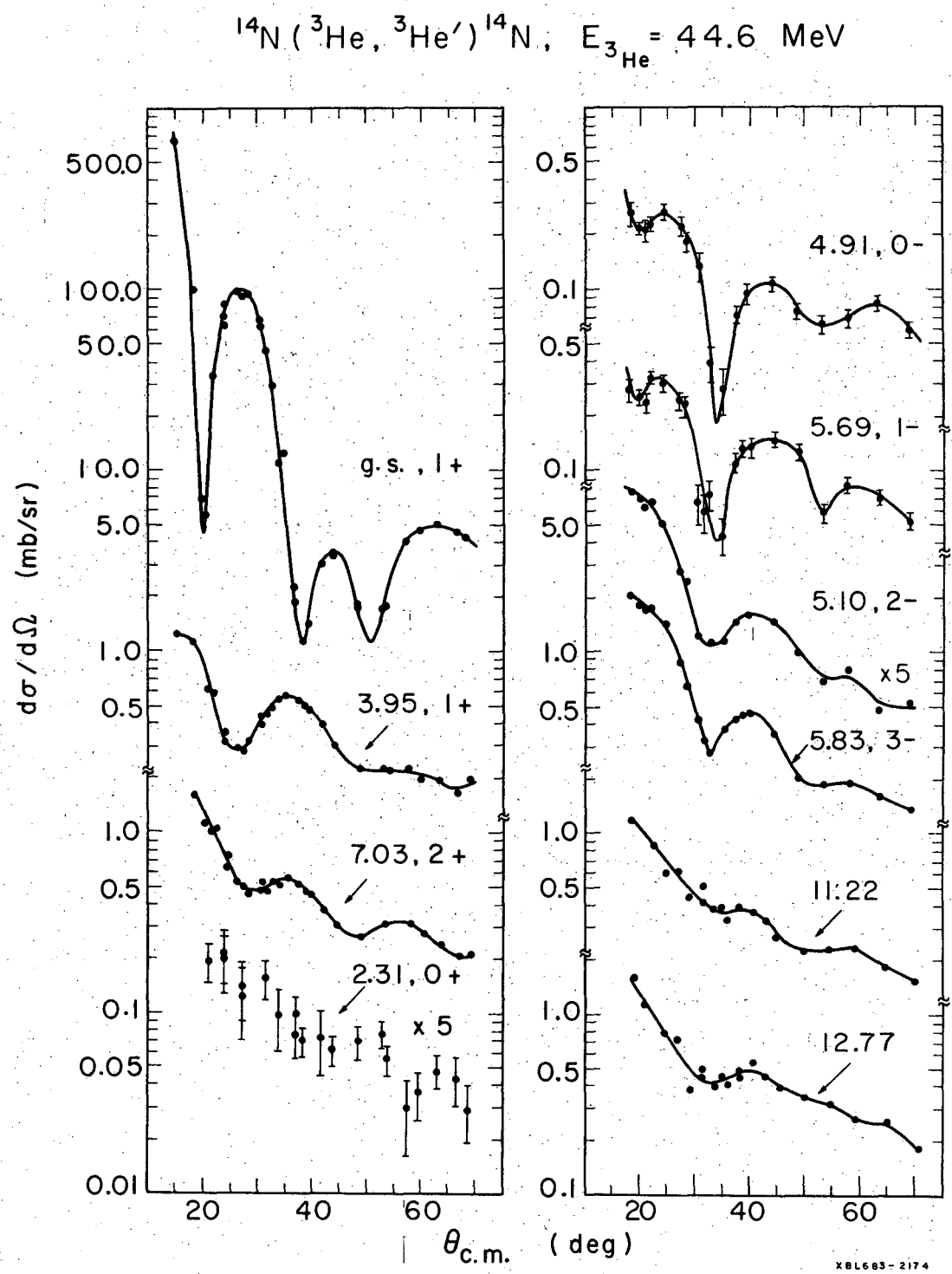

Fig. 19. Angular distributions from the $^{14}N(^{3}He,^{3}He')^{14}N$ reaction. The curves have no theoretical significance.

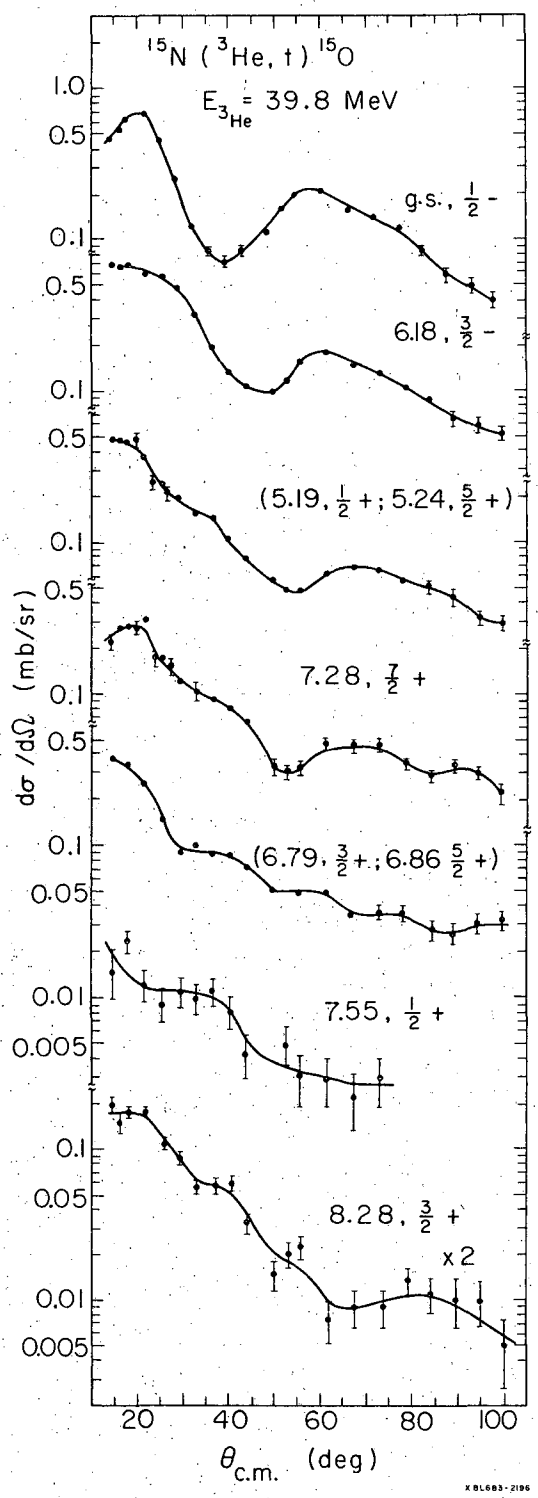

Fig. 20. Angular distributions from the $^{15}N(^{3}He,t)^{15}O$ reaction. The curves have no theoretical significance.

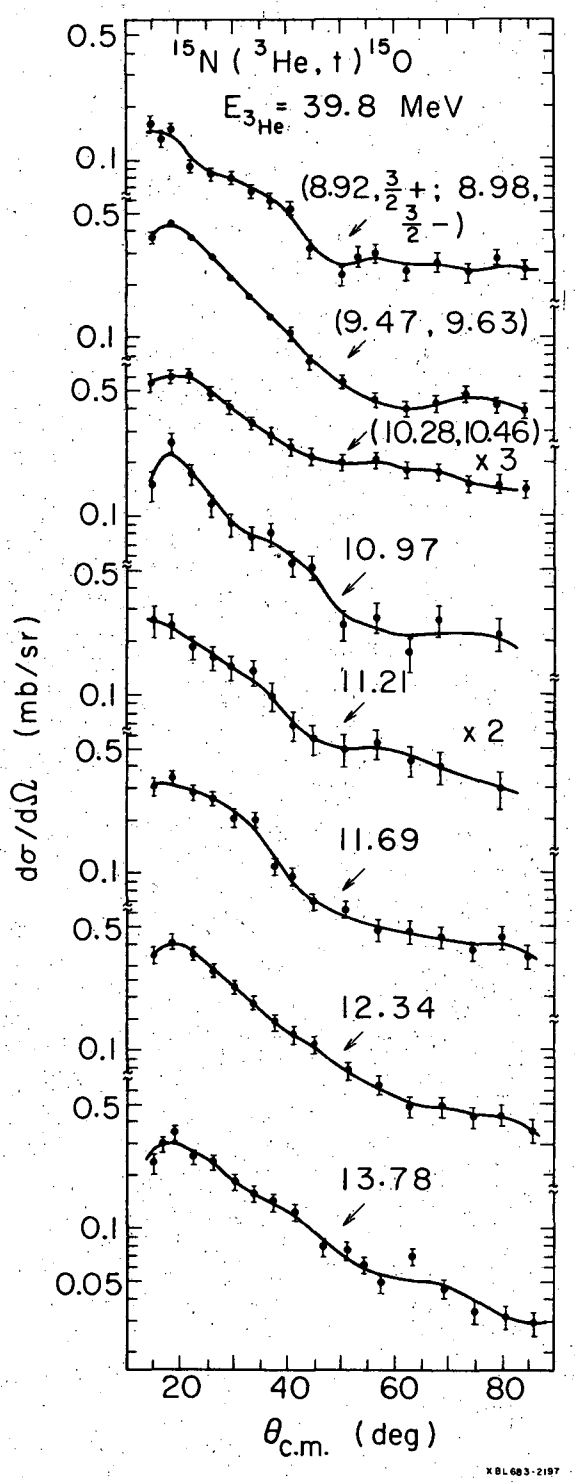

Fig. 21. Angular distributions from the $^{15}N(^{3}He,t)^{15}O$ reaction. The curves have no theoretical significance.

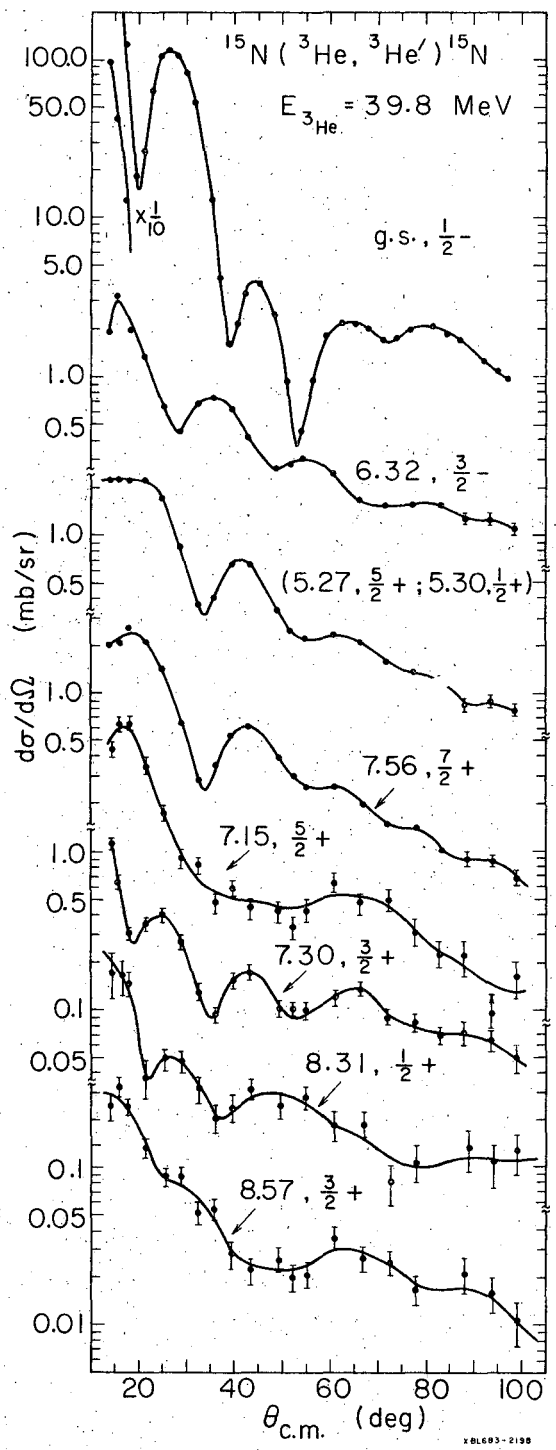

Fig. 22. Angular distributions from the $^{15}N(^{3}He,^{3}He')^{15}N$ reaction. The curves have no theoretical significance.

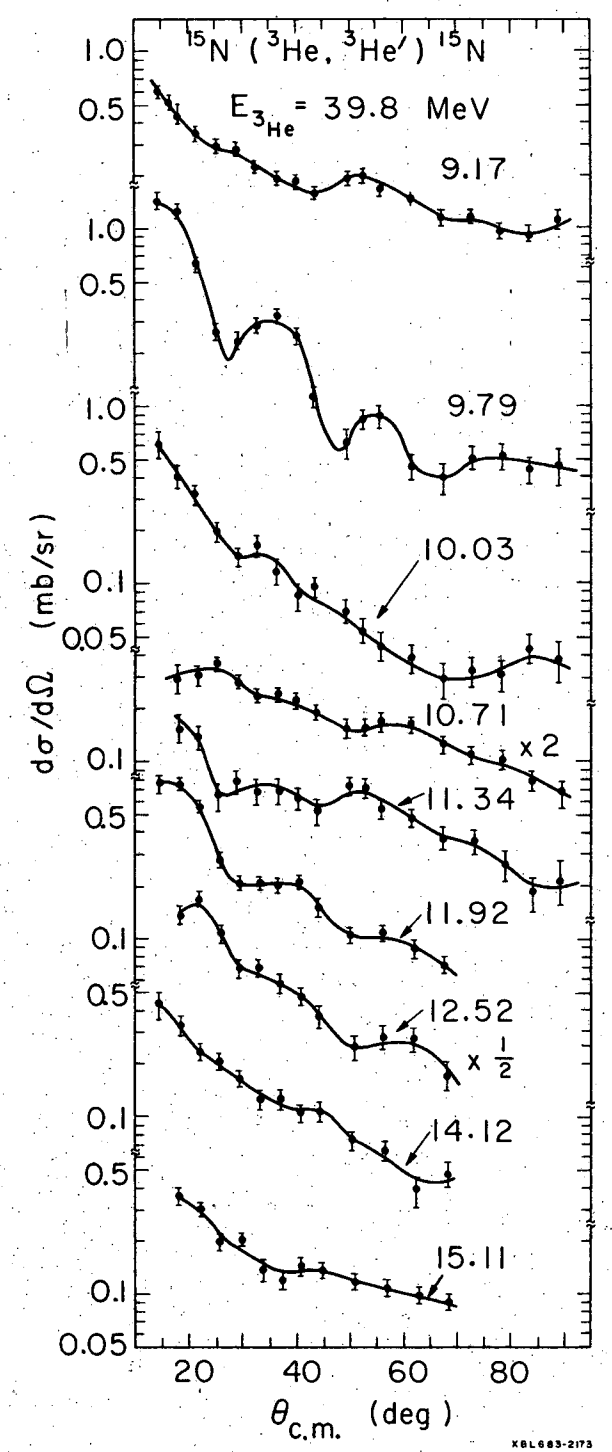

Fig. 23. Angular distributions from the $^{15}N(^3He,^3He')^{15}N$ reaction. The curves have no theoretical significance.

B. The $^{13}C(^{3}He,t)^{13}N$ and $^{13}C(^{3}He,^{3}He')^{13}C$ Reactions

A majority of the strongly populated levels observed in these reactions have negative parity and correspond to known p-shell hole states (see Table III). Some of these states, for example the 3/2- level observed in ^{13}N and ^{13}C at 11.85 and 11.84 MeV, respectively, were only identified recently in single-[49-51] and two-[35] nucleon pick-up reactions. The well known 3/2-, T = 3/2 levels in ^{13}N and ^{13}C are also observed in these reactions and will be discussed in Sec. VI.

C. The $^{14}C(^{3}He,t)^{14}N$ Reaction

The energy levels populated in the $^{14}C(^{3}He,t)^{14}N$ reaction are shown in Table IV. All of the well-known p-shell hole states are observed in this reaction including the 13.72-MeV 1+, T = 1 state which was first observed in the $^{15}N(^{3}He,\alpha)^{14}N$ reaction.[51] In addition, several T = 0 and T = 1 states are observed which involve the promotion of a p nucleon to the s-d shell.

D. The $^{14}N(^{3}He,t)^{14}O$ Reaction

In the $^{14}N(^{3}He,t)^{14}O$ reaction several new levels were observed in ^{14}O up to an excitation energy of 18 MeV. By comparing the angular distributions observed in this reaction with well-known single-particle transitions in the $^{15}N(^{3}He,t)^{15}O$ and $^{14}C(^{3}He,t)^{14}N$ reactions, it was possible to make spin and parity assignments of (1-), (0+), (3-), 2+, (2-) and 2+ for the levels observed in ^{14}O at 5.17, 5.91, 6.28, 6.60, 6.79 and 7.78 MeV, respectively (compare Table V). A detailed report on this experiment has been published elsewhere[18] and will not be discussed further here.

E. The $^{14}N(^{3}He,^{3}He')^{14}N$ Reaction

Several T = 0 levels are strongly populated in this reaction up to an excitation energy of 13 MeV; the results are summarized in Table IV. The angular distributions observed in this reaction (see Fig. 19) provide good examples of typical p1/2→ s1/2 (L = 1), p1/2→ d5/2 (L = 3), and p3/2→ p1/2 (L = 2) transitions. The pair of levels at 11.22 and 12.77 MeV have angular distributions which resemble L = 3 transitions and probably result from p3/2→ d3/2,d5/2 single-particle transitions.

F. The $^{15}N(^{3}He,t)^{15}O$ and $^{15}N(^{3}He,^{3}He')^{15}N$ Reactions

A comparison of the mirror levels populated in the $^{15}N(^{3}He,t)^{15}O$ and $^{15}N(^{3}He,^{3}He')^{15}N$ reactions is given in Table VI. All known levels of ^{15}N and ^{15}O were observed up to an excitation of 10 MeV. In the $^{15}N(^{3}He,t)^{15}O$ reaction a strong transition to the 6.18 MeV level is observed while a very small population of the (3/2)- level at 8.98 MeV is seen (see Fig. 11). This is in good agreement with the information obtained from the $^{16}O(^{3}He,\alpha)^{15}O$ (see Ref. 59) and $^{16}O(p,d)^{15}O$ (see Ref. 60) reactions which confirmed that the 6.18 MeV level contains most of the $p3/2^{-1}$ strength. Further supporting evidence is obtained from the $^{15}N(^{3}He,^{3}He')^{15}N$ reaction where the mirror level at 6.33 MeV is also strongly populated and has a characteristic L = 2 angular distribution, whereas the weaker level observed at 9.17 MeV does not have a well-defined angular distribution. The strong transition observed in ^{15}N at 9.79 MeV does have an L = 2 angular distribution (see Fig. 23) and corresponds to the population of the 5/2- and 7/2- levels at 9.76 and 9.83 MeV, respectively.

A majority of the remaining levels which are observed in these reactions correspond to positive parity states which are populated by promoting a p nucleon to the s-d shell. The spins of the low-lying positive parity states below 8.7 MeV can be explained by simple j-j configurations[57,61] (see Table VI); the validity of this model will be discussed further later.

V. A MICROSCOPIC DESCRIPTION OF THE (^{3}He,t) AND (^{3}He,^{3}He') REACTIONS

The success of a microscopic description of inelastic and charge-exchange scattering depends to a large extent upon the availability of nuclear wave functions which adequately describe the system. Among the levels which are populated in these (^{3}He,t) and (^{3}He,^{3}He') reactions, those which correspond to p shell states have been the subject of many experimental and theoretical investigations. Several intermediate-coupling shell-model calculations have been performed[64] which were successful in predicting many nuclear properties in addition to excitation energies. The recent effective-interaction calculations of Cohen and Kurath,[19] for example, were able to predict magnetic dipole moments, Gamow-Teller beta decays and M1 gamma transition rates.

The wave functions obtained from these calculations (denoted CK) were used to calculate nuclear structure factors G(JSLT) for the (^{3}He,t) and (^{3}He,^{3}He') reactions. The ability of the microscopic model to predict the shapes and relative magnitudes of the angular distributions for these transitions should provide a reliable test of the reaction mechanism and the applicability of a central two-body interaction. In addition, the measurement of (^{3}He,t) and (^{3}He,^{3}He') data allows us to obtain strengths for all four terms in the effective interaction simultaneously in the same series of experiments.

In order to carry out a microscopic analysis for other single-particle transitions, simple j-j configurations were assumed for the levels which were populated by promoting a p 1/2 nucleon to the s 1/2 or d 5/2 shell. Shell-model calculations indicate that this is a reasonably good approximation for the levels in A = 14[56] and A = 15[61] nuclei. For comparison, p shell transitions were also analyzed using simple j-j wave functions.

The theoretical calculations described in this work were carried out using a slightly modified version of the program DRC which has been described elsewhere.[65] This program calculates the quantity $\sigma(j_1 j_2 L\theta)$ which was defined in Eq. (12). Before a meaningful comparison with experiment could be made, it was necessary to investigate the effects of various parameters and approximations on the shapes and relative magnitudes of the

predicted angular distributions. In particular, optical model parameters, nuclear structure factors, binding energies and bound-state wave functions, range effects, and nonlocal potentials will now be discussed in detail.

A. Theoretical Calculations

1. Optical Model Parameters

The optical model parameters used in generating the distorted waves were obtained by fitting[66] the ^{3}He scattering data which was measured simultaneously in these experiments. Optical model parameters for tritons were assumed to be the same as those for ^{3}He particles. The general form of the optical potential used was

$$U(r) = U_c(r) - V_o(1+e^x)^{-1} - i\, W_o(1+e^{x'})^{-1} \quad , \qquad (19)$$

where

$$x = (r-r_o\, A^{1/3})/a \quad , \quad x' = (r-r_g\, A^{1/3})/b \ ,$$

and U_c is the Coulomb potential between a light particle of point-charge and a uniformly charged sphere.

The parameters obtained in this analysis are summarized in Table VII; typical fits are shown in Fig. 24. With the exception of ^{12}C (the difficulty in fitting elastic scattering data from this nucleus is well known[53,67-69] and will be discussed later) the sets of parameters obtained for each nucleus are almost identical and resemble the ^{3}He potentials for scattering from heavier nuclei.[70]

Unfortunately, when these parameters were used in theoretical calcultions they were unable to give reasonable fits for the (^{3}He,t) p1/2, p3/2→p1/2 dominant L = 0 transitions. In particular, the DWBA predictions were unable to reproduce the strong minima observed near $\theta_{c.m.} \cong 35$-45 degrees for dominant L = 0 transition with small negative Q values.

Table VII. Optical model potentials.

Potential	Channel	Energy (MeV)	V_o (MeV)	r_o (F)	a (F)	W_o (MeV)	r_g (F)	b (F)	r_c (F)
A[a]	$^{15}N+^{3}He$	39.8	160.0	1.23	.595	12.44	1.80	.858	1.3
B[a]	$^{14}N+^{3}He$	44.6	160.0	1.29	.565	11.37	1.78	.811	1.3
C[a]	$^{14}C+^{3}He$	44.8	160.0	1.31	.569	12.58	1.82	.795	1.3
D[a]	$^{13}C+^{3}He$	39.6	160.0	1.31	.565	14.86	1.73	.826	1.3
X[a]	Average set		160.0	1.29	.574	12.82	1.78	.822	1.3
E	$^{12}C+^{3}He$	49.8	160.0	1.40	.572	20.31	1.70	.537	1.3
F[b]	$^{12}C+^{3}He$	49.8	160.0	1.39	.542	12.58[c]	1.96	.571	1.3
M	$^{14}N+\alpha$[d]	40.5	195.0	1.28	.654	21.00	1.28	.654	1.3
V1[e]	$^{12}C+p$	46.3	41.5	1.143	.643	9.7	1.143	.643	1.2

[a]In order to fit the reaction data these potentials were modified by setting $r_o' = 0.93\ r_o$.

[b]This potential set was used in calculating the theoretical angular distributions for transitions leading to states in ^{12}C and ^{12}N.

[c]W_o was fixed at 12.58 MeV.

[d]Data obtained by Harvey et al.[62]

[e]Optical potential set obtained from Ref. 67.

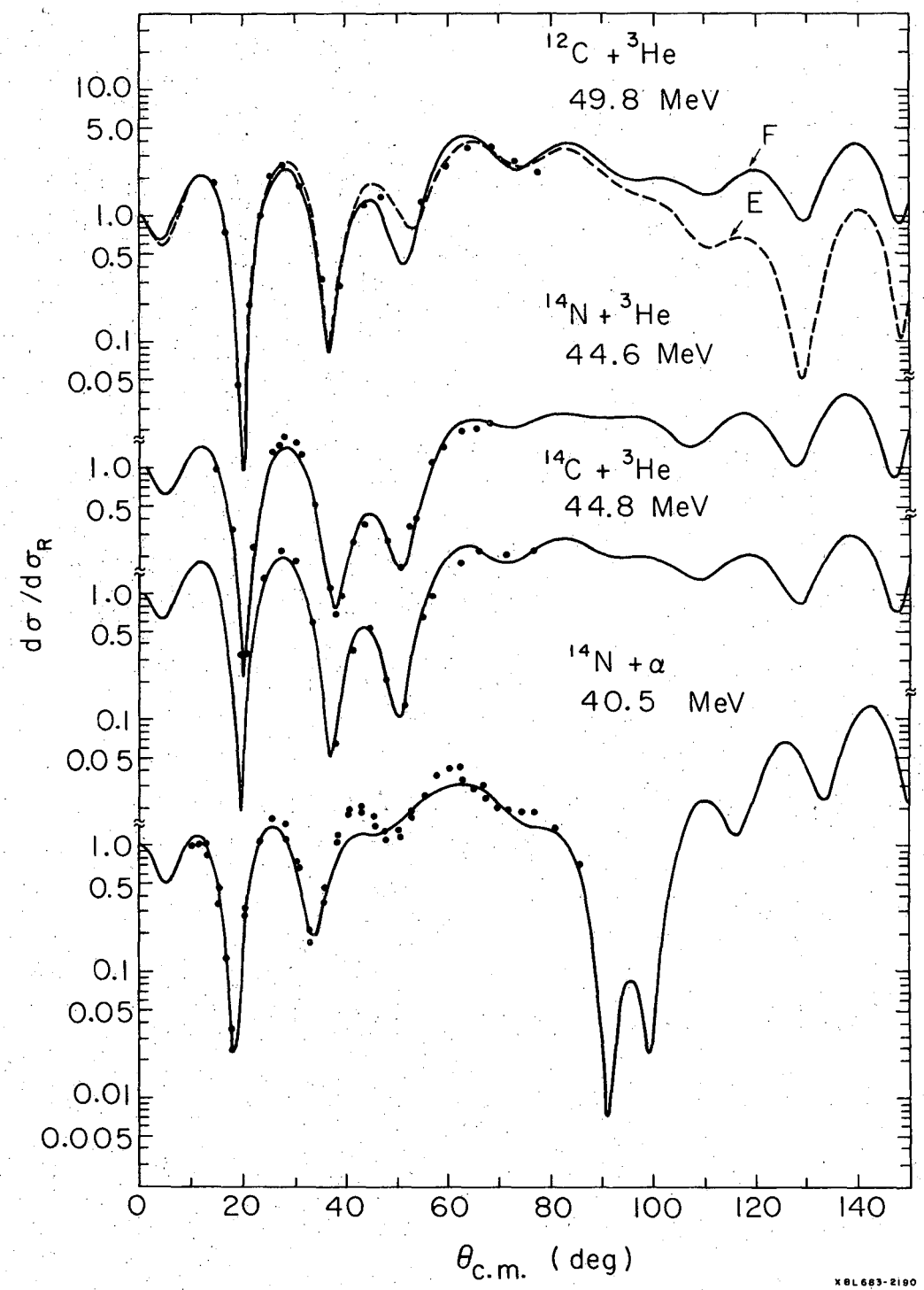

Fig. 24. Typical optical model fits obtained for the elastic scattering of ^{3}He and α particles from 1p shell nuclei using the parameters given in Table VII.

Identical results were obtained for several parameter sets in the same family with real well depths which varied from 160 to 200 MeV. Further investigation showed, however, that the predicted shape of these L = 0 transitions was very sensitive to small changes in the real radius, and good fits could be obtained if this parameter was decreased by ~7%. The ^{3}He(t) optical model parameters shown in Table VII, modified by setting $r'_o = 0.93\ r_o$, were used in calculating the theoretical angular distributions for all transitions observed in the A = 13-15 nuclei. Furthermore, since the energy dependence of the optical potentials for ^{3}He particles is known to be weak,[70] these parameters were assumed to be the same independent of the excitation energy of the final state. In Fig. 25 the theoretical angular distributions shown for several shell-model transitions illustrate that a small decrease in r_o does not strongly affect the magnitude of these transitions (i.e., the integrated cross sections differ by < 10%) and with the exception of the p1/2→p1/2, L = 0 and p1/2→d5/2, L = 1 (S = 1) transitions, it has very little effect on the predicted shapes of these angular distributions. However, the deep minimum which is now predicted for the ^{14}C(^{3}He,t)^{14}N (2.31 MeV, 0+) L = 0 transition at $\theta_{c.m.} \cong 35$ deg is in good agreement with the experimental data (compare Figs. 16 and 25).

Very few examples of pure or dominant p1/2→d5/2, L = 1 (S = 1) transitions were observed in these data. In general these states were either weakly populated or poorly resolved and therefore the quality of the fits for these transitions was not used as a criterion in determining optical model parameters (poor fits were obtained using either the modified or unmodified optical potentials; these results will be discussed later in Sec. VB).

a. <u>^{3}He scattering from ^{12}C.</u> Difficulties in fitting elastic proton[67] and ^{3}He[69] scattering data for ^{12}C have been reported elsewhere. In this analysis the major difference between the optical model parameters obtained for ^{12}C and those obtained for other p shell nuclei is the large imaginary depth W_o which was required in order to give the best fit (potential set E) to the elastic scattering data (see Table VII). Although there is known to be a strong coupling between the ground and first excited 2+ state of ^{12}C, an analysis using coupled equations for the scattering of

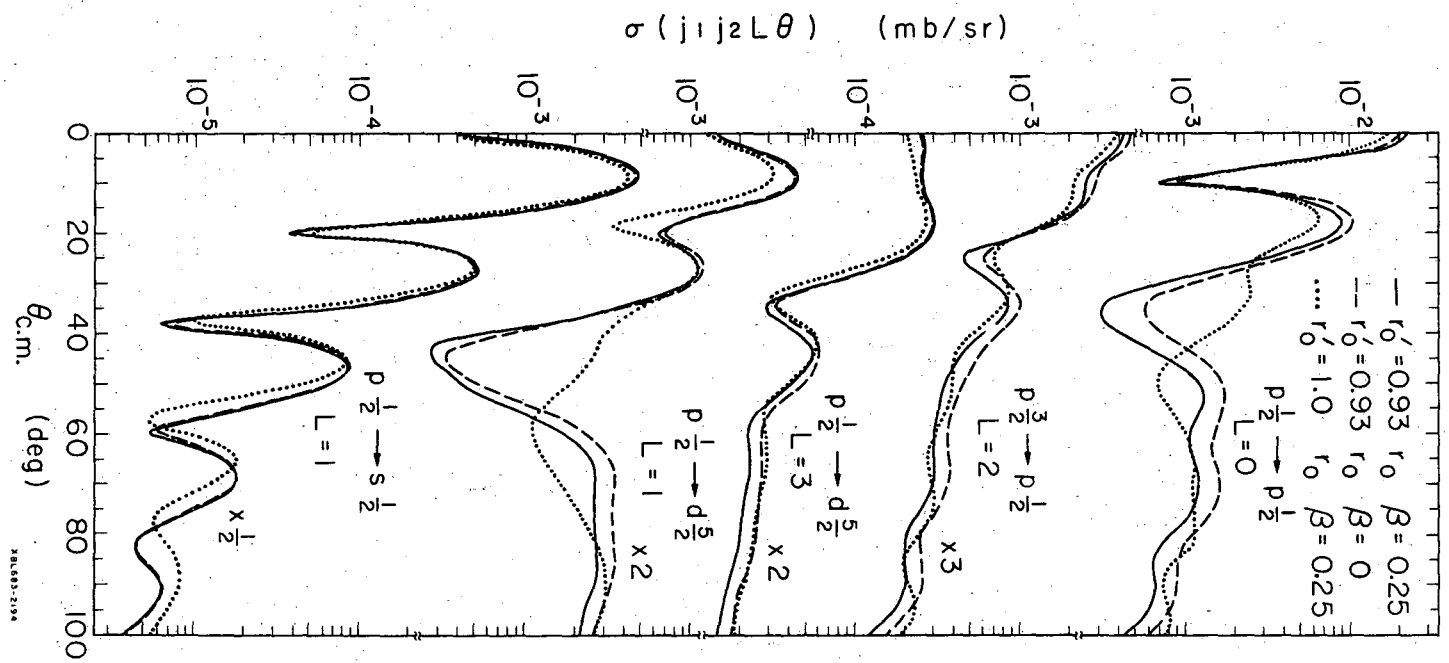

Fig. 25. Single-particle cross sections $\sigma(j_1 j_2 L\theta)$ for typical p1/2→p1/2, L = 0 [i.e., $^{14}C(^3He,t)^{14}N$ (2.31 MeV,0+)]; p3/2→p1/2, L = 2 [i.e., $^{14}N(^3He,^3He')^{14}N$ (3.95 MeV,1+)]; p1/2→d5/2, L = 3 [i.e., $^{15}N(^3He,^3He')^{15}N$ (7.56 MeV,7/2+)]; p1/2→d5/2, L = 1 [i.e., $^{14}N(^3He,t)^{14}O$ (6.28 MeV,(3-))]; and p1/2→s1/2, L = 1 [i.e., $^{13}C(^3He,^3He')^{13}C$ (3.09 MeV,1/2+)] transitions calculated using: 1) modified ($r_o' = 0.93\ r_o$) optical potentials (see Table VII) with a nonlocality range β=0.25 and β=0 and 2) unmodified ($r_o' = r_o$) optical potentials with a nonlocality range β=0.25.

46 MeV protons from ^{12}C indicated that the coupling effects produce only minor changes in the observed optical potential.[67] The large difference in W_o required to fit the ^3He scattering data for ^{12}C seems unreasonable particularly in view of the above evidence.

If W_o is fixed at 12.58 MeV the potential set F is obtained. This potential set is similar to those obtained for other nuclei and the fit to the elastic data is almost as good as the one obtained using the best fit parameter set E (compare Fig. 24). In particular, the curves which are obtained using these two parameter sets only differ significantly for $\theta_{c.m.} = \geq 100$ deg and therefore the present data are unable to distinguish between them. However, since the strengths of the imaginary potentials differ by almost a factor of two, the magnitudes of the theoretical angular distributions calculated using potential sets E and F were very different. In particular, although the shapes of the computed distributions were almost identical for both potential sets, the magnitudes for all transitions were almost twice as large using the potential set F.

Further, it was observed that the experimental L = 0 transitions leading to states in $^{12}C(^{12}N)$ were best fit using unmodified optical potentials (i.e., no change in r_o). This may be due to the fact that the observed L = 0 transitions in $^{12}C(^{12}N)$ have large negative Q values compared with those of the other nuclei. The unmodified potential set F was finally chosen in calculating the angular distributions which are compared with experiment in Sec. VB.

b. <u>Average optical potentials.</u> The difficulties encountered in obtaining a consistent optical potential set for ^{12}C suggest that possibly the search routine was also unable to obtain "true" optical model parameters for other 1p shell nuclei. If the inaccuracies introduced in this way primarily affect the magnitude of the calculated theoretical angular distributions, then these independent optical parameter sets can be used to predict the shapes of the experimental angular distribution. However, since the optical model parameters are not expected to vary greatly from one nucleus to another, an average optical potential set could be used for all nuclei in order to make a better comparison of the strengths for V_{ST} obtained from fitting different levels in different nuclei.

In the present analysis, the theoretical angular distributions which are compared with experiment were computed using the independent optical potential sets. However, the effect of using an average potential set was also investigated in the following manner. The potential set X was constructed by averaging the values of the parameters for the potential sets A, B, C and D (compare Table VII). When several representative transitions calculated using this potential set were compared with those predicted using independent optical parameters, it was found that only the magnitudes were affected (compare Fig. 26). In addition, the cross sections for different single-particle transitions were all changed by a similar amount in a given nucleus. As a result it was possible, without actually carrying out a complete analysis, to obtain average correction factors which could be applied to all values of V_{ST} obtained from a given target nucleus. These correction factors were 0.87, 0.89, 0.98, 1.19 and 0.98 for ^{12}C, ^{13}C, ^{14}C, ^{14}N, and ^{15}N, respectively. It will be shown in Sec. VB that in several cases the values of V_{ST} which were corrected in this manner were in somewhat better relative agreement than those obtained from the independent optical potentials.

2. Nuclear Structure Factors

The nuclear structure factors $G^2(JSLT)$ summarized in Tables VIII-XIII were computed using the relationships given in Sec. II. Spectroscopic factors $\mathcal{S}(JJ_iJ_f;TT_iT_f;j_1j_2)$ defined in Eq. (16) were calculated for p shell states using coefficients of fractional parentage obtained from the wave functions of Cohen and Kurath;[21,71] j-j coupling structure factors were also computed for p shell states in order to compare with the predictions of CK. (For certain transitions in mass 14, nuclear structure factors were also calculated using the intermediate-coupling wave functions of Visscher and Ferrell (VF)[72]).

Simple shell-model configurations consisting of an $(s1/2)^4(p3/2)^8$ core plus an s1/2 or d5/2 nucleon for A = 13 nuclei, a $(p1/2,s1/2)_{0-,1-;T=0,1}$ or $(p1/2,d5/2)_{2-,3-;T=0,1}$ configuration for A = 14 nuclei and a $[(p1/2)^2_0,s1/2]_{1/2+;T=1/2,3/2}$, $[(p1/2)^2_0,d5/2]_{5/2+;T=1/2,3/2}$

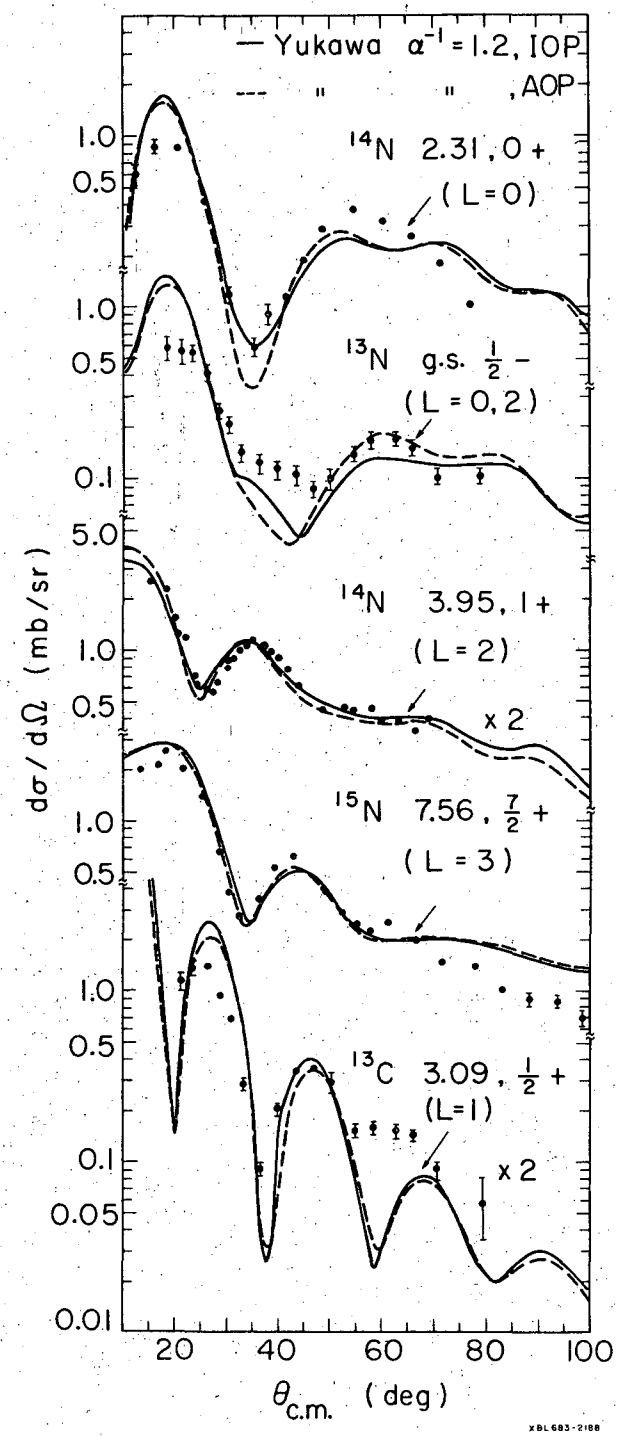

Fig. 26. DWBA predictions for representative (^{3}He,t) [i.e., ^{14}N 2.31-MeV, 0+; and ^{13}N g.s., 1/2-] and (^{3}He,^{3}He') [i.e., ^{14}N 3.95-MeV, 1+; ^{15}N 7.56-MeV, 7/2+; and ^{13}C 3.09-MeV, 1/2+] transitions obtained using: 1) the independent optical potentials IOP and 2) the average optical potential AOP (see Table VII). The curves have been normalized to give the best overall fit to the experimental data.

Table VIII. Nuclear structure factors $G^2(JSLT)$ for the states in mass 12.

Reaction	Energy (MeV)	J^{π},T	Dominant Single-Particle Transition	JSLT	$G^2(JSLT)$ Pure (jj)	$G^2(JSLT)$ Mixed (CK)
$^{12}C(^3He,^3He')^{12}C$	4.43	2+,0	p3/2→p1/2	2020	18.0	44.5
				2120	3.0	0.197
	12.71	1+,0	p3/2→p1/2	1120	0.333	0.0173
				1100	2.667	0.416
	15.11	1+,1	p3/2→p1/2	1121	0.333	0.0664
				1101	2.667	0.461
	16.11	2+,1	p3/2→p1/2	2021	2.0	1.074
				2121	3.0	0.960
$^{12}C(^3He,t)^{12}N$	0.0	1+,1	p3/2→p1/2	1121	0.667	0.133
				1101	5.333	0.922
	0.96	2+,1	p3/2→p1/2	2021	4.0	2.148
				2121	6.0	1.920

Table IX. Nuclear structure factors G^2(JSLT) for states in mass 13.

J^{π},T	Energy (MeV) ^{13}C	Energy (MeV) ^{13}N	Dominant Single-Particle Transition	JSLT	G^2(JSLT) $^{13}C(^3He,^3He')^{13}C$ Pure (jj)	G^2(JSLT) $^{13}C(^3He,^3He')^{13}C$ Mixed (CK)	G^2(JSLT) $^{13}C(^3He,t)^{13}N$ Pure (jj)	G^2(JSLT) $^{13}C(^3He,t)^{13}N$ Mixed (CK)
1/2-,1/2	0.0	0.0	p1/2→ p1/2	1121	-	-	2.667	1.895
				1101	-	-	0.333	0.322
				0001	-	-	1.000	1.000
1/2+,1/2	3.09	2.37	p1/2→ s1/2	1010	2.250		-	
				1011	0.250*		1.000	
				1110	0.500		-	
				1111	0.500		2.000	
				0110	0.250		-	
				0111	0.250		1.000	
3/2-,1/2	3.68	3.51	p3/2→ p1/2	2020	6.750	12.18	-	-
				2021	0.0833*	0.0453	0.333	0.181
				2120	1.125	0.644	-	-
				2121	0.125	0.164	0.500	0.656
				1120	0.125	0.0425	-	-
				1121	0.0139	0.0520	0.0555	0.208
				1100	1.000	0.507	-	-
				1101	0.111	0.594	0.444	2.374
5/2+,1/2	3.85	3.56	p1/2→ d5/2	3030	6.750		-	
				3031	0.750*		3.000	
				3130	1.000		-	
				3131	1.000		4.000	
				2130	0.050		-	
				2131	0.050		0.200	
				2110	1.200		-	
				2111	1.200		4.800	

Table IX. (continued)

J^{π},T	Energy (MeV) ^{13}C	Energy (MeV) ^{13}N	Dominant Single-Particle Transition	JSLT	G^2(JSLT) $^{13}C(^3He,^3He')^{13}C$ Pure (jj)	G^2(JSLT) $^{13}C(^3He,^3He')^{13}C$ Mixed (CK)	G^2(JSLT) $^{13}C(^3He,t)^{13}N$ Pure (jj)	G^2(JSLT) $^{13}C(^3He,t)^{13}N$ Mixed (CK)
5/2-,1/2	7.55	7.39	p3/2→p1/2	3120	-	0.00033	-	-
				3121	-	0.00611*	-	0.0244
				2020	5.40	11.68	-	-
				2021	0.600	0.517	2.40	2.062
				2120	0.900	0.0771	-	-
				2121	0.900*	0.486*	3.60	1.938
1/2-,1/2	8.86	8.92	p3/2→p1/2	1120	0.056	0.00241	-	-
				1121	0.056*	0.0253*	0.222	0.101
				1100	0.444	0.111	-	-
				1101	0.444*	0.147*	1.778	0.59
				0000	-	0.000	-	-
				0001	-	0.000	-	0.000
3/2-,1/2	11.84	11.85	p3/2→p1/2	2020	1.35	0.00738	-	-
				2021	0.150	0.137*	0.600	0.549
				2120	0.225	0.00245	-	-
				2121	0.225*	0.173	0.900	0.691
				1120	0.070	0.040	-	-
				1121	0.070*	0.0143*	0.278	0.0571
				1100	0.555	0.391	-	-
				1101	0.555*	0.0793*	2.222	0.318
3/2-,3/2	15.11	15.07	p3/2→p1/2	2021	0.667	0.593	0.667	0.593
				2121	1.000	0.636	1.000	0.636
				1121	0.111	0.045	0.111	0.045
				1101	0.889	0.316	0.889	0.316

*G(JSL1) and G(JSLO) have opposite signs for a given JSL.

Table X. Nuclear structure factors G^2(JSLT) for the $^{14}C(^3He,t)^{14}N$ reaction.

Energy (MeV)	J^π,T	Dominant Single-Particle Transition	JSLT	G^2(JSLT) Pure (jj)	Mixed (CK)	Mixed (VF)
0	1+,0	p1/2→ p1/2	1121	5.333	4.92	5.26
			1101	0.667	0.142	0.0000
2.31	0+,1	p1/2→ p1/2	0001	2.00	2.00	2.00
3.95	1+,0	p3/2→ p1/2	1121	0.333	0.0446	0.0450
			1101	2.667	4.80	4.205
4.91	0-,0	p3/2→ s1/2	0111	1.00		
5.10	2-,0	p1/2→ d5/2	2131	0.200		
			2111	4.80		
5.69	1-,0	p1/2→ s1/2	1011	1.00		
			1111	2.00		
5.83	3-,0	p1/2→ d5/2	3031	3.00		
			3131	4.00		
7.03	2+,0	p3/2→ p1/2	2021	2.00	0.789	1.252
			2121	3.00	4.32	3.94
9.17+10.43	2+,1	p3/2→ p1/2	2021	2.00	3.174	
			2121	3.00	1.133	
13.72	1+,1	p3/2→ p1/2	1121	0.333	0.132	
			1101	2.667	1.05	
-	2+,1[a]	p1/2,p3/2→ p1/2,3/2	2021	-	0.0391	
			2121	-	0.0539	

[a]This level has the dominant shell-model configuration $(p3/2)^{-2}$; therefore it cannot be populated in the j-j limit.

Table XI. Nuclear structure factors G^2(JSLT) for the $^{14}N(^3He,t)^{14}O$ reaction.

Energy (MeV)	J^{π},T	Dominant Single-Particle Transition	JSLT	G^2(JSLT) Pure (jj)	Mixed (CK)	Mixed (VF)
0	0+ ,1	p1/2→ p1/2	1121	1.778	1.640	1.753
			1101	0.222	0.0473	0.000
5.17	(1-),1	p1/2→ s1/2	1011	0.667		
			1111	1.333		
			0111	1.000		
-	(0-),1	p1/2→ s1/2	1011	0.333		
			1111	0.667		
6.28	(3-),1	p1/2→ d5/2	3031	1.333		
			3131	1.778		
			2131	0.156		
			2111	3.733		
6.60+7.78	2+ ,1	p3/2→ p1/2	3121	-	0.0748	
			2021	1.00	0.538	
			2121	1.50	1.470	
			1121	0.278	0.478	
			1101	2.222	2.122	
6.79	(2-),1	p1/2→ d5/2	3031	1.667		
			3131	2.222		
			2131	0.045		
			2111	1.067		
(10.24 or 10.89)	(1+),1	p3/2→ p1/2	2021	1.00	1.216	
			2121	1.50	1.36	
			1121	0.0556	0.0233	
			1101	0.444	0.187	
-	2+ ,1[a]	p3/2→ p1/2	3121	-	0.0257	
			2021	-	0.144	
			2121	-	0.202	
			1121	-	0.0103	
			1101	-	0.0001	

[a]This level has the dominant shell-model configurations $(p3/2)^{-2}$; therefore it cannot be populated in the j-j limit.

Table XII. Nuclear structure factors G^2(JSLT) for the $^{14}N(^3He,^3He')^{14}N$ reaction.

Energy (MeV)	J^π,T	Dominant Single-Particle Transition	JSLT	G^2(JSLT) Pure (jj)	Mixed (CK)	Mixed (VF)
2.31	0+,1	p1/2→ p1/2	1121	0.889	0.818	0.877
			1101	0.111	0.0237	0.0000
3.95	1+,0	p3/2→ p1/2	2020	4.50	4.38	3.91
			2120	0.75	0.731	0.696
			1120	0.028	0.217	0.503
			1100	0.222	0.043	0.0232
			0000	-	0.0000	0.0000
4.91	0-,0	p1/2→ s1/2	1010	1.50		
			1110	0.333		
5.10	2-,0	p1/2→ d5/2	3030	7.50		
			3130	1.111		
			2130	0.022		
			2110	0.533		
5.69	1-,0	p1/2→ s1/2	1010	3.00		
			1110	0.667		
			0110	0.500		
5.83	3-,0	p1/2→ d5/2	3030	6.000		
			3130	0.889		
			2130	0.078		
			2110	1.865		
7.03	2+,0	p3/2→ p1/2	3120	-	0.0454	0.138
			2020	4.50	3.98	1.80
			2120	0.75	0.605	0.809
			1120	0.139	0.0404	0.0011
			1100	1.111	1.345	1.272

Table XIII. Nuclear structure factors G^2(JSLT) for states in mass 15.

J^{π},T	Energy (MeV) ^{15}N	Energy (MeV) ^{15}O	Dominant Single-Particle Transition	JSLT	G^2(JSLT) $^{15}N(^3He,^3He')^{15}N$ Pure (jj)	G^2(JSLT) $^{15}N(^3He,^3He')^{15}N$ Mixed (CK)	G^2(JSLT) $^{15}N(^3He,t)^{15}O$ Pure (jj)	G^2(JSLT) $^{15}N(^3He,t)^{15}O$ Mixed (CK)
1/2-,1/2	0.0	0.0	p1/2→ p1/2	1121	-	-	2.667	2.667
				1101	-	-	0.333	0.333
				0001	-	-	1.00	1.00
5/2+,1/2	5.27	5.24	p1/2→ d5/2	3030	10.125		-	
				3031	0.125		0.500	
				3130	1.500		-	
				3131	0.167*		0.667	
				2130	0.075		-	
				2131	0.00833*		0.033	
				2110	1.800		-	
				2111	0.200*		0.800	
1/2+,1/2	5.30	5.19	p1/2→ s1/2	1010	3.375		-	
				1011	0.0417		0.167	
				1110	0.750		-	
				1111	0.0833*		0.333	
				0110	0.375		-	
				0111	0.0417*		0.167	
3/2-,1/2	6.32	6.18	p3/2→ p1/2	2020	4.500	4.500	-	-
				2021	0.500	0.500	2.00	2.00
				2120	0.750	0.750	-	-
				2121	0.750*	0.750*	3.00	3.00
				1120	0.083	0.083	-	-
				1121	0.083*	0.083*	0.333	0.333
				1100	0.667	0.667	-	-
				1101	0.667*	0.667*	2.667	2.667

Table XIII. (continued)

J^{π},T	Energy (MeV) ^{15}N	Energy (MeV) ^{15}O	Dominant Single-Particle Transition	JSLT	G^2(JSLT) $^{15}N(^3He,^3He')^{15}N$ Pure (jj)	G^2(JSLT) $^{15}N(^3He,^3He')^{15}N$ Mixed (CK)	G^2(JSLT) $^{15}N(^3He,t)^{15}O$ Pure (jj)	G^2(JSLT) $^{15}N(^3He,t)^{15}O$ Mixed (CK)
5/2+,1/2	7.15	6.86	p1/2→ d5/2	3030	2.41		-	
				3031	0.268*		1.071	
				3130	0.357		-	
				3131	0.357		1.428	
				2130	0.0351		-	
				2131	0.0351		0.141	
				2110	0.840		-	
				2111	0.840		3.36	
3/2+,1/2	7.30	6.79	p1/2→ s1/2	1010	3.00		-	
				1011	0.333*		1.333	
				1110	0.667		-	
				1111	0.667		2.667	
7/2+,1/2	7.56	7.28	p1/2→ d5/2	3030	7.72		-	
				3031	0.857*		3.43	
				3130	1.142		-	
				3131	1.142		4.57	
1/2+,1/2	8.31	7.55	p1/2→ s1/2	1010	0.375		-	
				1011	0.042*		0.167	
				1110	0.0833		-	
				1111	0.0833		0.333	
				0110	0.375		-	
				0111	0.375		1.500	
3/2+,1/2	8.57	8.28	p1/2→ d5/2	2130	0.040		-	
				2131	0.040		0.161	
				2110	0.960		-	
				2111	0.960		3.839	

Table XIII. (continued)

J^{π},T	Energy (MeV) ^{15}N	Energy (MeV) ^{15}O	Dominant Single-Particle Transition	JSLT	G^2(JSLT) $^{15}N(^3He,^3He')^{15}N$ Pure (jj)	G^2(JSLT) $^{15}N(^3He,^3He')^{15}N$ Mixed (CK)	G^2(JSLT) $^{15}N(^3He,t)^{15}O$ Pure (jj)	G^2(JSLT) $^{15}N(^3He,t)^{15}O$ Mixed (CK)
1/2+,3/2	11.62	-	p1/2→ s1/2	1011	0.333		0.333	
				1111	0.667		0.667	
				0111	0.333		0.333	
5/2+,3/2	-	-	p1/2→ d5/2	3031	1.00		1.00	
				3131	1.333		1.333	
				2131	0.067		0.067	
				2111	1.600		1.600	

*G(JSL1) and G(JSL0) have opposite signs for a given JSL.

$[(p1/2)^2_1, s1/2]_{1/2+,3/2+;T=1/2}$ or $[(p1/2)^2_1, d5/2]_{3/2+,5/2+,7/2+;\ T=1/2}$ configuration for A = 15 nuclei were assumed for levels which were formed by promoting a p nucleon to the s-d shell. The shell-model calculations of True[56] for levels in ^{14}N and of Halbert and French[61] for levels in ^{15}N and ^{15}O indicate that this should be a reasonably good approximation since these levels only contain small admixtures of other configurations. For example, the wave functions for the $(p1/2,s1/2)_{0-,1-;T=0,1}$ and $(p1/2,d5/2)_{2-,3-;T=0,1}$ levels of ^{14}N (see Ref. 56), which have been reasonably successful in predicting gamma-ray transition rates,[73,74] only contain (p1/2,d3/2) admixtures of $\leq 4\%$.

3. Bound-State Wave Functions, Binding Energies and Radial Form Factors

As mentioned previously, in order to simplify the theoretical calculations only one radial form factor $g_L^{j_1 j_2}(R')$ was computed corresponding to the dominant shell-model transition in the j-j limit (this resulted in Eq. (11)). Single-particle radial wave functions were calculated using a Woods-Saxon well with a radius of $1.25A^{1/3}$F, a diffuseness of a = 0.65 F, and a spin-orbit coupling of 25 times the Thomas term; a Coulomb potential with a radius of $1.25A^{1/3}$F was also included. The well depths were adjusted to give the binding energies computed from the separation energy scheme illustrated in Fig. 27. If this method is used, a definite relationship exists between the binding energies $EB_{1,2}$ of the particle in its initial j_1 and final j_2 states given by $EB_2 = EB_1 + Q(p,n)$ for the $(^3He,t)$ reaction and $EB_2 = EB_1 + Q(p,p')$ for the $(^3He,{}^3He')$ reaction.

In order to determine absolute values for $EB_{1,2}$ it is necessary to know: 1) whether neutrons or protons (or both) are excited to form the final state and 2) the parent state is the (A-1) nucleus which has the dominant configuration of the inactive (A-1) core of the target nucleus. In general, for p1/2→ d5/2, p1/2→ s1/2 and p1/2→ p1/2 transitions, in the j-j limit, the parent state corresponds to the ground state configuration of the (A-1) nucleus and therefore EB_1 is simply equal to the neutron or proton binding energy of the target nucleus. The transitions to levels in $^{15}N(^{15}O)$ with the configuration $(p1/2)^2_0 d5/2$ or $(p1/2)^2_0 s1/2$ are exceptions to this rule (see Fig. 27). (When this method gave negative values for EB_2, the nucleon in its final state was assumed for convenience to be bound by 400 keV.)

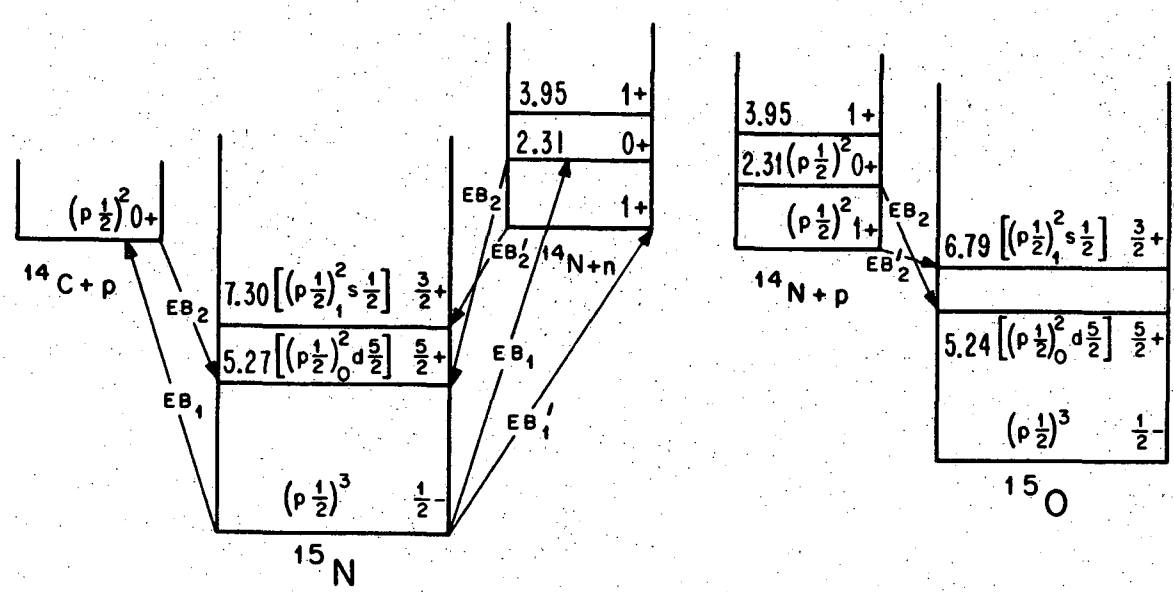

XBL685-2690

Fig. 27. The separation energy scheme used to determine the binding energies of the target nucleons involved in typical single-particle transitions (i.e., the $^{15}N(^3He,^3He')^{15}N$ (5.27 MeV,5/2+) and $^{15}N(^3He,t)^{15}O$ (5.24 MeV,5/2+) p1/2→ d5/2; and the $^{15}N(^3He,^3He')^{15}N$ (7.30 MeV,3/2+) and $^{15}N(^3He,t)^{15}O$ (6.79 MeV,3/2+) p1/2→ s1/2 transitions). $EB_1(EB_1')$ represents the binding energy of the p1/2 nucleon in its initial j_1 state while $EB_2(EB_2')$ represents the binding energy of the d5/2(s1/2) nucleon in its final j_2 state.

For p3/2→p1/2 transitions, the removal of a p3/2 neutron or proton (in the j-j limit) does not always overlap with the ground state configuration of the (A-1) nucleus but instead may have large coefficients of fractional parentage for several excited states. In this case the radial form factor should in principle be the sum of several radial form factors $g_L^{j_1 j_2}(R')$, each calculated using bound-state wave functions which were computed for separation energies corresponding to excited states in the (A-1) nucleus. If configuration-mixed wave functions are used for p shell states the situation becomes even more complex since p1/2,p3/2→p3/2 transitions also contribute to the population of a given final state. In the present analysis, when several excited states in the (A-1) nucleus were involved, in the j-j limit, (i.e., for p3/2→p1/2 transitions in mass 13 [(^{3}He,t) reaction only], 14 and 15 nuclei) the binding energy EB_1 was chosen to be equal to the neutron or proton binding energy of the target nucleus plus the excitation energy of the final state in the product nucleus. The validity of this approximation for p shell states depends upon the sensitivity of the predicted angular distributions to changes in the binding energies of the single-particle wave functions. In Fig. 28, integrated theoretical cross sections are plotted as a function of EB_1 (the definite relationship between EB_1 and EB_2 is still maintained) for several different single-particle transitions. In general it was found that both the shapes and magnitudes of the predicted distributions for L = 0 and L = 2 p-shell transitions were relatively insensitive to moderate changes in the binding energy EB_1.

One additional assumption was made in calculating the radial form factors for inelastic transitions where the excitation of protons and neutrons both contribute, as is the case for transitions in ^{12}C, ^{14}N, and ^{15}N (i.e., the 5.27 MeV, 5/2+ and 5.30 MeV, 1/2+ levels only). Since the neutron and proton binding energies are approximately equal for these nuclei, the radial form factors were computed assuming that the bound particles were protons. In ^{14}N calculations assuming that neutrons were excited gave almost identical angular distributions which differed in magnitude by < 5%. (The inelastic transition to the 3.68 MeV 3/2- level

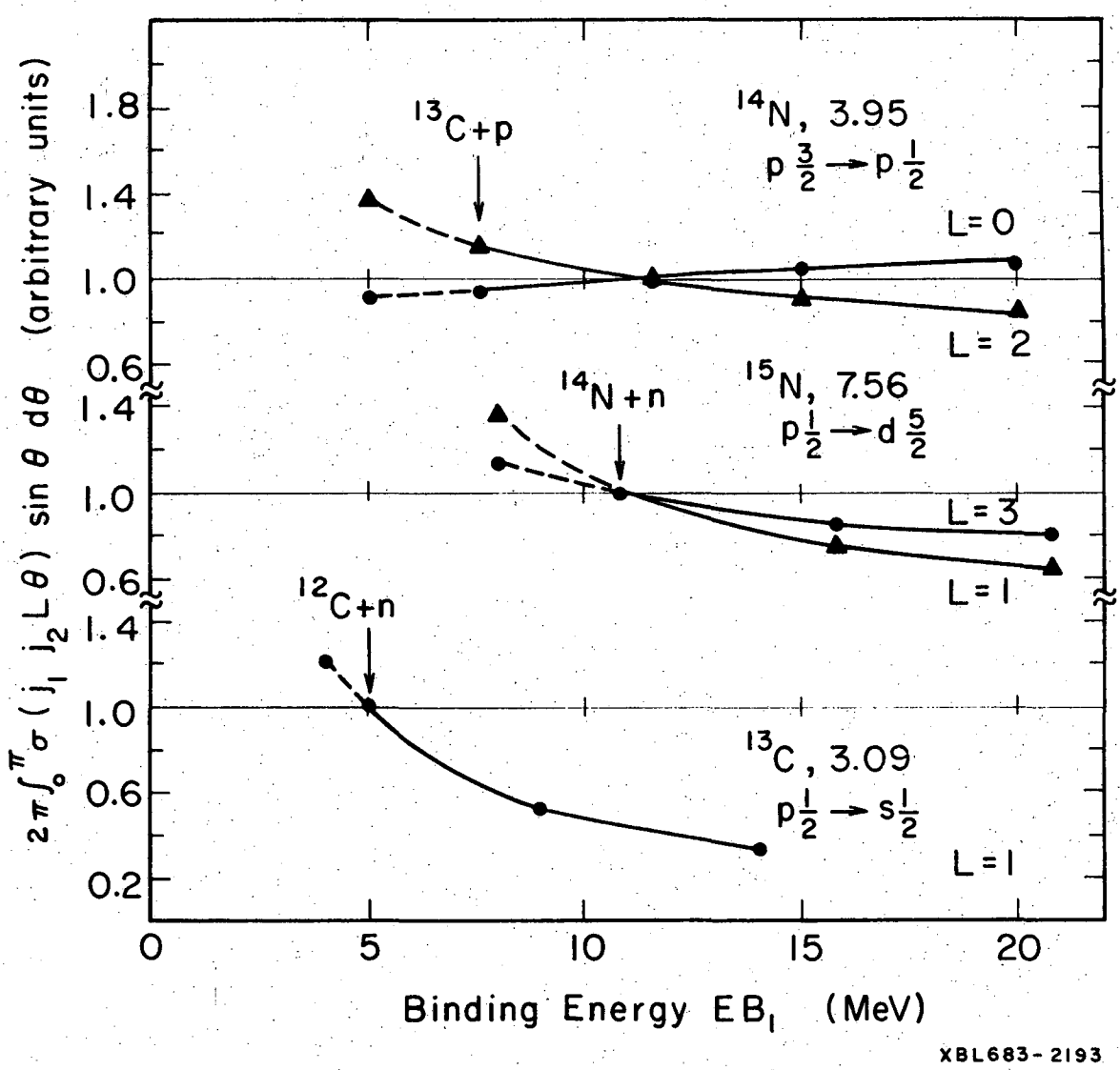

Fig. 28. Integrated single-particle cross sections as a function of the binding energy EB_1 (the fixed relationship between EB_1 and EB_2 was maintained) for several representative single-particle transitions. The cross sections have been normalized relative to those obtained using the binding energies predicted by the separation energy scheme described in Sec. VA-3.

in ^{13}C also involves both proton and neutron excitations. However, since the neutron and proton binding energies of ^{13}C differ by 12.586 MeV, the theoretical angular distribution for this transition was computed by averaging those calculated assuming that either protons or neutrons were excited.)

Typical radial form factors $g_L^{j_1 j_2}(R')$ are shown in Fig. 29 for a Yukawa interaction with $\alpha^{-1} = 1.2$ F. They exhibit a variety of shapes, including changes in sign, depending upon the single-particle wave functions involved.

4. Range Effects of a Yukawa Interaction

The theoretical angular distributions of different single-particle transitions and L transfers are shown in Fig. 30 for various ranges of the effective Yukawa interaction between 0.5 and 1.6 F. The predicted differential cross sections have been multiplied by α^6 in order to compare the strengths of different multipole transitions as a function of the range of the interaction (see Eq. (7)). It can be seen from Fig. 30 that the range of the interaction has two general effects on the predicted cross sections. First of all, the angular distributions have more structure and decrease more rapidly with increasing angle as the range is increased. Secondly, the strength of the higher multipole transitions is very sensitive to the range of the interaction. For example, in Fig. 30, the strength of the ^{14}N, 2.31 MeV (L = 0) transition varies by ± 10% between $\alpha^{-1} = 0.5$ and 1.6 F while the strength of the ^{14}N, 3.95 MeV (L = 2) transition decreases by a factor of five. Similar effects were also observed in an analysis of the $^{90}Zr(p,p')^{90}Zr$ reaction.[7]

A range of $\alpha^{-1} = 1.2$ F was finally chosen for the effective projectile-nucleon interaction since it gave the best overall fit to the experimental angular distributions observed for all L transfers. In order to compare the values of $\overline{V}_{ST}$ which were measured in these experiments with those obtained from analyses of the (p,p') and (p,n) reactions at $\alpha^{-1} = 1.0$ F, it is first necessary to convert the values of $\overline{V}_{ST}$ from an effective projectile-nucleon to an effective nucleon-nucleon interaction using Eq. (8). Equation (7) must then be used to convert from a range of

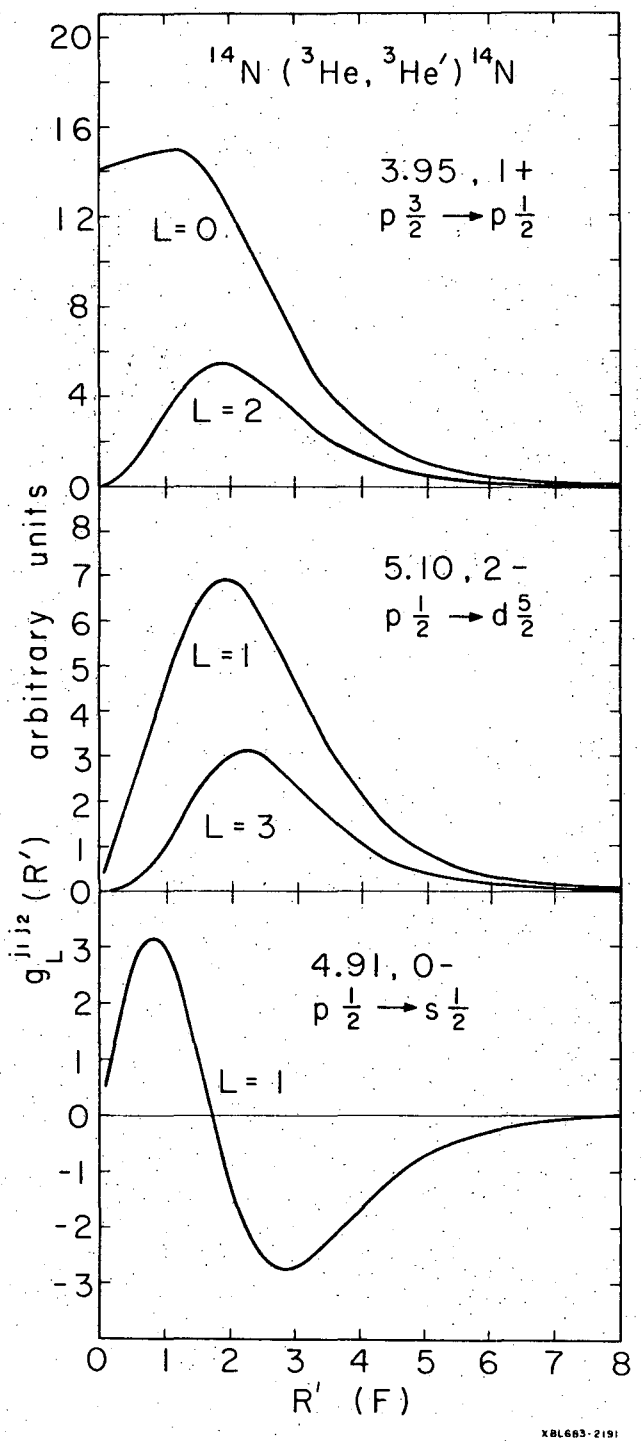

Fig. 29. Typical radial form factors $g_L^{j_1 j_2}(R')$ for various single-particle transitions observed in the $^{14}N(^3He,^3He')^{14}N$ reaction calculated using a Yukawa interaction with a range of α^{-1} = 1.2 F.

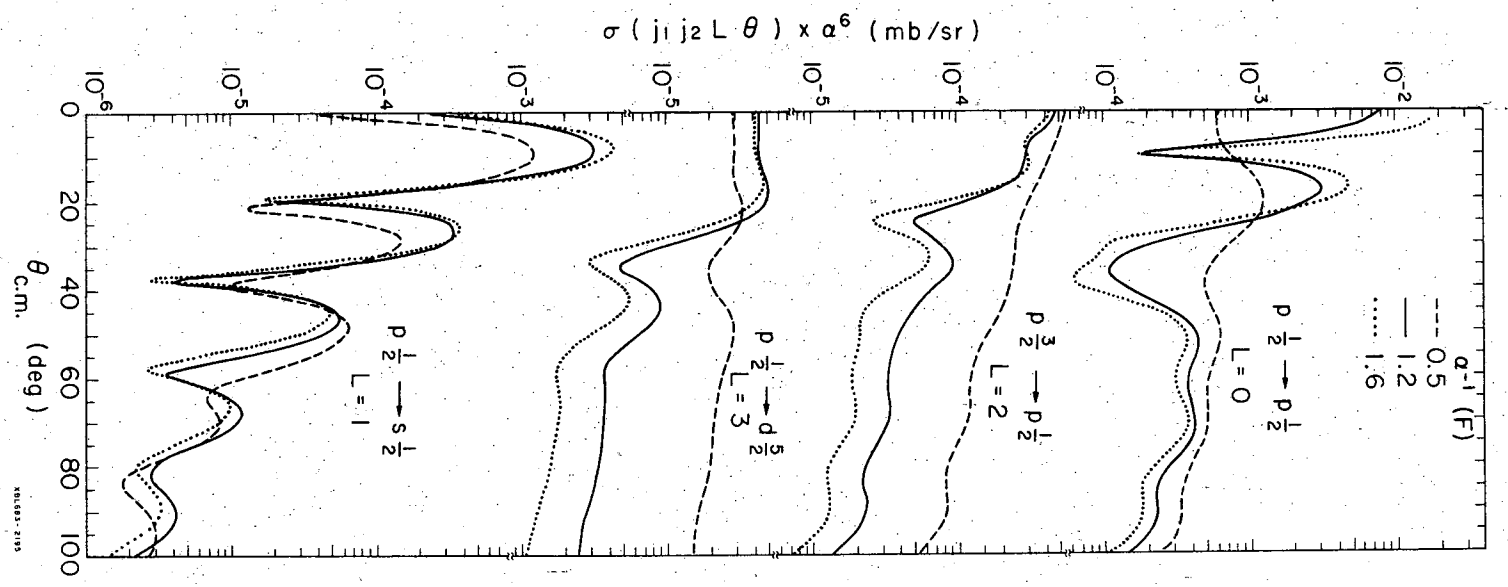

Fig. 30. Single-particle cross sections $\sigma(j_1 j_2 L\theta)$ for typical p1/2→ p1/2, L=0 [i.e., $^{14}C(^3He,t)^{14}N$ (2.31 MeV,0+)]; p1/2→ p3/2, L=2 [i.e., $^{14}N(^3He,^3He')^{14}N$ (3.95 MeV,1+)]; p1/2→ d5/2, L=3 [i.e., $^{15}N(^3He,^3He')^{15}N$ (7.56 MeV,7/2+)]; and p1/2→ s1/2, L=1 [i.e., $^{13}C(^3He,^3He')^{13}C$ (3.09 MeV,1/2+)] transitions calculated using three different ranges α^{-1} of the Yukawa interaction. All cross sections were computed using the independent optical potentials given in Table VII and have been multiplied by α^6 in order to compare the strength of a given single-particle transition (and L transfer) as a function of the range of the interaction.

1.2 to 1.0 F. The total conversion factors obtained for the (^{3}He,t) and (^{3}He,^{3}He') reactions were 1.18 and 1.10, respectively; all values quoted in this work have been converted in this manner.

5. Nonlocal Corrections

Since the optical-model and shell-model potential wells are known to be nonlocal, the wave functions calculated using an equivalent local potential should actually be reduced inside the nuclear surface.[75] This reduction can be produced using a damping factor obtained from the local energy approximation,[76]

$$G(r) = C[1-(\mu\beta^2/2\hbar^2)\ U(r)]^{-1/2} \quad , \qquad (20)$$

where μ is the reduced mass of the particle, β is the nonlocality range, $U(r)$ is the equivalent local potential and C is unity for scattering wave functions.

A nonlocal correction was included in this analysis for the ^{3}He and triton optical potentials only, using a nonlocality range of $\beta = 0.25$ F.[77] From Fig. 25 it can be seen that the nonlocal damping factor has very little effect on the shapes of the angular distributions but reduces the integrated cross sections for various single-particle transitions by 10 - 22% with the exception of the p1/2→ s1/2 transition which is reduced by only 1%.

B. Comparison with Experiment

In order to simplify the comparisons with experiment, the transitions observed in the (^{3}He,t) and (^{3}He,^{3}He') reactions will be discussed in groups according to the particular single-particle transition involved. Furthermore, transitions which deviate strongly from average behavior or transitions which give new spectroscopic information are discussed individually as the end of each section.

As mentioned previously, the theoretical curves which are compared with experiment were all calculated using independent optical potentials; however, strengths were obtained for both independent optical potentials and an average optical potential using the correction factors given in Sec. VA-1. The values quoted in this report will refer to those obtained from the average optical potential unless otherwise stated. In all cases, the theoretical curves were normalized to give the best overall fit to the experimental data; hence, independent values of V_{ST} were obtained for each transition. When two levels were unresolved experimentally, the theoretical angular distributions were computed by summing the contributions from each transition.

Since more than one term in the effective interaction usually contributed to the cross section of an individual transition, it was necessary to assume some relationship among the relative strengths of the individual terms in the effective interaction. Three different exchange mixtures - including the Wigner interaction (V_{00} only) and a Serber force - were used for (^{3}He,^{3}He') transitions, while V_{01} and V_{11} were generally assumed to be equal in the analysis of the (^{3}He,t) reaction; this will be discussed further later. It is important to mention once again that all strengths V_{ST} have been converted to an effective nucleon-nucleon interaction at α^{-1} = 1.0 F (see Sec. VA-4).

1. The (^{3}He,t) p1/2, p3/2→p1/2 Dominant L = 0 Transitions

Since the strengths of the higher multipole transitions decrease rapidly with increasing range (see Fig. 30), the ratio of the theoretical cross sections $\sigma(j_1 j_2 L\theta)$ for L = 0 : L = 2 transitions is ≅ 12:1 at a range

of α^{-1} = 1.2 F. As a result, most (^{3}He,t) transitions which are allowed by the selection rules to be L = 0 and/or 2 are predicted to be dominant L = 0 transitions. The 0+ ground state and the $(p3/2,p1/2)_{1+,T=1}$ levels in ^{14}O and the 1+ ground state of ^{14}N are the only exceptions to this rule; these levels all have L = 0 structure factors which are quite small.

As was mentioned previously, most of the dominant L = 0 transitions with small negative Q values have characteristic angular distributions which can only be reproduced using slightly modified optical potentials. The theoretical angular distributions for all L = 0 transitions are compared with experiment in Figs. 31 and 32; the solid curves were calculated using the mixed CK wave function. In general the fits to these angular distributions are reasonably good, particularly for those levels which have small negative Q values.

Dominant L = 0 transitions should provide the most accurate determination of the isospin V_{01} and spin-isospin V_{11} terms in the effective interaction. There are two reasons for this: First, many of these transitions - particularly the ground isobaric analog transitions - are very insensitive to configuration mixing. Secondly, L = 0 transitions are not expected to be enhanced by collective or core polarization effects.[9] Among the transitions which are observed in these experiments, five have been selected which should provide the best measurement of V_{01} and V_{11}; they are the g.s., 1/2- and 6.18 MeV, 3/2- levels in ^{15}O; the 2.31 MeV, 0+ and 3.95 MeV, 1+ levels in ^{14}N; and the g.s., 1/2- level in ^{13}N.

Three of these transitions are primarily (or only) dependent upon V_{01} while the other two are primarily (or only) dependent upon V_{11}. A ratio of $V_{11}/V_{01} \cong 0.8$ gave the best overall agreement for these transitions (compare Table XIV). This ratio was often used in subsequent calculations for other transitions and L transfers. However, when enhanced strengths were observed for V_{01} and V_{11}, the ratio predicted by the Serber force (V_{11}/V_{01} = 1.0) was used. In particular, for all pure L = 2 and all p1/2→ d5/2 transitions, V_{01} and V_{11} were assumed to be equal.

The values obtained for V_{01} and V_{11} from all L = 0 transitions are summarized in Table XIV. In general the overall agreement is reasonably good, while a slight improvement is observed using the average optical potential set. Furthermore, the average values for $V_{01} = 20.6 \pm 0.4$

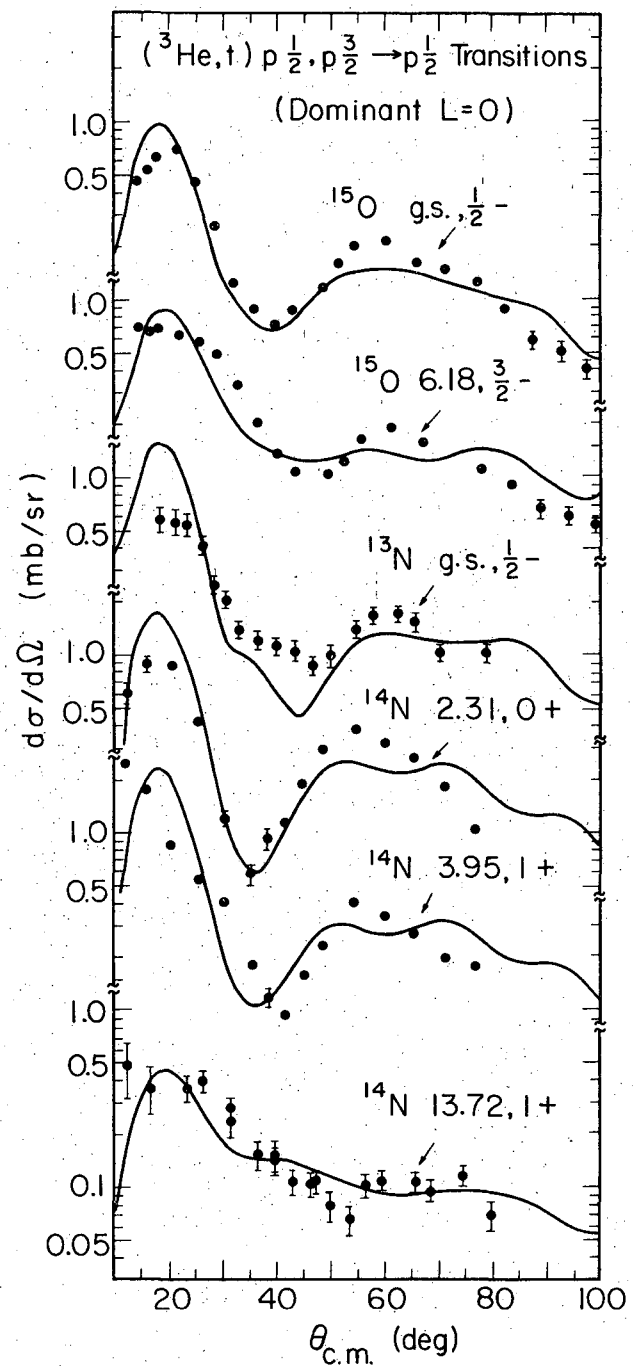

Fig. 31. Angular distributions for (^{3}He,t) p1/2,p3/2→ p1/2 (dominant L=0) transitions. The solid curves are DWBA predictions obtained using CK wave functions and the independent optical potentials given in Table VII.

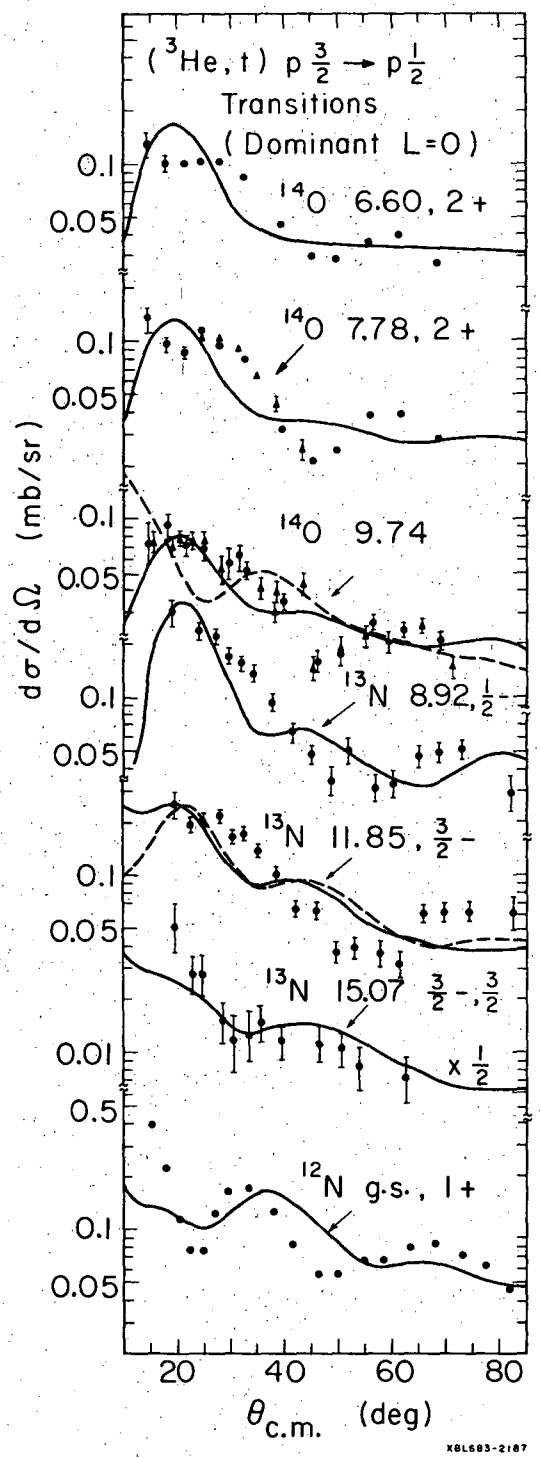

Fig. 32. Angular distributions for (^{3}He,t) p3/2→p1/2 (dominant L=0) transitions. The solid curves are DWBA predictions obtained using CK wave functions and the independent optical potentials given in Table VII. The dashed curve shown for the 9.74 MeV level in ^{14}O was calculated assuming that this level had the dominant configuration $(p3/2)^{-2}_{2+,T=1}$. The dashed curve shown for the 11.85 MeV level in ^{13}N was calculated using j-j wave functions.

Table XIV. Experimental strengths for the effective nucleon-nucleon interaction at α^{-1}=1.0 F obtained from (^{3}He, t) p 1/2, p 3/2 → p 1/2 (dominant L=0) transitions.

Reaction	Energy (MeV)	J^{π}, T	Independent Optical Potentials V_{01}(MeV) (jj)	V_{01} (CK)	V_{11}(MeV) (jj)	V_{11} (CK)	Average Optical Potential V_{01}(MeV) (jj)	V_{01} (CK)	V_{01} (VF)	V_{11}(MeV) (jj)	V_{11} (CK)	V_{11} (VF)
^{15}N(^{3}He, t)^{15}O	0.0	1/2-,1/2*	21.6	21.6	(17.3)[a]	(17.3)[a]	21.2	21.2		(17.0)[a]	(17.0)[a]	
	6.18	3/2-,1/2*	(22.2)	(22.2)	18.1	18.1	(21.7)	(21.7)		17.7	17.7	
^{14}C(^{3}He, t)^{14}N	2.31	0+ ,1 *	20.4	20.4	-	-	20.0	20.0	20.0	-	-	-
	3.95	1+ ,0 *	-	-	21.0	15.7	-	-	-	20.6	15.4	16.5
	13.72	1+ ,1	-	-	17.8	28.4	-	-		17.4	27.8	
^{14}N(^{3}He, t)^{14}O	6.60[b]	2+ ,1	(14.2)	(14.8)	11.3	11.8	(16.9)	(17.6)		13.4	14.0	-
	7.78[b]	2+ ,1	(13.8)	(14.4)	11.1	11.4	(16.4)	(17.1)		13.2	13.6	
	9.74[b]	(2+) ,1	c	67.6	c	67.6	c	80.5		c	80.5	
	6.60[d]	2+ ,1	(17.0)	(17.6)	13.6	14.2	(20.2)	(20.9)		16.2	16.9	
	7.78[d]	2+ ,1	(16.5)	(17.1)	13.2	13.7	(19.6)	(20.3)		15.7	16.3	
	9.74[d]	(2+) ,1	(16.9)	(17.6)	13.6	14.0	(20.1)	(20.9)		16.2	16.7	
^{13}C(^{3}He, t)^{13}N	0.0	1/2-,1/2*	22.6	23.3	(18.1)	(18.7)	20.1	20.7		(16.1)	(16.6)	
	3.51	3/2-,1/2 }	27.7	20.4	27.7	20.4	24.7	18.2		24.7	18.2	
	3.56[e†]	5/2+,1/2 }										
	8.92	1/2-,1/2	-	-	18.2	31.6	-	-		16.2	28.1	
	11.85	3/2-,1/2	(22.2)	(44.6)	19.7	44.6	(19.8)	(39.7)		17.5	39.7	
	15.07	3/2-,3/2	(21.4)	(31.0)	21.4	31.0	(19.0)	(27.6)		19.0	27.6	
^{12}C(^{3}He, t)^{12}N	0.0	1+ ,1	-	-	11.6	28.0	-	-		10.1	24.4	
			21.5±0.8	21.8+1.0	19.6±1.5	16.9±1.2	20.4±0.5	20.6±0.4		19.2±1.5	16.5±1.1	

[a] In some cases the calculated angular distributions are relatively insensitive to the values of either V_{01} or V_{11}. In these cases the strengths which are obtained are enclosed in brackets.

[b] The 6.60 and 7.78 MeV levels are assumed to have the configuration $[\frac{1}{\sqrt{2}}(p\ 3/2,\ p\ 1/2)^{-1} \pm \frac{1}{\sqrt{2}}(s,\ d)]_{2+,T=1}$ while the 9.74 MeV level is assumed to have the dominant configuration $(p\ 3/2)^{-2}_{2+,T=1}$ with a dominant L=2 distribution.

[c] The 9.74 MeV level is forbidden in the j-j limit.

[d] The 6.60, 7.78 and 9.74 MeV levels are all assumed to have the configuration $[(p\ 3/2,\ p\ 1/2)^{-1}+(s,\ d)]_{2+T=1}$ with $(p\ 3/2,\ p\ 1/2)^{-1}$ amplitudes of 35%, 35% and 30%, respectively.

[e] The contribution from the 3.56 MeV, p 1/2→d 5/2 transition is included.

* Only these transitions were included in computing average strengths.

† EB_2 was assumed to be equal to 400 keV (see Section VA-3).

and V_{11} = 16.5 ± 1.1 MeV are in very good agreement with those obtained from an analysis of the (p,n) reaction.[8,10-12] In particular, the (p,n) reactions on several target nuclei including ^{14}C, ^{52}Cr and ^{90}Zr (see Refs. 8, 11, and 12) yield values for V_{01} which range from 19 to 26 MeV and the ratio for the spin-isospin strength to the isospin strength is determined to be ≅ 0.6-1.0.[11,12] An independent measurement from the $^{7}Li(p,n)^{7}Be$ (431 keV) reaction at 44.7 MeV[10] gave a value for V_{11} = 15 MeV.

It is also interesting to compare the present results with those obtained previously in analyses of the (^{3}He,t) reaction on ^{17}O, ^{18}O, ^{27}Al, ^{30}Si, ^{39}K and ^{48}Ti at $E_{^3He}$ = 18-25 MeV.[13,14] Using a Yukawa potential with a range of α^{-1} = 1.0 F, values were obtained for V_{01} = 31 ± 6 and V_{11} = 20 ± 4 MeV [corrected to an effective nucleon-nucleon interaction at α^{-1} = 1.0 F (see Eq. (8))]. These strengths are somewhat larger than those obtained in the present analysis; this may be due to a possible energy dependence of the effective interaction.

a. The 8.92, 11.85 and 15.07 MeV levels in ^{13}N. The relatively large values of V_{01} and V_{11} which are predicted for these states may indicate that the wave functions of CK are unable to account for the configuration mixing in these states. This is particularly true for the 11.85 MeV level, since it will be shown later that the $^{13}C(^{3}He,^{3}He')^{13}C$ reaction, which populates the mirror level in ^{13}C at 11.84 MeV, predicts a value for V_{00} which is several times larger than values obtained for other transitions. In addition, evidence from an analysis of the $^{15}N(p,t)^{13}N$ reaction[35] indicates that the wave functions of CK underestimate the cross section for the 8.92 MeV, 1/2- level by a factor of six hundred.

b. The 9.74 MeV level in ^{14}O. Recent experimental evidence from the $^{16}O(p,t)^{14}O$ and $^{16}O(p,^{3}He)^{14}N$ reactions[78] indicates that the 9.74 MeV level in ^{14}O is the analog of a level observed in ^{14}N at 12.52 MeV. In addition, the transition to this level in the $^{16}O(p,t)^{14}O$ reaction has a characteristic L = 2 angular distribution similar to those observed for the 6.60 and 7.78 MeV levels in ^{14}O, indicating a possible spin assignment of (2+). The 12.52 MeV level in ^{14}N was also observed in the $^{15}N(^{3}He,\alpha)^{14}N$ reaction[49] and had a characteristic ℓ = 1 angular distribution. At first, it was thought that this level might correspond to one of the missing

$(p3/2)^{-2}$ states in ^{14}N; however, the spectroscopic factor which was obtained for this level was ≈3-5 times larger than the ones predicted by Cohen and Kurath[21] for these states.

One possible explanation for the population of the 9.74 MeV level in the $^{16}O(p,t)^{14}O$ reaction and the 12.52 MeV level in the $^{16}O(p,^{3}He)^{14}N$ and $^{15}N(^{3}He,\alpha)^{14}N$ reactions may be that these states have a $[(p3/2,p1/2)^{-1} + (s,d)]_{2+,T=1}$ configuration similar to those observed for the 9.17 and 10.43 MeV levels in ^{14}N[55] or their corresponding analogs at 6.60 and 7.78 MeV in ^{14}O. The spectroscopic factors which are obtained from the $^{15}N(^{3}He,\alpha)^{14}N$ reaction for the 9.17, 10.43 and 12.52 MeV levels are consistent with $(p3/2,p1/2)^{-1}$ amplitudes for these states of 43.4%, 37.7 % and 18.9%, respectively.[49]

The 9.74 MeV level is also observed in the $^{14}N(^{3}He,t)^{14}O$ reaction and has an angular distribution which resembles those obtained for the 6.60 and 7.78 MeV levels. In order to investigate the tentative assignment which has been proposed for this level, theoretical calculations were carried out for the levels in ^{14}O at 6.60, 7.78 and 9.74 MeV using the following models: 1) the 6.60 and 7.78 MeV levels were assumed to have the configuration $[\frac{1}{\sqrt{2}}(p3/2,p1/2)^{-1} \pm \frac{1}{\sqrt{2}}(s,d)]_{2+,T=1}$ while the 9.74 MeV level was assumed to have the dominant configuration $(p3/2)^{-2}_{2+,T=1}$ and 2) the 6.60, 7.78 and 9.74 MeV levels were all assumed to have the configuration $[(p3/2,p1/2)^{-1} + (s,d)]_{2+,T=1}$ with $(p3/2,p1/2)^{-1}$ amplitudes of 35%, 35% and 30%, respectively. Nuclear structure factors predict that the angular distributions for the $(p3/2)^{-2}$ and $(p3/2,p1/2)^{-1}$ configurations should be dominant L = 2 and L = 0 transitions, respectively. Since the 9.74 MeV level has an angular distribution which resembles other L = 0 transitions, the $(p3/2,p1/2)^{-1}$ configuration is favored (see Fig. 32). In addition, the values obtained for V_{01} and V_{11} for this transition are much too large if a $(p3/2)^{-2}$ configuration is assumed, while the model which considers the 6.60, 7.78 and 9.74 MeV levels to have similar configurations predicts values which are in good agreement with those obtained for other transitions (see Table XIV). This evidence supports a tentative $[(p3/2,p1/2)^{-1} + (s,d)]_{2+,T=1}$ assignment for the 9.74 MeV level in ^{14}O.

2. The (^{3}He,^{3}He') p3/2→ p1/2 (T_f=T_i) Transitions

In general, the (^{3}He,^{3}He') reaction is expected to be relatively insensitive to the spin-and isospin-dependent terms in the effective two-body interaction. This results from the following: (1) the Wigner interaction for complex projectiles is enhanced by a factor equal to the number of nucleons in the incoming projectile, and (2) evidence from the nucleon-nucleon (see Sec. VE) and nucleon-nucleus[7-9] scattering data indicates that V_{00} is probably two to three times larger than V_{10}, V_{01} and V_{11}. Consequently, if V_{00} is allowed, the (JSLT) =(LOLO) amplitudes are predicted to be the dominant terms for all inelastic transitions.

For p3/2→ p1/2 transitions, the (LOLO) = (0000) amplitude is generally forbidden by the selection rules, Eq. (14a,b,e), and therefore most of these transitions are predicted to have dominant L = 2 distributions. The experimental angular distributions obtained for p3/2→ p1/2 transitions are shown in Figs. 33 and 34; only those transitions in which $T_f = T_i$ will be discussed in this section. A comparison with those transitions which are restricted, Eq. (14a,e), to be pure L = 2 (i.e., the 4.43 MeV, 2+ level in ^{12}C and the 7.55 MeV, 5/2- level in ^{13}C) indicates that all p3/2→ p1/2 transitions have a characteristic L = 2 distribution with the exception of transitions which must be S = 1, Eq. (14a,b,e), (i.e., the 12.71 MeV, 1+ level in ^{12}C and the 8.86 MeV, 1/2- level in ^{13}C (see Ref. 79)).

In order to investigate the sensitivity of these (and other (^{3}He,^{3}He')) transitions to the spin- and isospin-dependence of the effective interaction, three different approximations were made concerning the exchange mixture in the central two-body force. First of all, the calculations were carried out assuming that only V_{00} contributes to the experimental cross sections (denoted Wigner force). Secondly, a Serber exchange mixture was used; this force predicts relative strengths in the ratio

$$V_{00} : V_{10} : V_{01} : V_{11} = -3 : 1 : 1 : 1 \quad .$$

Finally, a recent analysis of the (p,p') reaction[9] indicated that the proton-proton interaction was appreciably stronger than the proton-neutron interaction, implying that V_{00} and V_{01} have the same sign; more tentative

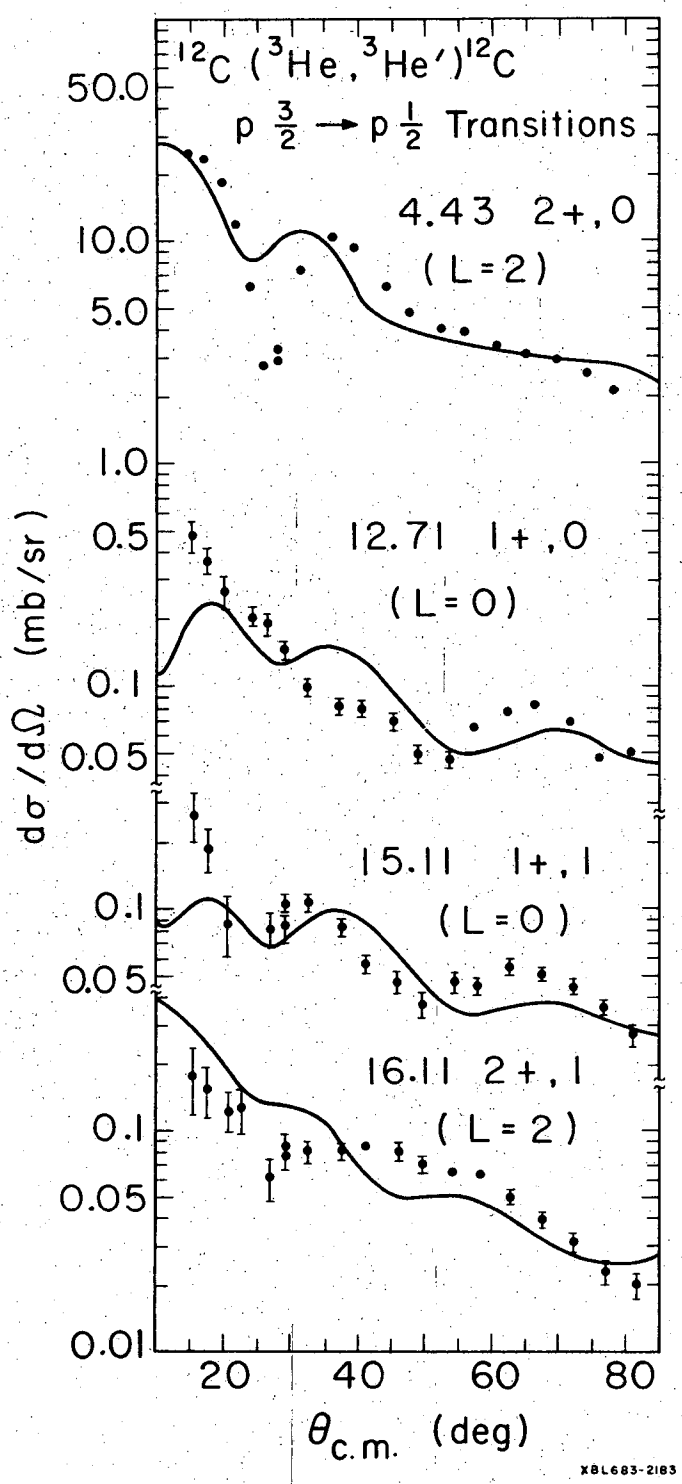

Fig. 33. Angular distributions for p3/2→p1/2 transitions observed in the $^{12}C(^3He,^3He')^{12}C$ reaction. The solid curves are DWBA predictions obtained using CK wave functions, a Serber exchange mixture, and the optical potential set F (see Table VII).

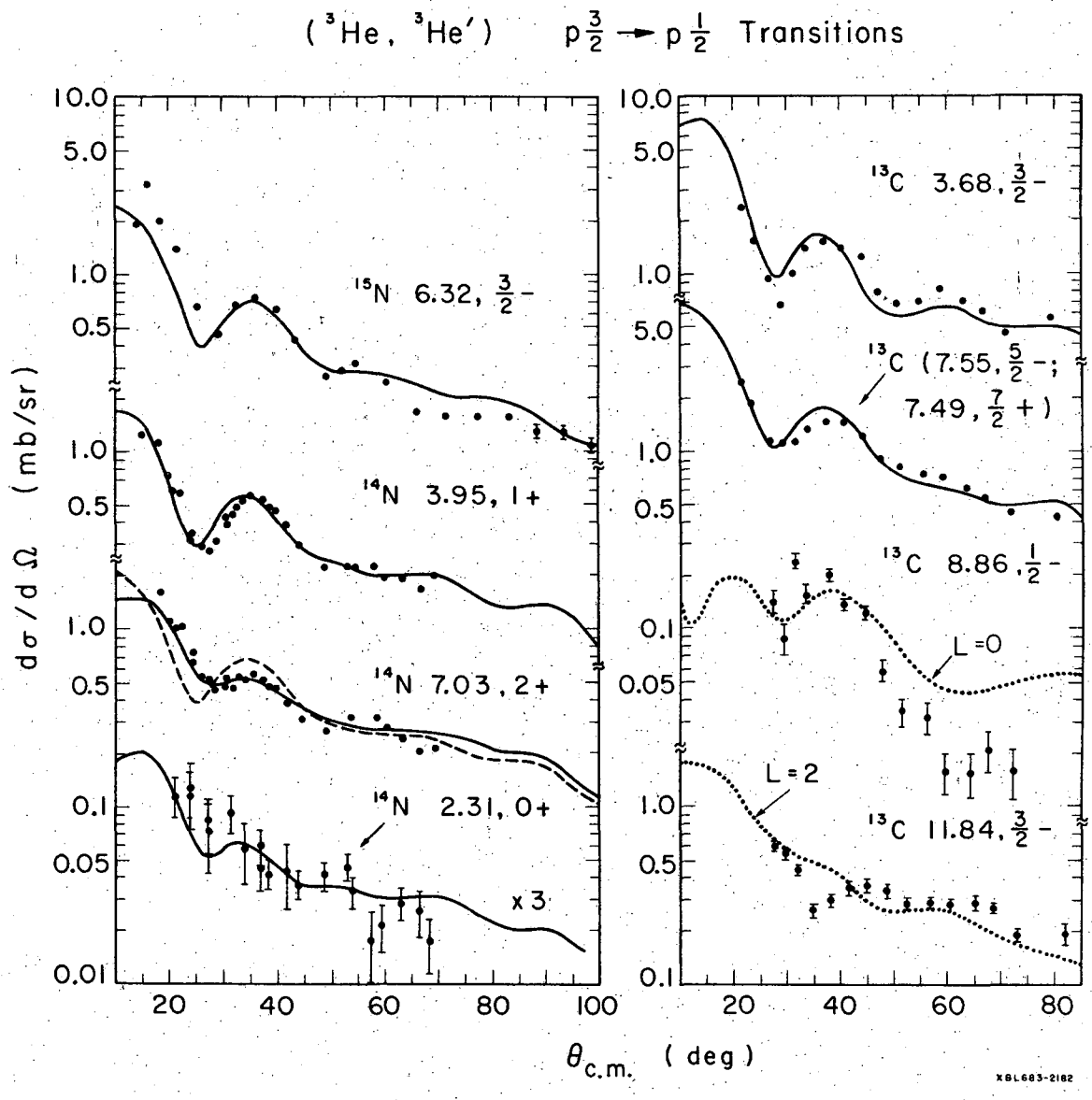

Fig. 34. Angular distributions for (^{3}He,^{3}He') p3/2→p1/2 transitions. The solid curves are DWBA predictions obtained using CK wave functions, a Serber exchange mixture, and the independent optical potentials given in Table VII. The dashed curve shown for the 7.03 MeV level in ^{14}N was calculated using a Wigner Force (i.e., V_{00} only). The dotted curves were computed using the unmodified ($r_o' = r_o$) potential set D (see Table VII). Force III was used for the 8.86 MeV level of ^{13}C while a Wigner interaction was assumed for the 11.84 MeV level.

results also showed that possibly V_{10} and V_{11} have opposite signs.[9] Since the inelastic transitions in mirror nuclei are dependent upon the signs of V_{ST} (i.e., T = 0 and 1 transfers are both allowed, see Eq. (14f, g)) an empirical exchange mixture denoted force III was also used. This force was assumed to give strengths in the ratio

$$V_{00} : V_{10} : V_{01} : V_{11} = -3 : -1 : -1 : 1 \quad .$$

This particular sign convention was chosen to satisfy the normalization condition:[4] $V_{00} + V_{10} - 3(V_{01} + V_{11}) = -1$.

The solid curves shown in Figs. 33 and 34 for $p3/2 \rightarrow p1/2$ (dominant L = 2) transitions were calculated using mixed CK wave functions and assumed the Serber exchange mixture (the S = 1 transitions will be discussed later). In general, the shapes of the theoretical distributions calculated using other exchange mixtures were almost identical. In order to obtain independent values of V_{00} for each transition and each exchange mixture, the theoretical curves have been normalized to give the best overall fit to the experimental data; the results are summarized in Table XV.

Several important conclusions are evident from these results. First of all, the values obtained for V_{00} are generally insensitive to the exchange mixture which is used, and therefore little information can be learned from these transitions concerning the spin and isospin dependence of the central interaction. Secondly, with the exception of the 11.84 MeV level in ^{13}C which will be discussed later, the relative agreement for all transitions is noticeably improved and the strength required for V_{00} is smaller using the mixed CK wave functions.

One of the most important results, however, is the magnitude of the strength obtained here for $V_{00} = 60.2 \pm 10$ MeV (the values quoted for V_{00} will refer to those obtained using a Serber exchange mixture unless otherwise stated) without including core polarization effects. In previous analyses of the (p,p') reaction, values for $V_{00} \cong 200$ MeV were obtained (for $\alpha^{-1} = 1.0$ F) for inelastic transitions in ^{18}O, ^{52}Cr, ^{54}Fe, ^{90}Zr, ^{92}Zr and ^{208}Pb when the ground and lower excited states were assumed to be well described by simple shell-model configurations.[8] If core polarization effects were included, however, V_{00} was reduced to approximately 80 MeV.[9]

Table XV. Experimental strengths for the effective nucleon-nucleon interaction at α^{-1}=1.0 F obtained from (^{3}He, ^{3}He'), p 3/2 → p 1/2 transitions.

				V_{00}(MeV)					
				Wigner Force		Serber Force		Force III	
		Energy (MeV)	J^{π},T	(jj)	(CK)	(jj)	(CK)	(jj)	(CK)
A. Independent Optical Potentials	^{15}N	6.32	3/2-,1/2	68.8	68.8	77.3	77.3	49.3	49.3
	^{14}N	3.95	1+ ,0	41.1	41.6	39.5	41.1	39.5	41.1
		7.03	2+ ,0	50.3	53.5	42.8	43.9	42.8	43.9
	^{13}C	3.68	3/2-,1/2	82.2	61.1	71.2	58.1	83.4	59.7
		7.55[a]	5/2-,1/2	112.6	76.3	126.5	82.0	98.3	71.1
		11.84*	3/2-,1/2	150.2	2013.0	168.4	332.4	77.0	157.8
	^{12}C	4.43	2+ ,0	106.6	67.8	105.8	67.8	105.8	67.8
				76.9±24	61.5±9	77.1±26	61.7±14	69.9±26	55.5±11
B. Average Optical Potential	^{15}N	6.32	3/2-,1/2	67.4	67.4	75.8	75.8	48.3	48.3
	^{14}N	3.95	1+ ,0	48.9	49.5	47.0	49.3	47.0	49.3
		7.03	2+ ,0	59.9	63.7	50.9	52.2	50.9	52.2
	^{13}C	3.68	3/2-,1/2	73.2	54.4	63.4	51.7	74.2	53.1
		7.55[a]	5/2-,1/2	100.2	67.9	112.6	73.0	87.5	63.3
		11.84*	3/2-,1/2	133.6	1792.0	149.8	296.0	68.5	140.3
	^{12}C	4.43	2+ ,0	92.7	59.0	92.0	59.0	92.0	59.0
				73.7±15	60.3±6	73.6±20	60.2±10	78.1±19	54.2±5

*Not included in computing average strengths.

[a]The contribution from the 7.49 MeV, 7/2+ level has been neglected.

In the present analysis, for p shell transitions, the wave functions of CK are unable to predict the observed E2 rates without including effective charges of βe for neutrons and $(1+\beta)e$ for protons where $\beta=0.5$.[20] However, the resulting enhancement factors for E2 transition matrix elements only range from 1.5 to 2.0. Therefore, core polarization effects should be less important but not negligible for 1p shell transitions.

Without specifically including core polarization in the microscopic analysis, it is difficult to determine how much this effect would alter the present (^{3}He,^{3}He') results; however, the relatively small values which were obtained for V_{00} indicate that core polarization is definitely less important in this treatment of 1p shell nuclei. Further evidence from an investigation of the ^{7}Li(p,p')^{7}Li (478 keV) reaction supports this conclusion:[10] at an incident proton energy of 44.7 MeV the strength required to fit the total cross section was V_{00} = 90 MeV (for a Yukawa with α^{-1} = 1.0 F). In addition, an analysis of the ^{12}C(p,p')^{12}C (4.43 MeV) reaction at E_p = 46 MeV[80] (see Sec. VD) gave a value of V_{00} = 86.9 MeV to be compared with V_{00} = 59.0 MeV obtained from the (^{3}He,^{3}He') reaction.

a. <u>The 11.84 MeV, 3/2 - level in ^{13}C</u>. The wave functions of CK predict that the ^{13}C(^{3}He,^{3}He')^{13}C (11.84 MeV, 3/2-) transition should be very sensitive to the spin-and isospin-dependent terms in the effective interaction (i.e., the 2020 amplitude is predicted to be very small). However, the strength required for V_{00} = 296 MeV in order to fit the observed cross section for this transition is several times larger than those obtained for other p3/2→p1/2 transitions. In addition, evidence from the ^{13}C(α,α')^{13}C reaction at E_α = 64.5 MeV[81] indicates that the 11.84 MeV level is populated with approximately the same relative intensity as was observed in the (^{3}He,^{3}He') reaction (compare Figs. 7 and 35). Since the (α,α') reaction is only dependent upon V_{00}, it is evident that the mixed CK wave functions are definitely unable to account for the population of this state.

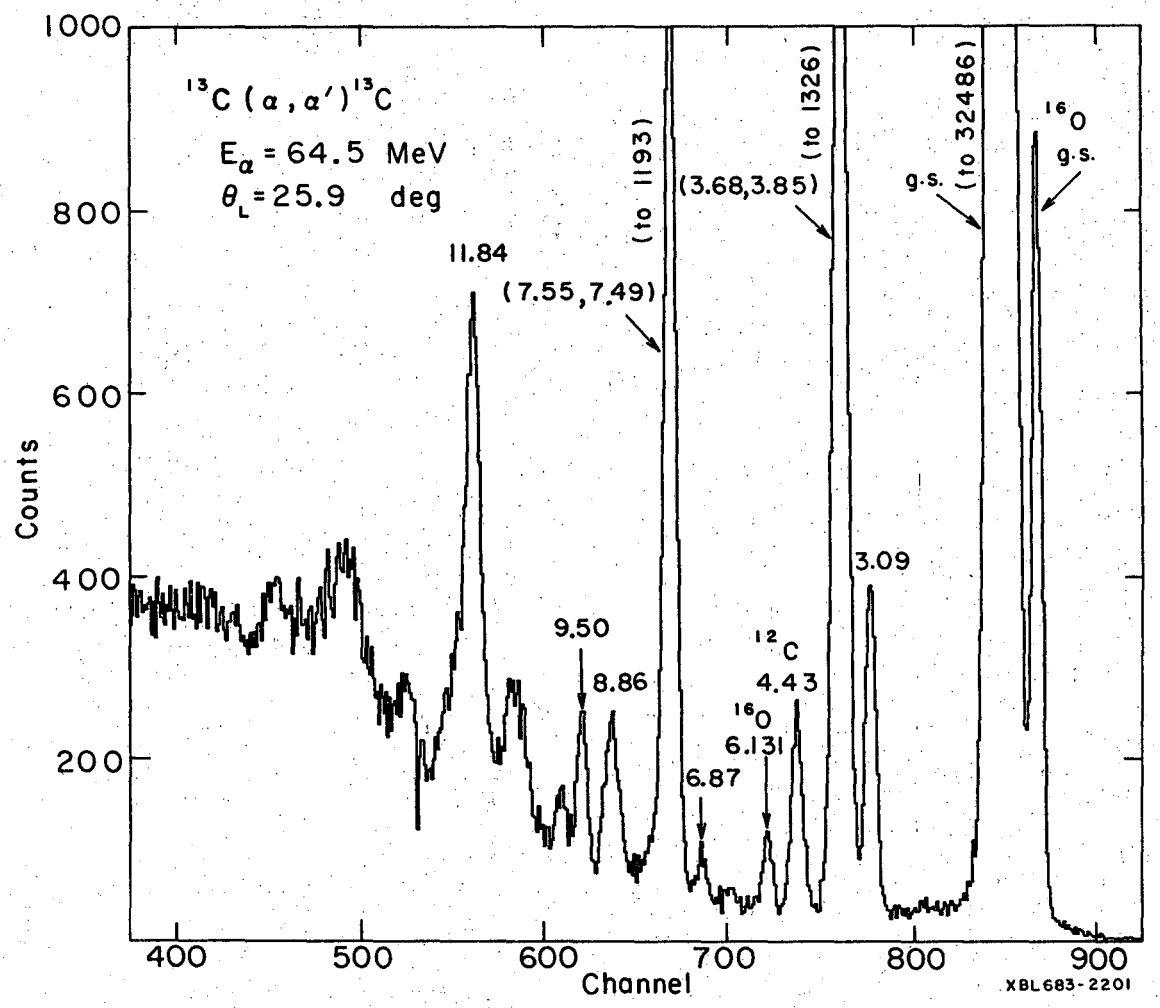

Fig. 35. Energy spectrum of the $^{13}C(\alpha,\alpha')^{13}C$ reaction at E_α = 64.5 MeV and a scattering angle of 25.9 deg.

b. The ^{12}C 12.71 MeV, 1+ and ^{13}C 8.86 MeV, 1/2 - levels. Since the ^{12}C 12.71 MeV, 1+ and ^{13}C 8.86 MeV, 1/2- levels are predicted to be dominant L = 0, S = 1 transitions, they provide a direct measure of the V_{10} term in the effective interaction (the 8.86 MeV level also depends upon V_{11}). Unfortunately, both of these levels are populated in the (α,α') reaction[62,81] with almost the same relative intensity as in the $(^3He,^3He')$ reaction (compare Figs. 7 and 35). The 12.71 MeV, 1+ level in ^{12}C is an example of the well-known unnatural parity states which have been investigated extensively in the (α,α') reaction.[82,83] In some cases it has been shown that the population of these states can be explained by multiple excitation processes.[83] As a result, the values obtained for V_{10} in a microscopic analysis of these data only provide an upper limit on the magnitude of this term.

The theoretical angular distributions for these transitions are compared with experiment in Figs. 33 and 34. Both transitions are best fit using unmodified optical potentials; however, the agreement is definitely not as good as that obtained for the $(^3He,t)$ L = 0 and $(^3He,^3He')$ L = 2 transitions. The values predicted for V_{10} and V_{11} are shown in Table XVI. If a Serber exchange mixture is used, the $^{13}C(^3He,^3He')^{13}C$ (8.86 MeV, 1/2-) transition is forbidden (or almost forbidden) using j-j (or CK) wave functions; however, if force III is used both transitions predict strengths of $V_{10} \approx 12 \pm 2$ and $V_{10} \approx 27$ MeV for j-j and CK wave functions, respectively. No conclusive determinations of this term have been obtained from (p,p') data; tentative results give $|V_{10}| \approx 40$ MeV.[9]

3. The $(^3He,t)$ p3/2→p1/2 Dominant L = 2 Transitions

The transitions which are discussed in this section can be divided into two groups: (1) those transitions which are restricted by the selection rules to be pure L = 2, and (2) those transitions which could be L = 0 and L = 2 but whose L = 0 amplitudes are predicted to be relatively small; this second group will be discussed individually later.

Table XVI. Experimental strengths for the effective nucleon-nucleon interaction at α^{-1}=1.0 F obtained from (^{3}He,^{3}He') transitions where V_{00} is forbidden.

	Dominant Single-Particle Transition		Energy (MeV)	J^{π},T		Serber Force (jj)	Serber Force (CK)	Force III (jj)	Force III (CK)
A. Independent Optical Potentials	p1/2→ d5/2	^{15}N	8.57	3/2+,1/2	V_{10},V_{11}	22.4		- [a]	
	p1/2→ p1/2	^{14}N	2.31	0+ ,1	V_{11}	12.4	17.0	12.4	17.0
	p3/2→ p1/2	^{13}C	8.86	1/2-,1/2	V_{10},V_{11}	- [a]	330	16.1	29.8
	p3/2→ p1/2	^{12}C	12.71	1+ ,0	V_{10}	12.2	31.0	12.2	31.0
	p3/2→ p1/2		15.11	1+ ,1	V_{11}	11.7	27.9	11.7	27.9
	p3/2→ p1/2		16.11[†]	2+ ,1	V_{01},V_{11}	33.8	53.0	33.8	53.0
B. Average Optical Potential	p1/2→ d5/2	^{15}N	8.57	3/2+,1/2	V_{10},V_{11}	22.0		- [a]	
	p1/2→ p1/2	^{14}N	2.31	0+ ,1	V_{11}	14.7	20.2	14.7	20.2
	p3/2→ p1/2	^{13}C	8.86	1/2-,1/2	V_{10},V_{11}	- [a]	294	14.3	26.5
	p3/2→ p1/2	^{12}C	12.71	1+ ,0	V_{10}	10.6	27.0	10.6	27.0
	p3/2→ p1/2		15.11	1+ ,1	V_{11}	10.2	24.3	10.2	24.3
	p3/2→ p1/2		16.11[†]	2+ ,1	V_{01},V_{11}	29.4	46.1	29.4	46.1

[†] EB_2 was assumed to be equal to 400 keV (see Sec. VA-3).

[a] Forbidden in the j-j limit.

The pure L = 2 transitions all have characteristic angular distributions which are similar to the corresponding (^{3}He,^{3}He') distributions but have much less structure and are not as well reproduced by theoretical calculations (see Fig. 36). The values obtained for V_{01} and V_{11} shown in Table XVII are all consistently higher than those required for L = 0 transitions. It would be necessary to use a range of $\alpha^{-1} \cong 0.5$ F in order to obtain agreement between the relative strengths required for L = 0 and L = 2 transitions; however, the fits obtained at this range would be very poor for all transitions (compare Fig. 30). The apparent enhancement of the (^{3}He,t) L = 2 transitions may be due to collective or core polarization effects as discussed previously for (^{3}He,^{3}He') p3/2→p1/2 transitions. The structureless features of the angular distributions for these transitions might indicate, however, that other mechanisms such as multiple excitation or particle-exchange are contributing.

a. <u>The ^{14}N(^{3}He,t)^{14}O (g.s.,0+) and ^{14}C(^{3}He,t)^{14}N (g.s.,1+) transitions.</u> The ^{14}N(^{3}He,t)^{14}O (g.s.,0+) reaction and the inverse of the ^{14}C(^{3}He,t)^{14}N (g.s.,1+) reaction correspond to transitions between identical initial and final states. When detailed-balance[40] and phase-space corrections are applied, the angular distributions for these transitions should be identical (see also Sec. VI). Evidence from the well-known β decay of ^{14}C predicts that the L = 0 amplitudes for these transitions are approximately equal to zero.[72] Experimentally it is observed (compare Figs. 16, 17 and 36) that both of these transitions have a distinct angular distribution which is neither pure L = 0 or pure L = 2 in character. Theoretical calculations using mixed CK or VF wave functions predict a dominant L = 2 distribution while those using j-j wave functions also include a strong L = 0 component; none of these give a good fit to the experimental data. The values obtained for V_{11} are shown in Table XVII; both levels predict similar results. Using mixed wave functions, the strengths required are comparable to, or slightly larger than, those predicted for L = 0 transitions.

It is interesting to compare these results with those obtained in a recent microscopic analysis of the ^{14}C(p,n)^{14}N reaction at E_p = 13.3 MeV.[11] When a Yukawa interaction with a range of 1.4 F was used, comparison with

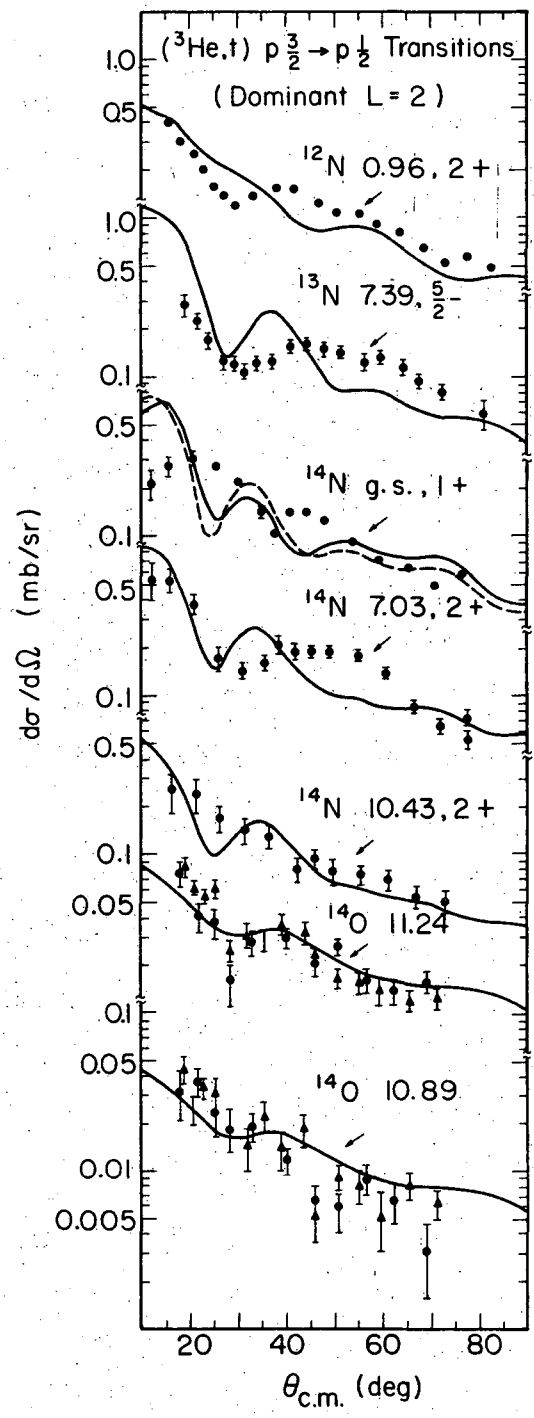

Fig. 36. Angular distributions for the (^{3}He,t) p3/2→p1/2 dominant L = 2 transitions. The solid curves are DWBA predictions obtained using CK wave functions and the independent optical potentials given in Table VII. The dashed curve shown for the ground state of ^{14}N was computed using VF wave functions.

Table XVII. Experimental strengths for the effective nucleon-nucleon interaction at α^{-1}=1.0 F obtained from (^{3}He,t), p3/2→p1/2 (dominant L=2) transitions.

			Independent Optical Potentials				Average Optical Potential					
			V_{01}(MeV)		V_{11}(MeV)		V_{01}(MeV)			V_{11}(MeV)		
Reaction	Energy (MeV)	J^{π},T	(jj)	(CK)	(jj)	(CK)	(jj)	(CK)	(VF)	(jj)	(CK)	(VF)
^{14}C(^{3}He,t)^{14}N	0.0	1+,0	-	-	18.1	24.2	-	-	-	17.7	23.7	25.9
	7.03	2+,0*	36.2	35.9	36.2	35.9	35.5	35.2	34.8	35.5	35.2	34.8
	10.43[a]	2+,1*	45.8	49.3	45.8	49.3	44.9	48.3		44.9	48.3	
^{14}N(^{3}He,t)^{14}O	0.0	1+,0	-	-	12.7	17.5	-	-	-	15.1	20.8	23.7
	10.89[b]	(1+),1	11.8	14.9	9.4	11.9	14.0	17.7		11.2	14.2	
	11.24[b]	(1+),1	16.2	20.7	13.0	16.5	19.3	24.6		15.5	19.6	
^{13}C(^{3}He,t)^{13}N	7.39	5/2-,1/2*	37.2	45.3	37.2	45.3	33.1	40.3		33.1	40.3	
^{12}C(^{3}He,t)^{12}N	0.96[†]	2+,1*	33.7	52.7	33.7	52.7	29.3	45.8		29.3	45.8	
			38.2±4	45.8±5	38.2±4	45.8±5	35.7±5	42.4±5		35.7±5	42.4±5	

*Only these transitions were included in computing average strengths.

†EB_2 was assumed to be equal to 400 keV (see Sec. VA-3).

[a]The 10.43 MeV level is assumed to have the configuration $[\frac{1}{\sqrt{2}}(p3/2,p1/2)^{-1} + \frac{1}{\sqrt{2}}(s,d)]_{2+,T=1}$.

[b]These values for V_{ST} were obtained assuming that either the 10.89 or the 11.24 MeV level had the dominant configuration $(p3/2,p1/2)^{-1}_{1+,T=1}$.

experiment showed not only a poor fit to the ground state transition but also a strength for V_{11} (using mixed VF wave functions) which was three times larger (or $\approx$ 58 MeV at α^{-1} = 1.0 F) than the value of 19.2 MeV required to fit the 3.95 MeV (dominant L=0) transition. In contrast, the corresponding values required in the $^{14}C(^{3}He,t)^{14}N$ reaction are 25.9 and 16.5 MeV, respectively. This discrepancy may indicate that contributions from other reaction mechanisms such as particle exchange are not as important for complex projectiles at higher incident energies.

b. The 10.89 and 11.24 MeV levels in ^{14}O. The 10.89 and 11.24 MeV levels in ^{14}O are both possible candidates for the analog to the 13.72 MeV, $(p3/2,p1/2)^{-1}_{1+,T=1}$ level in ^{14}N which should occur near 11.4 MeV in ^{14}O if level shifts are neglected. Theoretical calculations predict that the angular distribution for this state should correspond to a dominant L = 2 transition. Unfortunately, the 10.89 and 11.24 MeV levels are both weakly populated in the $(^{3}He,t)$ reaction and therefore a meaningful comparison of the shapes of the experimental angular distributions could not be made (compare Fig. 36). However, approximate values were obtained for V_{01} which are given in Table XVII. Although it appears that the values predicted for the 11.24 MeV level are in better agreement with those for other L = 2 transitions, the 10.89 MeV level cannot be ruled out.

4. The $(^{3}He,^{3}He')$ p1/2→ d5/2 Transitions

In principle, an L = 1 (S = 1) and/or L = 3 (S = 0,1) transfer is allowed for a p1/2→ d5/2 transition. However, since (LOLO) amplitudes are strongly enhanced for complex projectiles (see Sec. VB-2), the $(^{3}He,^{3}He')$ p1/2→ d5/2 transitions are all predicted to have dominant L = 3 distributions (the 3/2+ level in ^{15}N at 8.57 MeV is the only exception; it is restricted by the selection rules, Eq. (14a,e), to be pure L = 1 (S = 1) and will be discussed further later). The angular distributions for these L = 3 transitions shown in Figs. 37 and 38, have a similar shape which is fairly well reproduced by the theoretical calculations. The values obtained for V_{00} are summarized in Table XVIII. Once again, they are relatively insensitive to the spin- and isospin-dependent terms in the effective interaction. The overall agreement is very good considering the simple model which was assumed for the wave functions of these states. The average strengths obtained for V_{00} are slightly larger than those computed earlier for L = 2

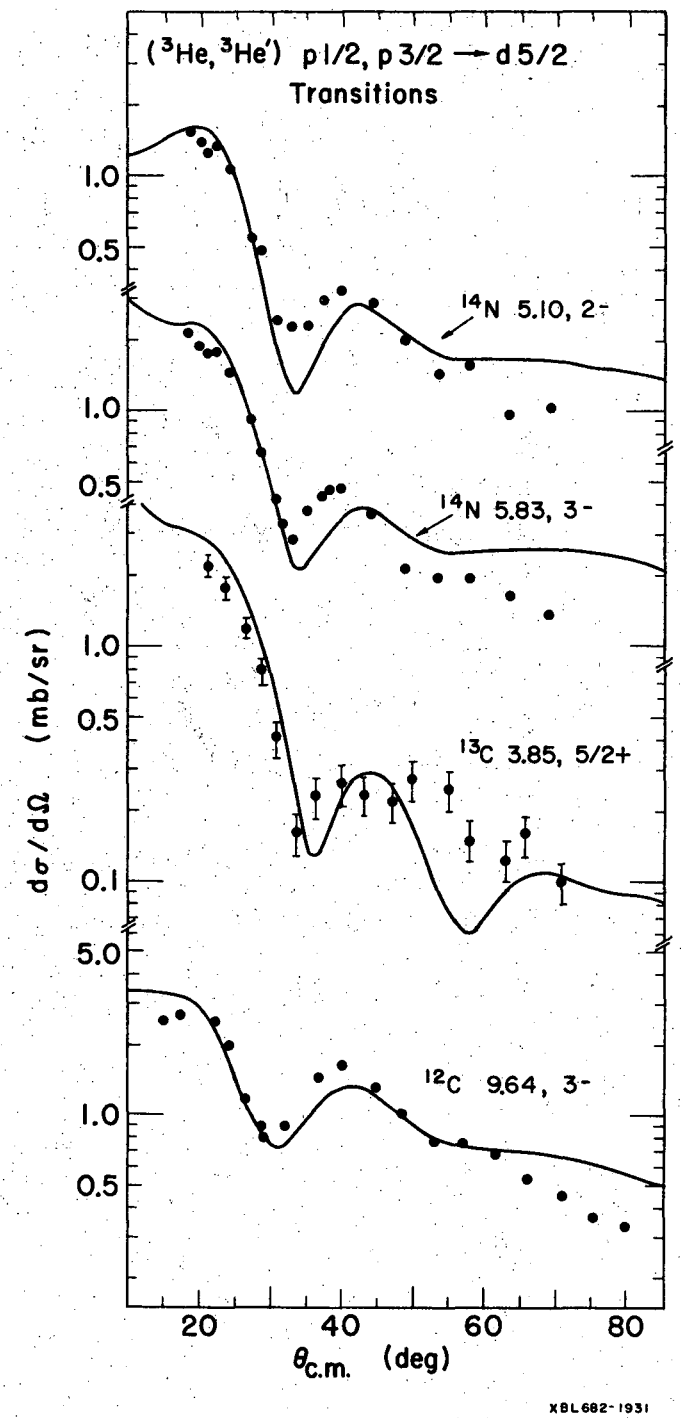

Fig. 37. Angular distributions for (^{3}He,^{3}He') p1/2,p3/2→ d5/2 transitions. The solid curves are DWBA predictions obtained using j-j wave functions, a Serber exchange mixture, and the independent optical potentials given in Table VII. (The 9.64-MeV, 3-level in ^{12}C was assumed to have the configuration $(p3/2)^7_{3/2}$ d5/2).

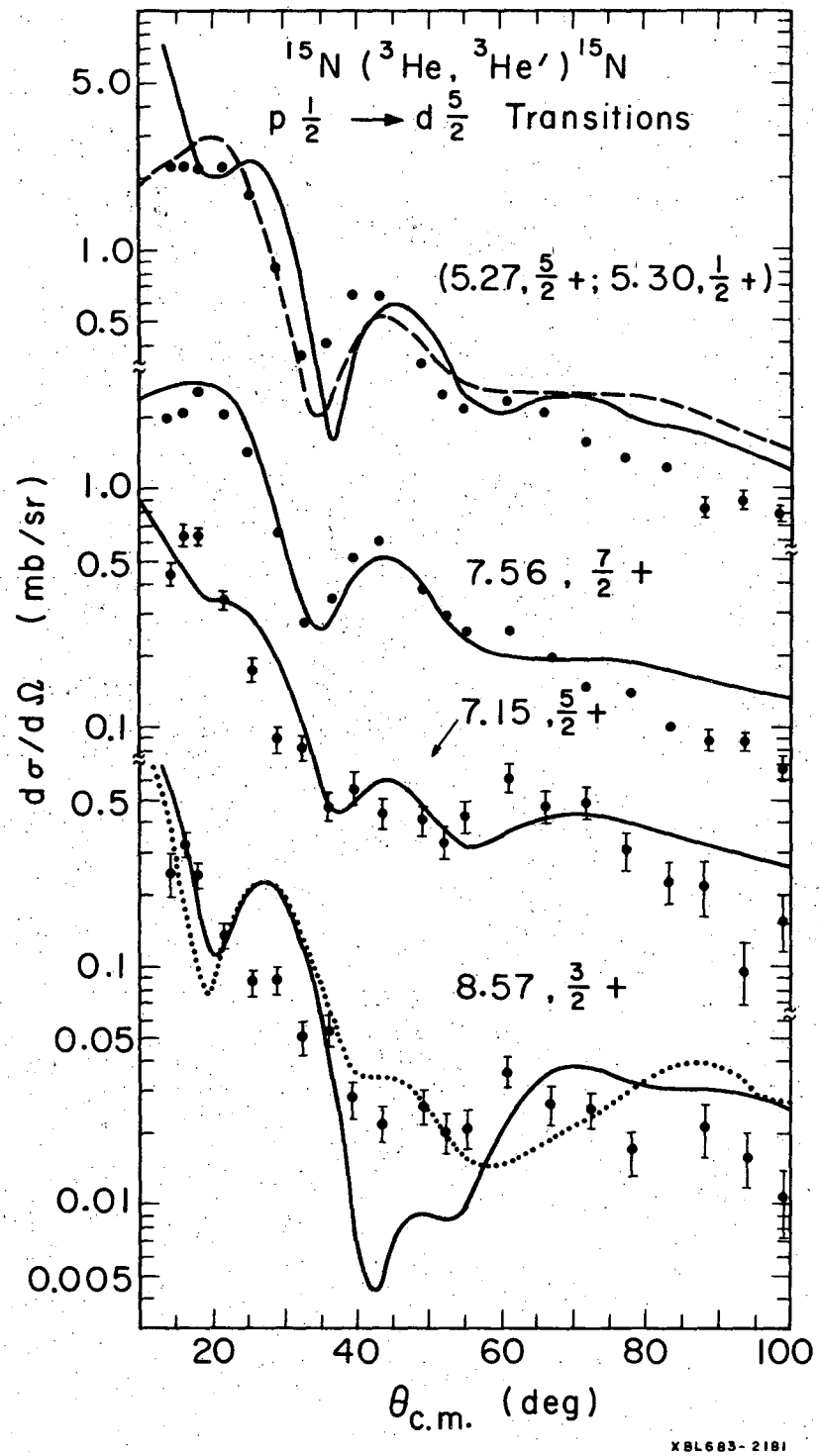

Fig. 38. Angular distributions for p1/2→ d5/2 transitions observed in the $^{15}N(^3He,^3He')^{15}N$ reaction. The solid curves are DWBA predictions obtained using j-j wave functions, a Serber exchange mixture, and the modified ($r_o' = 0.93\ r_o$) optical potential set A (see Table VII). The dashed curve shown for the unresolved levels at 5.27 and 5.30 MeV was computed neglecting the contribution from the 5.30 MeV, 1/2+ level. The dotted curve shown for the 8.57 MeV, 3/2+ level was computed using the unmodified potential set A.

Table XVIII. Experimental strengths for the effective nucleon-nucleon interaction at α^{-1}=1.0 F obtained from (^{3}He,^{3}He') p1/2→ s1/2,d5/2 transitions.

Single-Particle Transition		Energy (MeV)	J^{π},T	V_{00}(MeV) Independent Optical Potentials: Wigner Force	Serber Force	Force III	Average Optical Potential: Wigner Force	Serber Force	Force III
p1/2→ d5/2	^{15}N	5.27	5/2+,1/2	71.7	73.9	66.2	70.3	72.4	64.9
		5.30	1/2+,1/2						
		5.27[a]	5/2+,1/2*	93.0	93.8	82.6	91.1	91.9	80.9
		7.15	5/2+,1/2	68.6	50.2	77.2	67.2	49.2	75.7
		7.56	7/2+,1/2	95.2	83.6	107.3	93.3	81.9	105.2
	^{14}N	5.10	2- ,0	57.8	56.3	56.3	68.8	67.0	67.0
		5.83	3- ,0	75.5	72.6	72.6	89.8	86.4	86.4
	^{13}C	3.85	5/2+,1/2	75.0	52.6	84.3	66.8	46.8	75.0
				74.0±8	64.9±12	77.3±12	76.0±10	67.3±13	79.0±11
p1/2→ s1/2	^{15}N	7.30	3/2+,1/2	61.6	53.2	69.3	60.4	52.1	67.9
		8.31	1/2+,1/2	70.8	53.1	79.9	69.4	52.0	78.3
	^{14}N	4.91	0- ,0	45.0	44.4	44.4	53.6	52.8	52.8
		5.69	1- ,0	38.9	38.1	38.1	46.3	45.3	45.3
	^{13}C	3.09	1/2+,1/2	45.0	38.2	50.6	40.0	34.0	45.0
				52.3±11	45.4±6	56.5±15	53.9±9	47.2±6	57.9±12

*Not included in computing average strengths.

[a]The contribution from the 5.30 MeV, p1/2→ s1/2 transition is neglected.

transitions using the wave functions of CK; however, they are in better agreement with the values computed for L = 2 transitions using simple j-j wave functions. These results are consistent with those obtained from an analysis of E3 transitions rates.[73,74,84] In particular, if the shell-model wave functions of True[56] are used to predict the observed E3 transition rates in mass 14 nuclei, then an effective charge $\beta = 0.5$ is required[73] (i.e., the same β required to predict the observed E2 rates using CK wave functions) whereas if j-j wave functions are used, a slightly larger value of β is required.

The 8.57 MeV, 3/2+ level in ^{15}N is predicted to be a dominant L = 1, S = 1 transition. Theoretical fits are shown in Fig. 38 for both the modified and unmodified optical potential set; the latter appears to give a better overall account of the experimental data. The values obtained for $V_{10} = V_{11} = 22.0$ MeV using a Serber exchange mixture (see Table XVI) can only be considered as upper limits since this level is also populated in the (α,α') reaction[62] with approximately the same relative intensity as in the $(^3He,^3He')$ reaction (see Sec. VC).

5. <u>The $(^3He,t)$ p1/2→ d5/2 Transitions</u>

In contrast with the $(^3He,^3He')$ p1/2→ d5/2 transitions, the corresponding $(^3He,t)$ transitions are predicted to have mixed (L = 1 and/or L = 3) amplitudes ranging from almost pure L = 1 to pure L = 3 (compare Table XIX). In general, the experimental angular distributions for these transitions have a similar shape (compare Figs. 39, 40 and Ref. 18) while the theoretical curves vary, depending upon the relative strengths of the L = 1 and 3 components (when two levels were unresolved, the theoretical curves were obtained by adding the contributions from each level).

Those transitions which are restricted to be L = 3, such as the 7.28 MeV, 7/2+ level in ^{15}O, have angular distributions which resemble the corresponding $(^3He,^3He')$ transitions (i.e., the 7.56 MeV, 7/2+ level in ^{15}N); however, the oscillatory structure of these distributions is not as well defined as that predicted by theory (e.g., the predicted minimum at $\theta_{c.m.} \cong 35$ deg is completely filled in while the predicted maximum at $\theta_{c.m.} \cong 42$ deg appears to occur at a slightly smaller angle). The theoretical

Table XIX. Experimental strengths for the effective nucleon-nucleon interaction at α^{-1}=1.0 F obtained from (^{3}He,t), p1/2→ d5/2 transitions.

Reaction	Energy (MeV)	J^{π},T	Dominant L Transfer	Independent Optical Potentials V_{01}(MeV)	Independent Optical Potentials V_{11}(MeV)	Average Optical Potential V_{01}(MeV)	Average Optical Potential V_{11}(MeV)
^{15}N(^{3}He,t)^{15}O	5.19[a]	1/2+,1/2	1	59.0	59.0	57.8	57.8
	5.24	5/2+,1/2	1,3				
	6.79[a]	3/2+,1/2	1	23.6	23.6	23.1	23.1
	6.86	5/2+,1/2	1,3				
	7.28[†]	7/2+,1/2	3	40.5	40.5	39.7	39.7
	8.28[†]	3/2+,1/2	1	-	15.8	-	15.5
^{14}N(^{3}He,t)^{14}O	6.28[†]	(3-),1	1	19.1	19.1	22.7	22.7
	6.79[†]	(2-),1	1,3	21.0	21.0	25.0	25.0
^{14}C(^{3}He,t)^{14}N	5.10	2- ,0	1	-	31.6	-	31.0
	5.83	3- ,0	3	43.9	43.9	43.0	43.0
^{13}C(^{3}He,t)^{13}N	3.51[b]	3/2-,1/2	0	20.4	20.4	18.2	18.2
	3.56[†]	5/2+,1/2	1,3				
				32.5±13	30.6±12	32.8±12	30.7±11

[†] Eb_2 was assumed to be equal to 400 keV (see Sec. VA-3).

[a] The contributions from these p1/2→s1/2 transitions were included.

[b] The angular distribution for the 3.51 MeV level was calculated using CK wave functions.

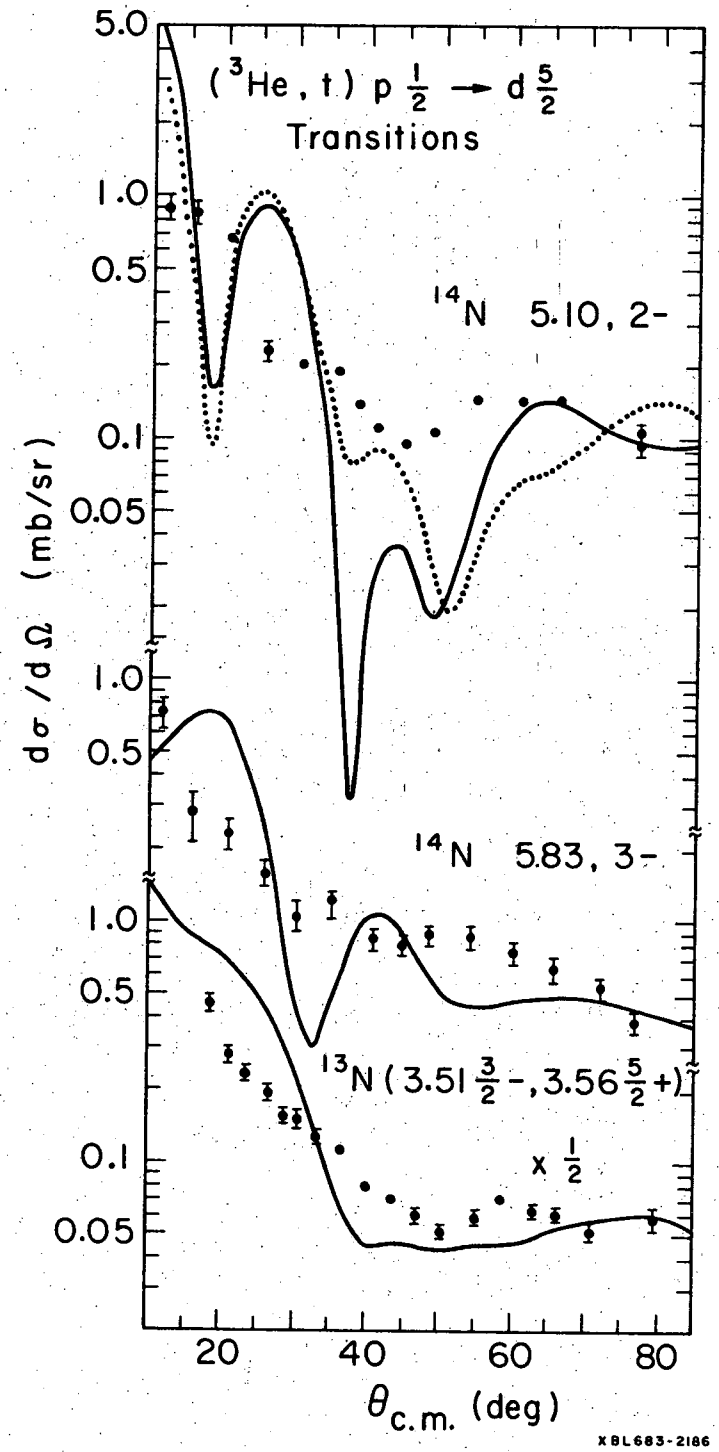

Fig. 39. Angular distributions for (^{3}He,t) p1/2→ d5/2 transitions. The solid curves are DWBA predictions obtained using simple j-j wave functions (CK wave functions were used to calculate the distribution for the 3.51 MeV, 3/2-level in ^{13}N) and the independent optical potentials given in Table VII. The dotted curve shown for the 5.10 MeV level in ^{14}N was computed using the unmodified potential set C (see Table VII).

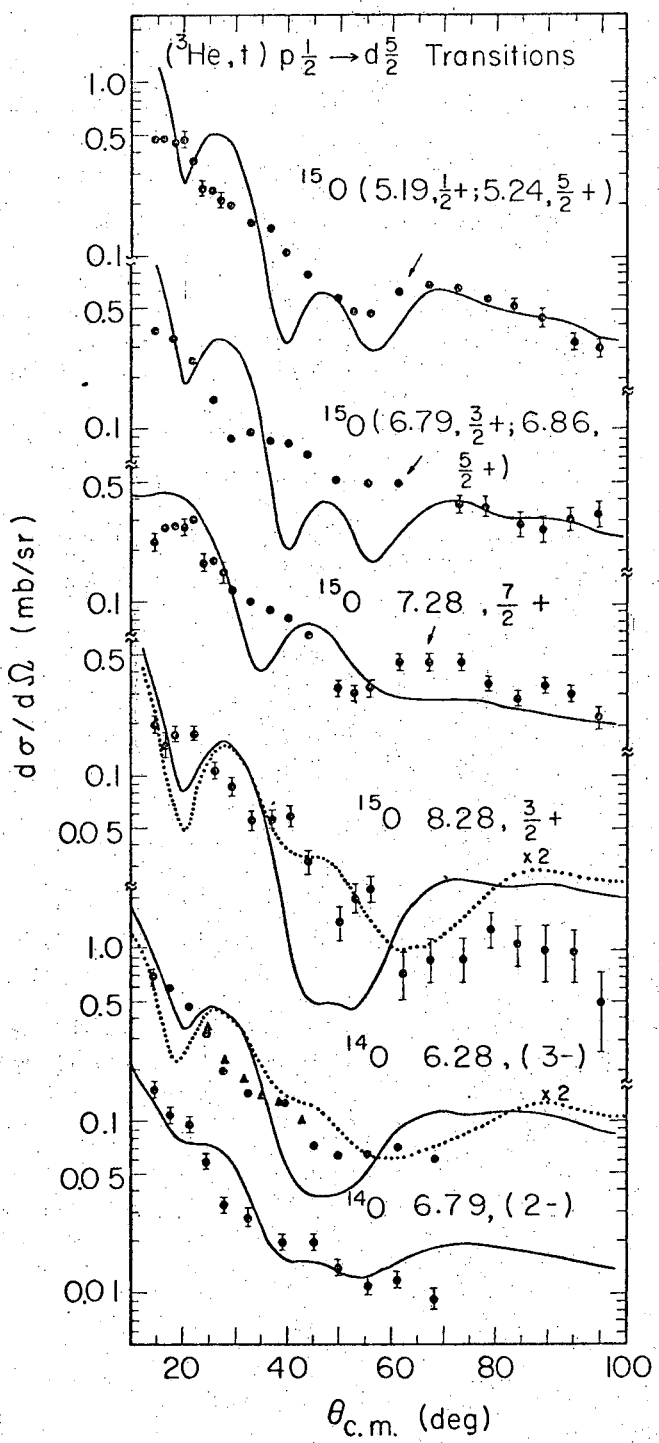

Fig. 40. Angular distributions for (^{3}He,t) p1/2→ d5/2 transitions. The solid curves are DWBA predictions obtained using j-j wave functions and the independent optical potentials given in Table VII. The dotted curves were calculated using unmodified ($r_0' = r_0$) optical potentials. The theoretical curves for unresolved levels were obtained by summing the predicted distributions for each level.

angular distributions for those transitions predicted to have strong or dominant L = 1 components are not in very good agreement with the experimental data. The curves shown in Figs. 39 and 40 were calculated using modified and unmodified optical potentials. Although the latter give a better fit to the data in the region $\theta_{c.m.} \cong 40\text{-}60$ deg, both potential sets predict minima at $\theta_{c.m.} \cong 20$ deg while the experimental data indicate maxima (compare Figs. 39 and 40).

The values obtained for V_{01} and V_{11} are shown in Table XIX; the relative agreement is not as good as that obtained for other single-particle transitions. In addition, the average strengths predicted for $V_{01} = 32.8 \pm 12$ and $V_{11} = 30.7 \pm 11$ MeV are larger than the values required for L = 0 transitions, indicating that the experimental cross sections for (^{3}He,t) p1/2→ d5/2 transitions are also enhanced.

6. The (^{3}He,^{3}He') p1/2→ s1/2 Transitions

The experimental angular distributions for p1/2→ s1/2 transitions which are shown in Fig. 41 have more structure and deeper minima than those observed for other single-particle transitions. Theoretical calculations predict a well-defined oscillatory structure for these transitions; however, the fits obtained are not as good as those for (^{3}He,^{3}He') L = 2 and L = 3 transitions.

Predicted values for V_{00} are summarized in Table XVIII; the overall agreement is surprisingly good considering the simple j-j configurations which were assumed for these states. In addition, the average strength obtained for $V_{00} = 47.2 \pm 6$ MeV does not change significantly if the contributions from the spin and isospin terms in the effective interaction are neglected (compare Table XVIII). Since core polarization effects for L = 1 transitions should be small, it also is of interest that the values obtained for V_{00} are ≈ 10-20 MeV smaller than those obtained for L = 2 and L = 3 transitions.

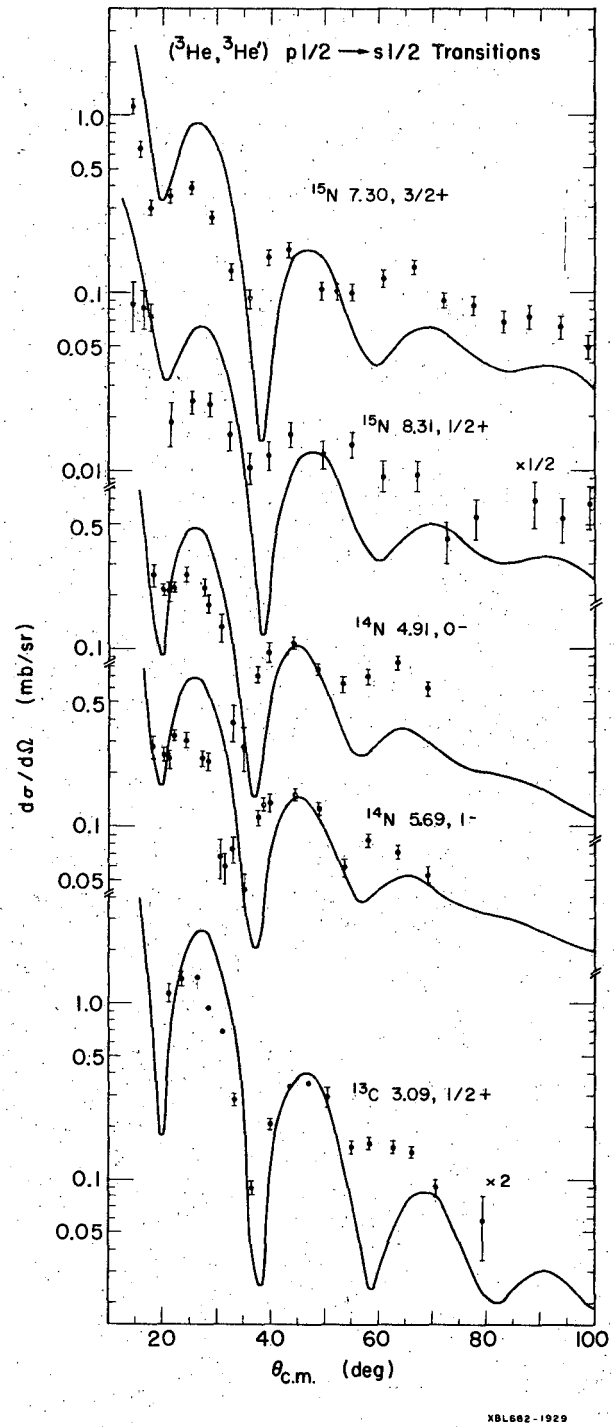

Fig. 41. Angular distributions for (^{3}He,^{3}He') p1/2→ s1/2 transitions. The curves are DWBA predictions obtained using j-j wave functions, a Serber exchange mixture, and the independent optical potentials given in Table VII.

7. The (^{3}He,t) p1/2→ s1/2 Transitions

In general, the levels which are populated in the (^{3}He,t) reaction by the promotion of a p1/2 nucleon to an s1/2 nucleon have much smaller cross sections than other single-particle transitions to low-lying orbitals.[16,18] The angular distributions for these states which are shown in Fig. 42 have much less structure than theoretically predicted. However, the values obtained for V_{01} = 19.4 ± 3 and V_{11} = 17.3 ± 5 MeV (see Table XX) are approximately equal to those for L = 0 transitions indicating that these transitions are not collectively enhanced.

C. The (^{3}He,^{3}He') and (α,α') Reactions on 1p Shell Nuclei

The microscopic analysis of the (^{3}He,^{3}He') reaction has shown that this reaction is in general very insensitive to the spin- and isospin-dependent terms in the effective interaction and therefore the cross sections for strongly excited states are determined primarily by the (LOLO) amplitude. Since the (α.α') reaction is only dependent upon this term, a direct comparison of these two reactions populating identical final states could provide further evidence to support this conclusion.

An investigation of the elastic and inelastic scattering of 40.5 MeV α particles from several targets including ^{12}C, ^{13}C, ^{14}N, ^{15}N and ^{16}O has been reported by Harvey et al.[62] It was found that the angular distributions obtained from these reactions could also be characterized according to the particular shell-model transition involved. A comparison of the (^{3}He,^{3}He') and (α,α') distributions indicates that the shapes are very similar, especially for L = 2 and L = 3 transitions; however, the magnitude of the (α,α') distribution is always approximately two to three times larger.

In Table XXI, relative integrated cross sections are compared for transitions observed in the (^{3}He,^{3}He') and (α,α') reactions on several 1p shell nuclei. The transitions have been grouped according to the particular shell-model transition involved, and in each case the cross sections have been arbitrarily normalized relative to the one single-particle transition

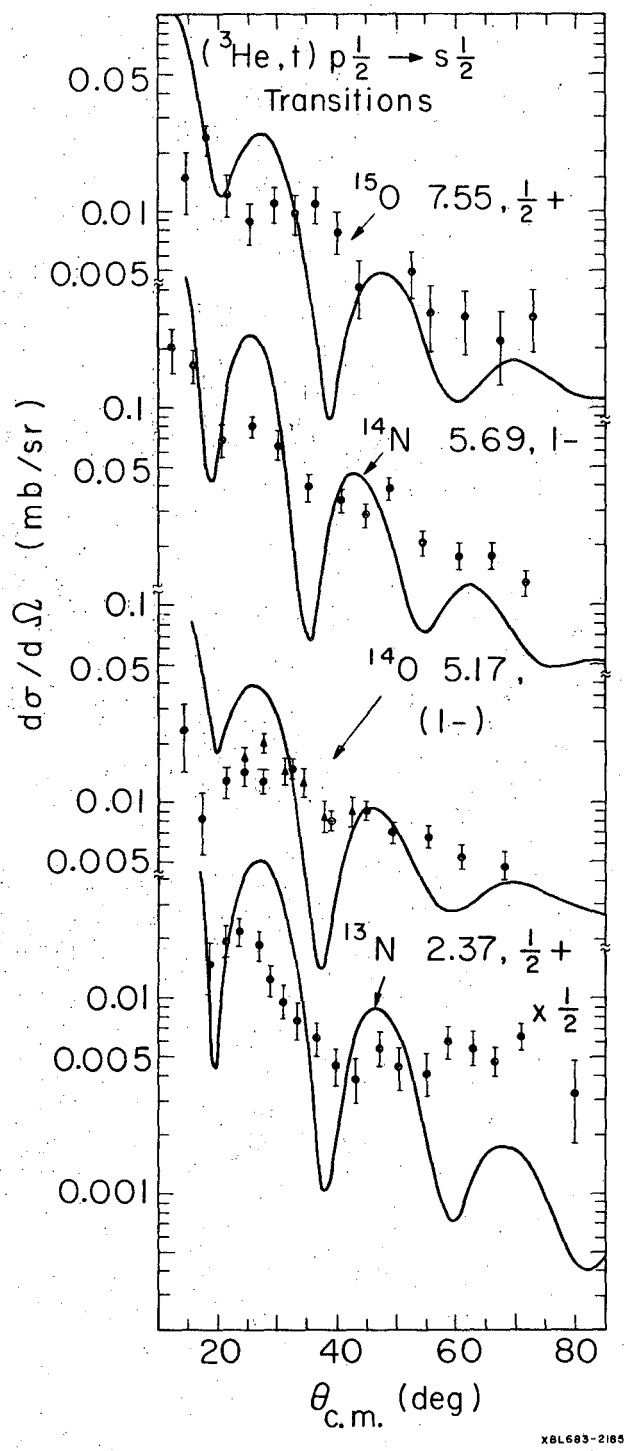

Fig. 42. Angular distributions for (^{3}He,t) p1/2→ s1/2 transitions. The curves are DWBA predictions obtained using j-j wave functions and the independent optical potentials given in Table VII.

Table XX. Experimental strengths for the effective nucleon-nucleon interaction at α^{-1}=1.0 F obtained from (^{3}He,t), p1/2→ s1/2 transitions.

Reaction	Energy (MeV)	J^{π},T	Independent Optical Potentials		Average Optical Potential	
			V_{01}(MeV)	V_{11}(MeV)	V_{01}(MeV)	V_{11}(MeV)
^{15}N(^{3}He,t)^{15}O	6.79	3/2+,1/2	23.6	23.6	23.1	23.1
	6.86[a]	5/2+,1/2				
	7.55[†]	1/2+,1/2	19.8	15.8	19.4	15.5
^{14}N(^{3}He,t)^{14}O	5.17[†]	1- ,1	16.2	13.0	19.3	15.5
^{14}C(^{3}He,t)^{14}N	5.69	1- ,0	23.5	23.5	23.0	23.0
^{13}C(^{3}He,t)^{13}N	2.37[†]	1/2+,1/2	13.5	10.7	12.0	9.5
			19.3±4	17.3±5	19.4±3	17.3±5

[†]EB_2 was assumed to be equal to 400 keV (see Sec. VA-3).

[a]The contribution from the 6.86 MeV, p1/2→ d5/2 transition is included.

Table XXI. A comparison of inelastic ^{3}He and α-particle scattering on 1p shell nuclei.

Dominant Single-Particle Transition		Energy (MeV)	J^π,T	Integrated Cross Sections ($\theta_{c.m.}$=20- 80 deg.) Absolute (mb) (^{3}He,^{3}He')	Absolute (mb) (α,α')[a]	Relative (^{3}He,^{3}He')	Relative (α,α')	G^2(LOLO) Relative (CK)	G^2(LOLO) Relative (jj)
p3/2→ p1/2	^{15}N	6.32	3/2-,1/2	1.70	3.80	1.31	1.56	1.03	1.0
	^{14}N	3.95	1+ ,0	1.30	2.44	1.0	1.0	1.0	1.0
		7.03	2+ ,0	1.61	2.59	1.24	1.06	0.91	1.0
	^{13}C	3.68	3/2-,1/2	4.25	12.10	3.27	4.95	2.78	1.5
		7.55	5/2-,1/2	4.29	12.60	3.30	5.16	2.66	1.2
		8.86	1/2-,1/2	0.289[b]	c	0.22	d	0.0000	e
		11.84	3/2-,1/2	1.58	c	1.22	d	0.0017	0.3
	^{12}C	4.43	2+ ,0	22.9	41.1	17.6	16.8	10.15	4.0
						$\sigma_\alpha/\sigma_{^3He}$ = 1.88		$G^2_\alpha/G^2_{^3He}$ = 1.78	
p1/2→ d5/2	^{15}N	5.27	5/2+,1/2	2.02	7.38	1.34	1.42		1.69[f]
		5.30	1/2+,1/2						
		7.15	5/2+,1/2	0.308	0.591	0.204	0.114		0.402
		7.56	7/2+,1/2	1.91	9.16	1.26	1.76		1.28
		8.57	3/2+,1/2	0.174	0.516	0.115	0.10		e
	^{14}N	5.10	2- ,0	1.10	3.68	0.728	0.71		1.25
		5.83	3- ,0	1.51	5.18	1.0	1.0		1.0
	^{13}C	3.85	5/2+,1/2	1.43	4.18	0.947	0.807		1.12

Table XXI. (continued)

Dominant Single-Particle Transition		Energy (MeV)	J^{π},T	Integrated Cross Sections ($\theta_{c.m.}$=20 - 80 deg.) Absolute (mb) (^{3}He,^{3}He')	Absolute (mb) (α,α')[a]	Relative (^{3}He,^{3}He')	Relative (α,α')	G^2(LOLO) Relative (CK)	G^2(LOLO) Relative (jj)
	^{12}C	9.64	3- ,0	4.19	22.7	2.78	4.38		-
						$\sigma_{\alpha}/\sigma_{^3He}$ = 3.43		$G^2_{\alpha}/G^2_{^3He}$ = 1.78	
p1/2→ s1/2	^{15}N	7.30	3/2+,1/2	0.659	3.23	1.58	1.98		2.0
		8.31	1/2+,1/2	0.109	0.747	0.262	0.458		0.25
	^{14}N	4.91	0- ,0	0.416	1.63	1.0	1.0		1.0
		5.69	1- ,0	0.464	1.82	1.11	1.12		2.0
	^{13}C	3.09	1/2+,1/2	0.690	3.41	1.66	2.09	1.5	1.5
						$\sigma_{\alpha}/\sigma_{^3He}$ = 3.92		$G^2_{\alpha}/G^2_{^3He}$ = 1.78	

[a]Harvey et al., see Ref. 62.

[b]$\theta_{c.m.}$ = 25 - 80 deg.

[c]Not reported in Ref. 62.

[d]These levels are populated in the (α,α') reaction at E_{α} = 64.5 MeV with approximately the same relative intensities as those observed in the (^{3}He,^{3}He') reaction (compare Figs. 7 and 35).

[e]Forbidden in the j-j limit.

[f]The contribution from the 5.30 MeV, 1/2+ level has been neglected.

involved, and in each case the cross sections have been arbitrarily normalized relative to the one single-particle transition in that group which was predicted to be the most insensitive to spin- and isospin-dependent terms. The overall agreement is excellent considering the simplicity of the comparison which is made. In addition, the nuclear structure factors G^2(LOLO) are able to reproduce the observed trends in the relative magnitudes without actually carrying out a DWBA calculation.

If these reactions are only dependent upon the Wigner term V_{00}, then the predicted cross sections for identical states should be proportional to the square of the number of nucleons in the projectile. In Table XXI it can be seen that the ratio of the integrated cross sections $\sigma_\alpha/\sigma_{^3He}$ ranges from 1.88 - 3.92 while the theoretically predicted value is 16/9 = 1.78.

In order to provide a better comparison for these reactions, a microscopic analysis was carried out for the $^{14}N(\alpha,\alpha')^{14}N$ reaction using the optical potential shown in Table VII. A Yukawa potential with a range of α^{-1} = 1.2 F was chosen for the effective projectile-nucleon interaction while a nonlocality range β = 0.25 was assumed for the α particle. The results are shown in Fig. 43; the agreement between theory and experiment is reasonably good considering the fact that no attempt was made to vary the parameters in order to improve the theoretical fits.

The values obtained for V_{00} which have been converted to an effective nucleon-nucleon interaction at α^{-1} = 1.0 F (i.e., Eq. (8) was used[85] with γ = 0.329[5] and a range correction from 1.2 to 1.0 F was applied) are compared with those determined for the (^3He,$^3He'$) reaction in Table XXII. Reasonably consistent results are obtained for p3/2→p1/2 and p1/2→s1/2 transitions but the strengths required to fit the (α,α') p1/2→d5/2 transitions are somewhat larger. It can be concluded, however, that the microscopic description is able to account for the observed experimental data from both reactions.

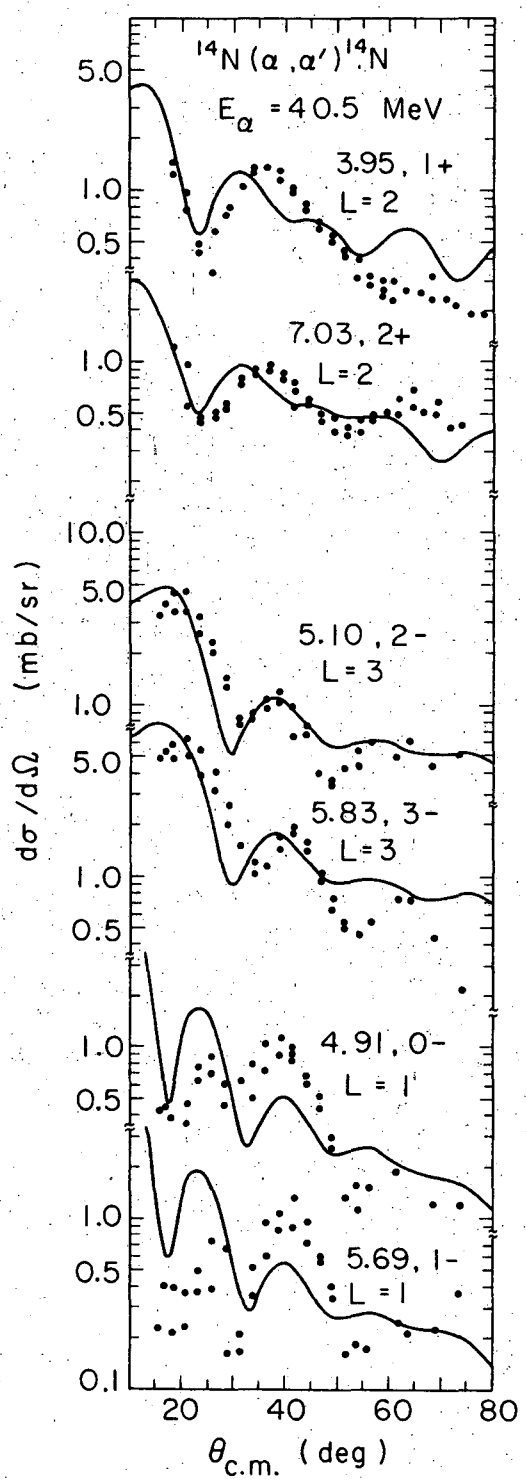

Fig. 43. Angular distributions from the $^{14}N(\alpha,\alpha')^{14}N$ reaction at E_α = 40.5 MeV. The solid curves are DWBA predictions obtained using the optical potential set M (see Table VII). Mixed CK wave functions were used for p shell transitions while simple j-j configurations were assumed for p1/2→ s1/2, d5/2 transitions.

Table XXII. A comparison of the experimental strengths for the effective nucleon-nucleon interaction at $\bar{\alpha}^{-1}$=1.0 F obtained from the $^{14}N(^{3}He,^{3}He')^{14}N$ and $^{14}N(\alpha,\alpha')^{14}N$ reactions at $E_{^3He}$=44.6 and E_{α}=40.5 MeV, respectively.

			V_{00}(MeV)					
			$(^3He,^3He')^a$				(α,α')	
			Wigner Force		Serber Force		Wigner Force	
Energy (MeV)	J^{π}	Dominant Single-Particle Transition	(jj)	(CK)	(jj)	(CK)	(jj)	(CK)
3.95	1+	p3/2→ p1/2	48.9	49.5	47.0	49.3	53.4	54.2
7.03	2+		59.9	63.7	50.9	52.2	54.6	58.0
4.91	0-	p1/2→ s1/2	53.6	-	52.8		58.5	
5.69	1-		46.3	-	45.3		45.4	
5.10	2-	p1/2→ d5/2	68.8	-	67.0		82.7	
5.83	3-		89.8	-	86.4		112.0	

[a]All values quoted were obtained using the average optical potential.

D. The $^{12}C(p,p')^{12}C$ and $^{12}C(^3He,^3He')^{12}C$ Reactions

An investigation of the $^{12}C(p,p')^{12}C$ reaction at $E_p = 46$ MeV has been reported recently by Petersen et al.[80] These data were analyzed using both an extended version of the collective model which included spin and isospin oscillations[67,86] and also a microscopic description which made use of the distorted-wave impulse-approximation (DWIA).[80] In the DWIA procedure, the projectile-nucleon interaction is replaced by the transition matrix for free nucleon-nucleon scattering.[1,29] Since the interaction is determined, the agreement with experiment provides a test of the nuclear wave functions used to describe the initial and final states provided the DWIA is valid at this energy. Fair agreement was obtained when the wave functions of Gillet[87] were used to describe the levels of ^{12}C.

A comparison of the effective interaction required to fit these data using the wave functions of CK with that required to fit the corresponding ($^3He,^3He'$) data should provide a sensitive test of the approximations made in determining the absolute strength of the effective nucleon-nucleon interaction from the scattering of complex projectiles (see Eq. (8)). The calculations were performed using the optical parameter set V1 (see Table VII).[67] A Yukawa potential with a range of $\alpha^{-1} = 1.0$ F was chosen for the effective interaction while the nonlocality range for a proton was assumed to be $\beta = 0.85$ F. The results are shown in Fig. 44; theoretical angular distributions for restricted L = 2 transitions are very similar to those obtained previously using the collective[67] and microscopic[80] models while the dominant L = 0 distributions are still unable to fit the experimental data at small angles. The values obtained for V_{ST} are compared with those from the ($^3He,^3He'$) reaction in Table XXIII. The overall agreement is fair, indicating that the approximations which were made in the ($^3He,^3He'$) reaction are probably valid.

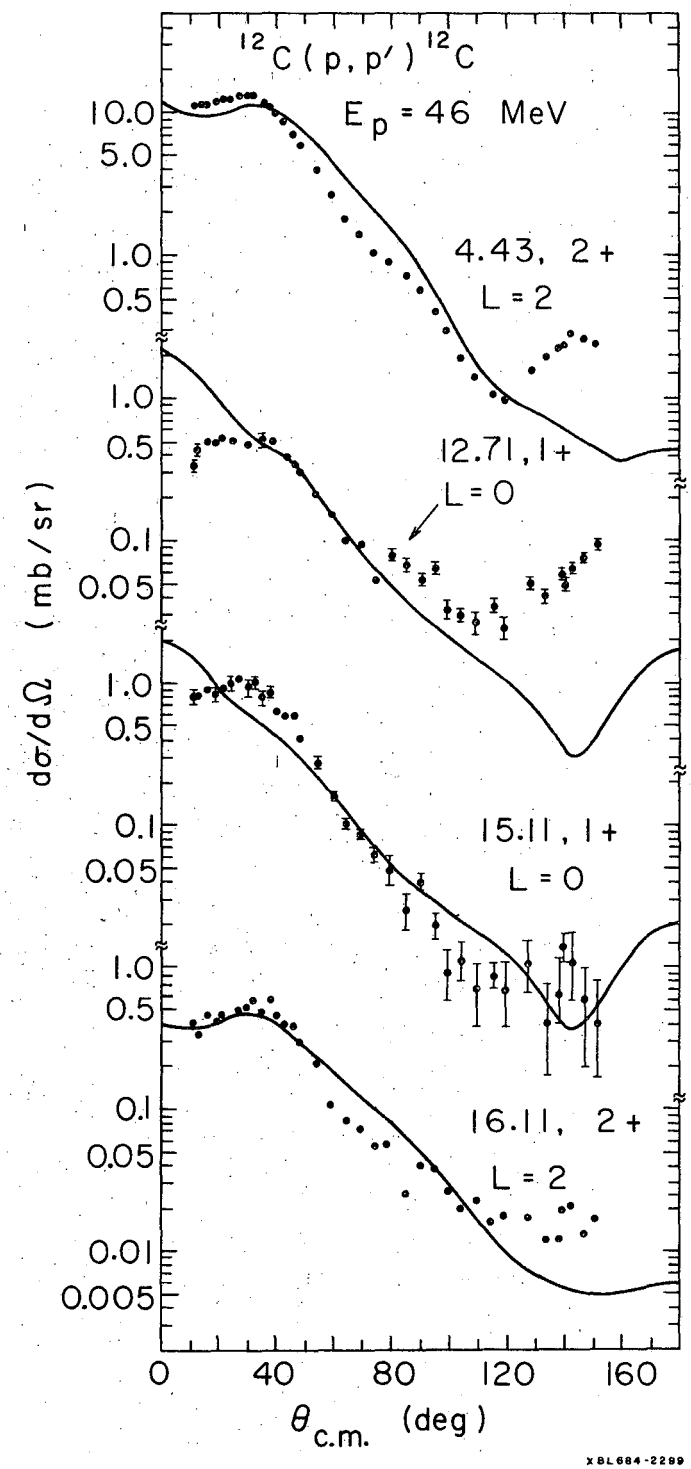

Fig. 44. Angular distributions from the $^{12}C(p,p')^{12}C$ reaction at $E_p = 46$ MeV. The solid curves are DWBA predictions obtained using CK wave functions, a Serber exchange mixture, and the optical potential set V1 (see Table VII).

Table XXIII. A comparison of the experimental strengths for the effective nucleon-nucleon interaction at α^{-1}=1.0 F obtained from the $^{12}C(^{3}He,^{3}He')^{12}C$, $^{12}C(^{3}He,t)^{12}N$ and $^{12}C(p,p')^{12}C$ reactions at $E_{^3He}$=49.8 MeV and E_p=46 MeV, respectively.

Energy (MeV)				$(^3He,^3He')^a$				$(^3He,t)^a$		(p,p')			
				Wigner Force		Serber Force		Serber Force		Wigner Force		Serber Force	
^{12}C	^{12}N	J^{π},T	V_{ST}	(jj)	(CK)	(jj)	(CK)	(jj)	(CK)	(jj)	(CK)	(jj)	(CK)
4.43	-	2+,0	V_{00}	92.7	59.0	92.0	59.0	-	-	137.0	87.1	127.0	86.9
12.71	-	1+,0	V_{10}	-	-	10.6	27.0	-	-			9.4	23.7
15.11	0.0	1+,1	V_{11}	-	-	10.2	24.3	10.1	24.4	-	-	10.8	26.1
16.11	0.96	2+,1	V_{01}, V_{11}	-	-	29.4	46.1	29.3	45.8	-	-	20.2	31.6

[a] All values quoted were obtained using the average optical potential.

E. A comparison of the Effective and Free Nucleon-Nucleon Interaction

It is interesting to compare the effective nucleon-nucleon interaction required to fit the (^{3}He,t) and (^{3}He,^{3}He') scattering data with those used in simple shell-model calculations and those required to fit low-energy nucleon-nucleon scattering data. In order to facilitate this comparison it is helpful to briefly summarize the different forms in which a simple local interaction is generally used. In particular, a simple local interaction with an arbitrary spin-isospin exchange mixture can be written in one of three equivalent forms given by:

$$V(r_{12}) = V_0[W + MP^x + BP^\sigma - HP^\tau]\, g(r_{12}) \quad , \tag{21}$$

where V_0 is in MeV, W, M, B and H are constants and P^x, P^σ and P^τ are space, spin and isospin exchange operators; or

$$V(r_{12}) = V_0[A_{TE}P_{TE} + A_{SE}P_{SE} + A_{TO}P_{TO} + A_{SO}P_{SO}]\, g(r_{12}) \quad , \tag{22}$$

where A_{TE}, A_{SE}, A_{TO} and A_{SO} are constants and P is a projection operator for the triplet-even, singlet-even, triplet-odd and singlet-odd states; or

$$V(r_{12}) = [V_{00} + V_{10}\, \underset{\sim}{\sigma}_1\cdot\underset{\sim}{\sigma}_2 + \underset{\sim}{\tau}_1\cdot\underset{\sim}{\tau}_2(V_{01}+V_{11}\, \underset{\sim}{\sigma}_1\cdot\underset{\sim}{\sigma}_2)]\, g(r_{12}) \ , \tag{23}$$

where V_{ST} are in MeV. Expressions have been given elsewhere[3,4] which relate the coefficients of the individual terms for different parameterizations.

The coefficients predicted for several different exchange mixtures[3,56,88-90] are given in Table XXIV. Although most of these potentials have been used in shell-model calculations, the strengths were chosen to fit low-energy nucleon-nucleon scattering data. In particular all of these exchange mixtures, with the exception of the Serber force, have a singlet-even potential which reproduces low energy proton-proton scattering data[56,90-92] data and in addition, the ratio of the singlet-even to triplet-even strengths is approximately equal to that required to reproduce the binding energy of the deuteron (or neutron-proton scattering data).[3,56,92,93]

Table XXIV. A comparison of V_{ST} for various exchange mixtures used in nucleon-nucleon scattering and shell-model calculations.

$$V(r_{12}) = V_o\ (W+MP^x+BP^\sigma-HP^\tau)\ \exp-(\alpha r_{12})/\alpha r_{12}$$

where α^{-1} = 1.0 F and V_o = -135 MeV (A_o = 1697 MeV F^3)

Exchange Mixture	W	M	B	H	A_{TE}	A_{SE}	A_{TO}	A_{SO}	V_{00} [a]	V_{10} [a]	V_{01} [a]	V_{11} [a]
1. Serber	0.5	0.5	0.0	0.0	1.0	1.0	0.0	0.0	-50.6	16.9	16.9	16.9
2. Glendenning & Veneroni [b,c]	0.4	0.4	0.1	0.1	1.0	0.6	0.0	0.0	-40.5	6.8	20.2	13.5
3. True [d]	0.406	0.406	0.094	0.094	1.0	0.625	0.0	0.0	-41.1	7.4	20.0	13.7
4. Ferrell-Visscher [e]	0.317	0.5	0.0	0.183	1.0	0.634	-0.366	0.0	-13.5	16.9	29.2	16.9
5. Rosenfeld [f]	-0.13	0.93	0.46	-0.26	1.0	0.6	-0.34	-1.78	0.0	0.0	13.5	31.0
Effective nucleon-nucleon interaction					(^{3}He,t)				-	-	|20.6|	|16.5|
					(^{3}He,^{3}He')				|60.2|	|(11-27)|		

[a] All values of V_{ST} were calculated using a Yukawa potential with α^{-1}=1.0 F and V_o=-135 MeV.

[b] A Yukawa with α^{-1}=1.13 F and V_o=-84 MeV (A_o=1523 MeV F^3) reproduces the proton-proton scattering length and effective range (see Ref. 91).

[c] Used by Glendenning and Veneroni[3] in a microscopic analysis of (p,p') reaction on even nickel isotopes; radial dependence: Gaussian, $\beta^{-1/2}$=1.85 F, V_o=-52 MeV (A_o=1835 MeV F^3).

[d] Used by True[56] in a shell-model calculation for levels in ^{14}N; radial dependence: Gaussian, $\beta^{-1/2}$=1.82 F, V_o=-52 MeV (A_o=1760 MeV F^3).

[e] Used in a shell-model calculation of 0+ states in ^{16}O (see Ref. 90); radial dependence: Gaussian, $\beta^{-1/2}$=1.732 F, V_o=-51.9 MeV (A_o=1502 MeV F^3).

[f] A Yukawa with α^{-1}=1.37 F and V_o=-50 MeV (A_o=1615 MeV F^3) gives the singlet-triplet separation for the deuteron.[92]

In order to compare the absolute values for V_{ST} predicted by these exchange mixtures with those obtained in the present analysis, a Yukawa interaction with a range of α^{-1} = 1.0 F and V_o = -135 MeV was chosen. This potential gives a volume integral of A_o = 1697 MeV F^3 which is reasonably similar to those used previously for all exchange mixtures (compare Table XXIV).

Since the Rosenfeld mixture is charge symmetric, while the Ferrell-Vischer exchange mixture was chosen to fit additional properties in ^{4}He and ^{16}O, (see Ref. 90) the first three exchange mixtures listed in Table XXIV should provide the best comparison with the present data. In particular, it can be seen that the values predicted for V_{01} = 16.9-20.2 and V_{11} = 13.5-16.9 MeV are in very good agreement with the values of V_{01} = 20.6 and V_{11} = 16.5 MeV obtained in the (^{3}He,t) analysis, while the values predicted for V_{00} = 40.5-50.6 MeV are somewhat lower than those observed in the (^{3}He,^{3}He') reaction of $V_{00} \cong$ 60.2 MeV. However, if one assumes that the enhancements due to core polarization effects are identical to the enhancements observed in the E2 matrix elements (i.e., 1.5-2.0, see Sec. VB-2),[20] then the values for $V_{00} \cong$ 60.2 MeV are reduced to $\approx$ 30.1-40.2 MeV.

VI. THE (^{3}He,t) AND (^{3}He,^{3}He') REACTIONS POPULATING ANALOG FINAL STATES

A comparison of the (^{3}He,t) and (^{3}He,^{3}He') reactions populating analog final states where $T_f = T_i + 1$ was also of interest in these experiments. In general these transitions were weakly populated; however, it was possible to observe the lowest T = 3/2 levels in mass 9 and 13, the ground isobaric triad in mass 14, and several T = 1 levels in mass 12.

Assuming the charge independence of nuclear forces, the ratio of the differential cross sections for these transitions is given by [see Eqs. (9) and (10)]:

$$\frac{d\sigma(^3\mathrm{He},t)}{d\sigma(^3\mathrm{He},^3\mathrm{He}')} = \frac{k_t}{k_{^3\mathrm{He}}} \times \left| \frac{C_t'(T'T'1;P_i'-P_f')}{C_{^3\mathrm{He}'}'(T'T'1;P_i'-P_f')} \cdot \frac{C_{^3\mathrm{He},t}(T_iT_f1;P_i-P_f)}{C_{^3\mathrm{He},^3\mathrm{He}'}(T_iT_f1;P_i-P_f)} \right|^2$$

$$= \frac{2k_t}{k_{^3\mathrm{He}}} \times \left| \frac{C_{^3\mathrm{He},t}}{C_{^3\mathrm{He},^3\mathrm{He}'}} \right|^2 \qquad (24)$$

For example, a comparison of the ^{12}C(^{3}He,t)^{12}N (g.s.,1+) and ^{12}C(^{3}He,^{3}He')^{12}C (15.11 MeV, 1+) reactions at $E_{^3\mathrm{He}} = 49.8$ MeV gives:

$$\frac{d\sigma(^3\mathrm{He},t)}{d\sigma(^3\mathrm{He},^3\mathrm{He}')} = 2 \times \frac{1.61}{1.69} \times \left| \frac{(011;01)}{(011;00)} \right|^2 = 1.90 \quad .$$

This expression, Eq. (24), has ignored the differences between the t and ^{3}He energies, Coulomb potentials, and internal wave functions in the exit channels. These will be discussed further later.

A. T = 3/2 Levels in Mass 9, 13 and 15

The $^{9}Be(^{3}He,t)^{9}B$ and $^{9}Be(^{3}He,^{3}He')^{9}Be$ reactions were investigated at $E_{^{3}He}$ = 39.8 MeV; typical energy spectra are shown in Fig. 45. The well-known 3/2-, T = 3/2 levels in ^{9}Be at 14.39 MeV and in ^{9}B at 14.67 MeV[94] are both weakly populated in these reactions. Isospin-coupling factors predict that the differential cross sections for T = 3/2 levels populated in the $(^{3}He,t)$ and $(^{3}He,^{3}He')$ reactions should be identical. Although angular distributions were not obtained for these transitions, the observed intensities were approximately equal at three forward angles between θ_L = 13.4 and 16.4 deg.

The lowest T = 3/2 levels in ^{13}C and ^{13}N were also weakly populated in the $(^{3}He,t)$ and $(^{3}He,^{3}He')$ reactions (compare Fig. 7). Unfortunately, an accurate comparison of the differential cross sections for these transitions could not be made due to poor statistics plus ^{12}C and hydrogen target impurities which made the observation of the T = 3/2 level in ^{13}C impossible at forward angles.

Since $p1/2 \rightarrow s1/2$ transitions are generally weakly populated in the $(^{3}He,t)$ reaction (compare Fig. 42), it was not possible to observe the lowest T = 3/2 levels in ^{15}N and ^{15}O which are presumed to have the dominant configuration $[(p1/2)^{2}_{0}\ s1/2]_{1/2+,T=3/2}$. In particular, assuming pure j-j configurations, these transitions are predicted to have a differential cross section which is 1.5 times smaller than that observed for the 7.55 MeV level in ^{15}O. However, this level has a peak cross section of only 23 μb. and is barely observable in a typical energy spectrum (compare Fig. 11). The situation for observing the T = 3/2 levels becomes even more hopeless when one notes that the 11.62 MeV 1/2+, T = 3/2 level in ^{15}N is known to have a width of ≈ 450 keV.[44]

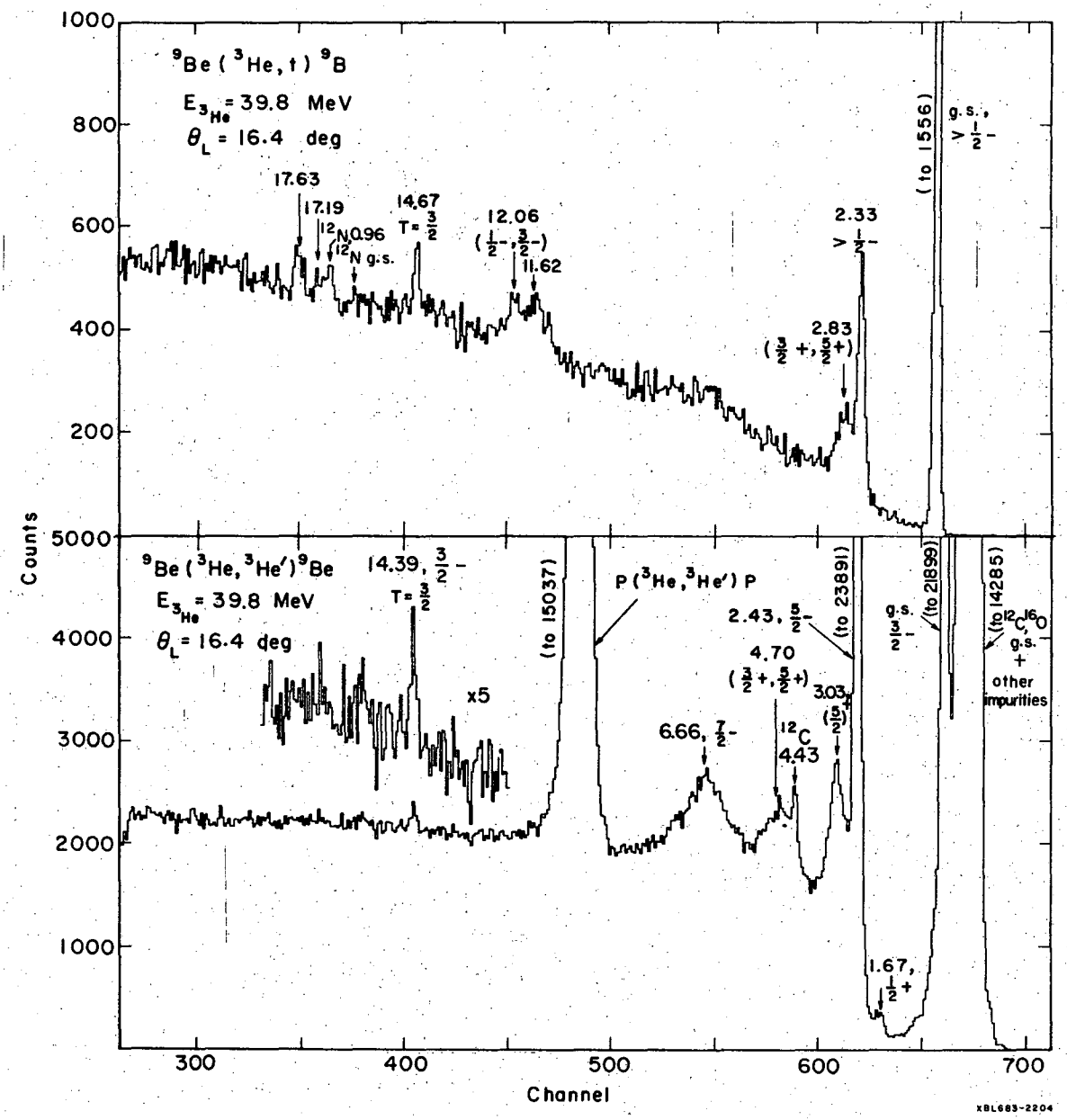

Fig. 45. Energy spectra of the ^{9}Be(^{3}He,t)^{9}B and ^{9}Be(^{3}He,^{3}He′)^{9}Be reactions at $E_{^3He}$ = 39.8 MeV and a scattering angle of 16.4 deg. The ^{9}B spectrum has been adjusted to align the mirror levels populated in both reactions.

B. The $^{14}N(^{3}He,t)^{14}O$ (g.s.,0+), $^{14}N(^{3}He,^{3}He')^{14}N$ (2.31 MeV,0+) and $^{14}C(^{3}He,t)^{14}N$ (g.s.,1+) Reactions

The $^{14}N(^{3}He,t)^{14}O$ (g.s.,0+), $^{14}N(^{3}He,^{3}He')^{14}N$ (2.31 MeV, 0+) and the inverse of the $^{14}C(^{3}He,t)^{14}N$ (g.s.,1+) reactions all correspond to transitions between identical initial and final states. The experimental angular distributions which were obtained for these transitions are compared in Fig. 46; the magnitudes have been adjusted to correct for detailed balance, isospin-coupling and phase space factors. In general, these transitions all have similar angular distributions while the corrected integrated cross sections are approximately equal (compare Table XXV). Although the DWBA calculations failed to fit the shapes of these distributions the strengths required for V_{11} are in good relative agreement (compare Table XXV).

A similar comparison of the cross sections observed in the $^{14}N(p,n)^{14}O$ (g.s.,0+), $^{14}N(p,p')^{14}N$ (2.31 MeV,0+), $^{14}N(n,n')^{14}N$ (2.31 MeV,0+) and $^{14}C(p,n)^{14}N$ (g.s.,1+) reactions at $E_p \cong 5$-14 MeV has been reported;[95] comparable results were obtained.

C. T = 1 Levels in ^{12}C and ^{12}N

Several T = 1 levels were populated in both the $^{12}C(^{3}He,t)^{12}N$ and $^{12}C(^{3}He,^{3}He')^{12}C$ reactions (compare Fig. 6). In addition, accurate angular distributions were obtained for the ground and first excited T = 1 levels in ^{12}C and ^{12}N which provide the best comparison of the (^{3}He,t) and (^{3}He,$^{3}He'$) reactions populating analog final states. The two lowest T = 1 levels located in ^{12}C at 15.11 and 16.11 MeV have well-known p shell configurations with spins and parities 1+ and 2+, respectively. While the analogs to these levels in ^{12}N are presumed to be the ground and first excited (0.96 MeV) states,[42] the spin and parity of the latter has not been definitely determined. A comparison of corresponding (^{3}He,$^{3}He'$) and (^{3}He,t) angular distributions for these levels is shown in Fig. 47; the (^{3}He,$^{3}He'$) distributions have been multiplied by 1.90 in order to correct for phase-space and isospin-coupling factors. In general the agreement is very good;

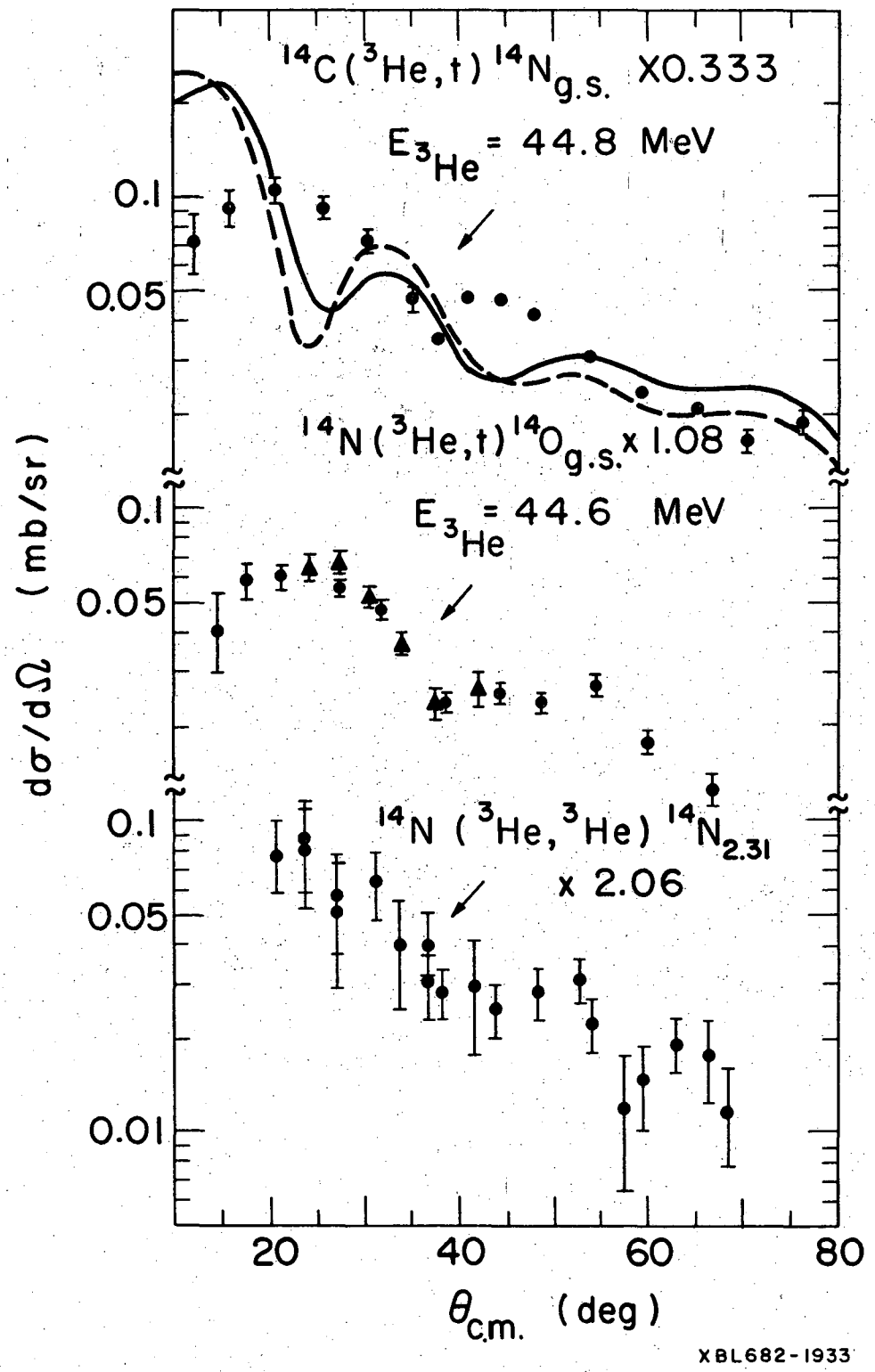

Fig. 46. Angular distributions for the $^{14}C(^3He,t)^{14}N$(g.s.,1+), $^{14}N(^3He,t)^{14}O$ (g.s.,0+) and $^{14}N(^3He,^3He')^{14}N$(2.31 MeV,0+) transitions. The cross sections have been corrected for detailed-balance, phase-space and isospin-coupling factors. The solid and dashed curves are DWBA fits to the $^{14}C(^3He,t)^{14}N$ (g.s.,1+) transition computed using CK and VF wave functions.

Table XXV. A comparison of the (^{3}He,t) and (^{3}He,^{3}He') reactions populating analog states in the mass 14 triad.

Reaction	$E_{^3He}$ (MeV)	Cross Sections ($\theta_{c.m.}$=15 - 80 deg.) Absolute (μb)	Corrected[a] (μb)	V_{11}(MeV) (Average Optical Potential) (jj)	(CK)	(VF)
$^{14}N(^3He,t)^{14}O$ (g.s.,0+)	44.6	117 ± 18[b]	126 ± 19[b]	15.1	20.8	23.7
$^{14}N(^3He,^3He')^{14}N$ (2.31 MeV,0+)	44.6	68 ± 17[b]	140 ± 35[b]	14.7	20.2	23.3
$^{14}C(^3He,t)^{14}N$ (g.s.,1+)	44.8	569 ± 113[b]	189 ± 37[b]	17.7	23.7	25.9

[a]See Fig. 46.

[b]Estimated errors include uncertainties in the absolute differential cross section plus statistical errors.

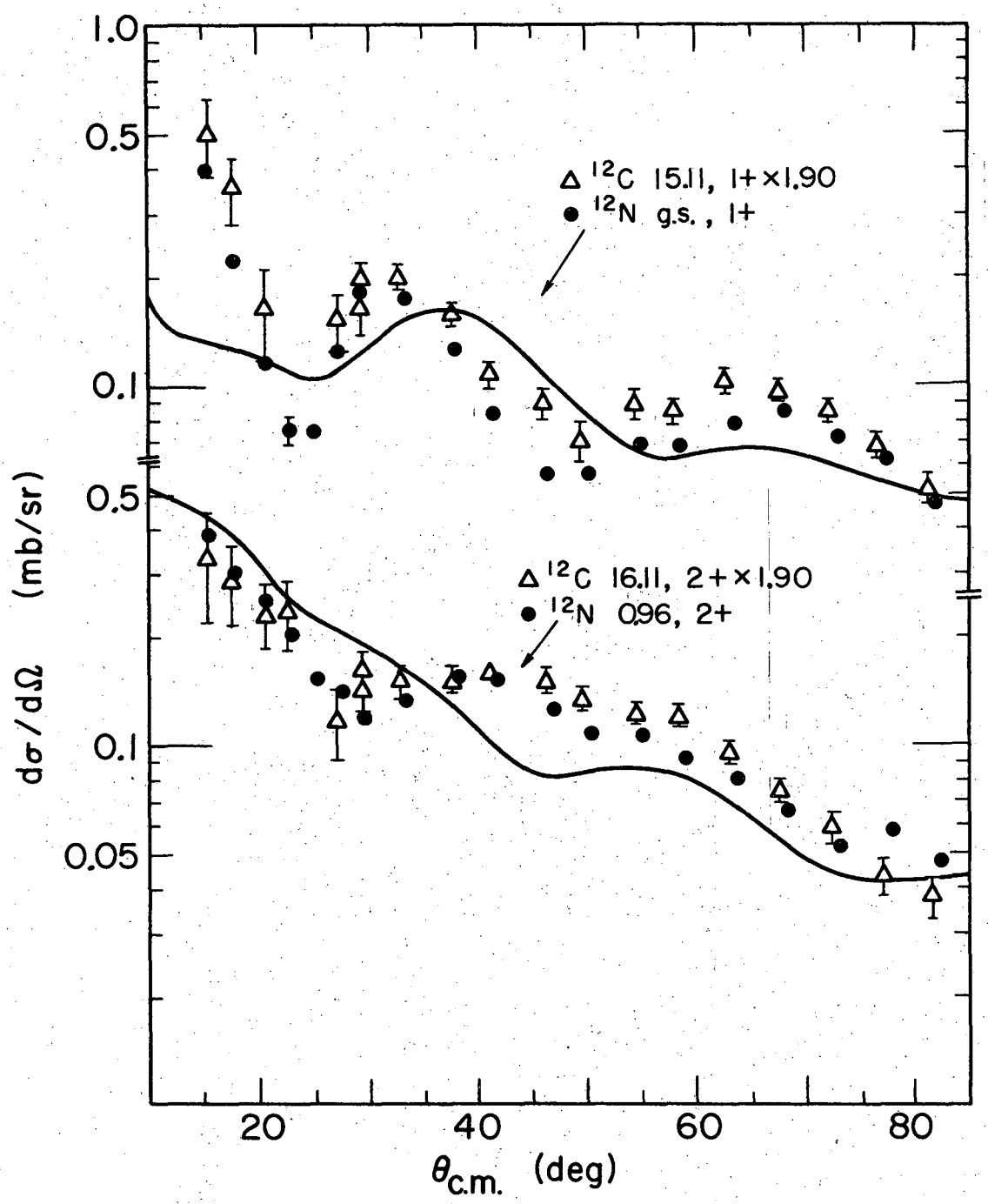

XBL 682-1932

Fig. 47. Angular distributions for the $^{12}C(^{3}He,t)^{12}N$ ground, 1+ and 0.96-MeV, 2+ states and for the $^{12}C(^{3}He,^{3}He')^{12}C$ 15.11-MeV, 1+ and 16.11-MeV, 2+ states. The $(^{3}He,^{3}He')$ cross sections have been mutiplied by 1.90 to correct for phase-space and isospin-coupling factors. The solid curves are DWBA fits to the $(^{3}He,t)$ transitions computed using mixed CK wave functions and the optical potential set F.

however, the (^{3}He,^{3}He') transitions appear to be approximately 10% larger. Although this difference may be due to an incorrect background subtraction for the (^{3}He,^{3}He') transitions, the detailed microscopic analysis also gives an explanation for this effect.

First of all, DWBA calculations predict similar (differing in magnitude by $\leq 5\%$) single-particle cross sections $\sigma(j_1 j_2 L\theta)/k_f$ for the corresponding (^{3}He,t) and (^{3}He,^{3}He') transitions. Therefore, the effects of the differing energies and Coulomb scattering in the exit channels are small. However, a comparison of the theoretical effective projectile-nucleon interaction for tritons or ^{3}He particles indicates that the internal wave functions of the complex projectiles may affect the experimental ratio of these (^{3}He,t) and (^{3}He,^{3}He') transitions. In particular, Eq. (8) predicts that the values for $\overline{V}_{ST}$ should be 1.07 times larger for (^{3}He,^{3}He') transitions (i.e., the cross sections of (^{3}He,^{3}He') transitions should be 1.15 times larger.) As a result, the observed increase in the experimental cross sections for these (^{3}He,^{3}He') transitions can be accounted for and the values obtained for V_{ST} from both reactions are in good agreement (compare Table XXIII). In addition, it can be concluded that the 0.96 MeV level in ^{12}N has a spin and parity of 2+ and is the analog of the 16.11 MeV level in ^{12}C.

All T = 1 levels observed in the ^{12}C(^{3}He,t)^{12}N and ^{12}C(^{3}He,^{3}He')^{12}C reaction are summarized and compared with previous data[42-49] in Tables I and II. With the exception of the 17.26, 17.77 and 19.2 MeV levels, all well-known T = 1 states in ^{12}C were observed up to an excitation energy of 20 MeV. In addition, all previously reported levels in ^{12}N were observed with the exception of the 1.65 MeV level. Since the spins and parities of several T = 1 levels in ^{12}C are well-known, tentative assignments can be made for other excited states in ^{12}N by a comparison of the known excitation energies (see also Ref. 42) and relative intensities of the T = 1 levels populated in the (^{3}He,t) and (^{3}He,^{3}He') reactions. The results are summarized in Table XXVI and also compared with known levels in ^{12}B.[43-45,96] Unfortunately, in most cases a meaningful comparison of the corresponding (^{3}He,t) and (^{3}He,^{3}He') distributions could not be made due to poor statistics, large decay widths and unknown contributions from T = 0 levels (in ^{12}C). The individual assignments will now be discussed in detail.

Table XXVI. T=1 levels in the mass 12 triad.

^{12}B			^{12}C				^{12}N	
J^{π} [a]	Energy[a] (MeV)	Level Shift (keV)[b]	Energy (MeV)	$J^{\pi};T$	Dominant Shell-Model Configuration	Level Shift (MeV)[b]	Energy (MeV)	J^{π}
1+	0.0	-	15.11	1+;1	$(p3/2)^7_{3/2}$ p1/2	-	0.0	1+
2+	0.953	(+47)	16.11	2+;1	$(p3/2)^7_{3/2}$ p1/2	40	0.96	2+
2-	1.674	214	16.57	2-;1	p^7s	260	1.20	(2-)
1-	2.62	470	17.26	1-;1	p^7s	500	1.65	
(≤ 3+)	2.72	60	17.77	0+;1	p^8	230	2.43	
(≤ 3+)	3.39	100	18.40[c]	(;1)		190	3.10	
2+	3.76	60	18.81	2+;1	p^8	200	3.50	
(1-)	4.30	210	19.2	1-,2-;1	p^7 (s;d)	--		
3-	4.54	70	19.58	(;1)		230	4.24	

[a] (See Refs. 43-45, 96).

[b] The level shifts are calculated relative to the ground state multiplet.

[c] A level observed previously in ^{12}C at 18.40 MeV is known to have J^{π}=0-; however, the isobaric spin of this level is unknown (see Ref. 46).

1. The 1.20 and 1.65 MeV Levels in ^{12}N

The 16.57 MeV 2- and 17.26 MeV 1- levels in ^{12}C have the dominant shell-model configuration p^7s.[46,47] On the basis of excitation energies, the analogs to these states in ^{12}N can be tentatively identified as the 1.20 and 1.65 MeV levels, respectively.[42] In addition, since ^{12}C is unbound at 15.957 MeV and ^{12}N is unbound at 0.595 MeV, the large level shifts observed for these states from ^{12}B to ^{12}C and from ^{12}C to ^{12}N (compare Table XXVI) are consistent with the Thomas-Ehrman effect which should be most pronounced for an s state proton.[97] The fact that no visible peaks were observed in the (^3He,$^3He'$) or (^3He,t) reaction corresponding to the ^{12}C 17.26 and ^{12}N 1.65 MeV levels is also consistent with the known large width (≈1.0 MeV) of the 17.26 MeV level.[44] The experimental angular distributions obtained for the ^{12}N, 1.20 MeV and ^{12}C, 16.57 MeV transitions are compared in Fig. 48. The agreement is acceptable considering the statistical uncertainty of the (^3He,$^3He'$) distribution. This evidence further supports a (2-) assignment for the 1.20 MeV level in ^{12}N.

2. The 2.43 and 3.50 MeV Levels in ^{12}N

Evidence from the $^{15}N(p,\alpha)^{12}C$ (see Ref. 98) and the $^{13}C(^3He,\alpha)^{12}C$ reactions[49] indicates that the 17.77 MeV 0+ and 18.81 MeV 2+ levels in ^{12}C have large p shell components. In particular, the spectroscopic factor obtained in the (^3He,α) reaction for the 17.77 MeV level[49] was in good agreement with the theoretical value computed by CK for the lowest 0+, T = 1 level predicted to occur in ^{12}C at 19.597 MeV.[21] In the present work, the 2.43 and 3.50 MeV levels observed in ^{12}N have been tentatively identified as the analogs to 17.77 MeV and 18.81 MeV levels in ^{12}C. Both the relative intensities (compare Fig. 6) and the excitation energies (compare Table XXVI) are in agreement with these assignments. In addition, the mixed CK wave functions predict that the lowest 0+, T = 1 level should be very weakly populated in the (^3He,t) and (^3He,$^3He'$) reactions, as is observed experimentally.

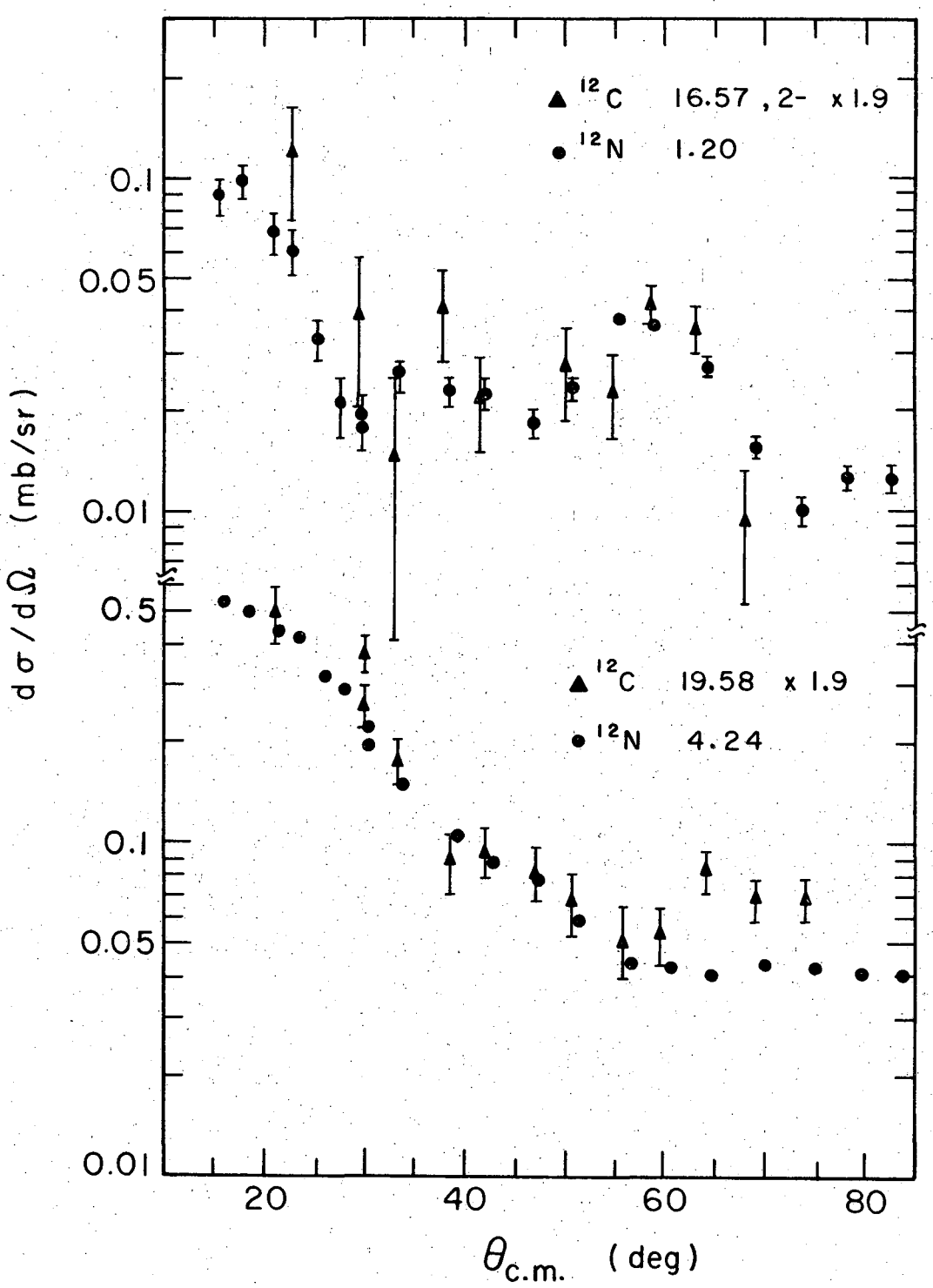

XBL683-2184

Fig. 48. Angular distributions for the $^{12}C(^3He,t)^{12}N$ 1.20-MeV, (2-) and 4.24-MeV states and for the $^{12}C(^3He,^3He')^{12}C$ 16.57-MeV, 2- and 19.58-MeV states. The $(^3He,^3He')$ cross sections have been multiplied by 1.9 to correct for phase-space and isospin-coupling factors.

3. The 3.10 MeV Level in ^{12}N

Neglecting level shifts, the analog to the 3.10 MeV level in ^{12}N is predicted to occur in ^{12}C at 18.21 MeV. In the $^{12}C(^{3}He,^{3}He')^{12}C$ reaction a level is observed at 18.4 MeV which probably corresponds to the analog of the ^{12}N 3.10 MeV level. Although a T = 1 state is not known to occur at this excitation energy in ^{12}C, a level has been reported previously[46] at 18.40 MeV with spin and parity 0- but unknown isobaric spin.

4. The 4.24 MeV Level in ^{12}N

A broad level or group of levels is observed in the $^{12}C(^{3}He,t)^{12}N$ and $^{12}C(^{3}He,^{3}He')^{12}C$ reactions at 4.24 and 19.58 MeV, respectively. The angular distributions obtained for these transitions are compared in Fig. 48; the $(^{3}He,^{3}He')$ distribution has been multiplied by a factor of 1.9 in order to correct for phase-space and isospin-coupling factors. Both distributions have approximately the same shape and magnitude indicating that these transitions correspond to analog final states in ^{12}N and ^{12}C. Although no known T = 1 levels occur at this excitation energy in ^{12}C, a 3- level has been reported in ^{12}B at 4.54 MeV. In addition, a comparison of the relative excitation energies of the ^{12}B - 4.54 MeV, ^{12}C - 19.58 MeV and ^{12}N - 4.24 MeV states give level shifts which are comparable to those observed for other excited triads (compare Table XXVI).

VII. CONCLUSIONS

A microscopic analysis of the (^{3}He,t) and (^{3}He,^{3}He') reactions on 1p shell nuclei has been carried out using a local potential with an arbitrary spin-isospin exchange mixture. Spectroscopic factors were calculated using the intermediate-coupling wave functions of Cohen and Kurath[19] for p shell states while simple j-j configurations were assumed for the levels which were formed by promoting a p1/2 nucleon to the s1/2 or d5/2 shell. A Yukawa interaction with a range of α^{-1} = 1.2 F was found to give the best overall agreement for all transitions. The average strengths obtained for V_{ST} are summarized in Table XXVII and also compared with the results obtained in previous analyses of the (p,p'),[7-10] (p,n)[8,10-12] and (^{3}He,t)[13,14] reactions. In all cases, the values obtained for the effective projectile-nucleon interaction at α^{-1} = 1.2 F have been converted to an effective nucleon-nucleon interaction at α^{-1} = 1.0 F using the relationships given previously by Wesolowski et al.[14] and Johnson et al.[7] (see Eqs. (7) and (8)). Several important results were obtained from this analysis. First, the average values computed for V_{01} = 19.4-20.6 and V_{11} = 16.5-17.3 MeV from the p3/2,p1/2→p1/2, dominant L = 0 and p1/2→s1/2, L = 1 transitions were in very good agreement with those obtained previously in analyses of the (p,n) reaction.[8,10-12] Second, the strengths required to fit the (^{3}He,t) p3/2→p1/2, L = 2 and p1/2→d5/2, L = 1, 3 transitions were enhanced while the experimental angular distributions for these transitions had less structure than those predicted by theoretical calculations. This suggests that core polarization effects or particle-exchange could be contributing to the cross sections for these transitions. A similar effect has been observed for L = 2 transitions in the (p,n) reaction.[11,12]

Further, it was found that the transitions which were strongly populated in the (^{3}He,^{3}He') reaction were generally insensitive to the spin- and isospin-dependent terms in the effective interaction. In addition, the absolute strengths obtained for V_{00} were much smaller than those required to fit the inelastic transitions observed in the (p,p') reaction on several heavier nuclei.[8] As a result, it can be concluded that core polarization effects are much less important for 1p shell nuclei. Unfor-

Table XXVII. Average strengths for the effective nucleon-nucleon interaction at α^{-1}=1.0 F obtained from (^{3}He,^{3}He') and (^{3}He,t) transitions.

	(^{3}He,t) Present Work						(Previous Work)	
	p1/2,p3/2→ p1/2 (L=0)		p3/2→ p1/2 (L=2)		p1/2→ d5/2 (L=1,3)	p1/2→ s1/2 (L=1)	(p,n)[a] L=0	(^{3}He,t)[b] L=0
V_{ST}	(jj)	(CK)	(jj)	(CK)	(jj)	(jj)		
V_{01}	20.4 ± 0.5	20.6 ± 0.4	35.7 ± 5	42.4 ± 5	32.8 ± 12	19.4 ± 3	19-26	31 ± 6
V_{11}	19.2 ± 1.5	16.5 ± 1.1	35.7 ± 5	42.4 ± 5	30.7 ± 11	17.3 ± 5	$\frac{V_{11}}{V_{01}} \cong$ 0.6-1.0	20 ± 4

		(^{3}He,^{3}He') Present Work				(p,p') Previous Work		
		p3/2→ p1/2 (L=2)		p1/2→ d5/2 (L=3)	p1/2→ s1/2 (L=1)		Without[c] Core Polarization	With[d] Core Polarization
V_{ST}	Exchange Mixture	(jj)	(CK)	(jj)	(jj)	Target		
V_{00}	Wigner	73.7 ± 15	60.3 ± 6	76.0 ± 10	53.9 ± 9	^{7}Li	90	-
V_{00}	Serber	73.6 ± 20	60.2 ± 10	67.3 ± 13	47.2 ± 6	^{12}C	86.9[e]	-
V_{00}	Force III	78.1 ± 19	54.2 ± 5	79.0 ± 11	57.9 ± 12	^{18}O, ^{90,92}Zr, ^{208}Pb	≈200	≈80
		(L=0)		(L=1)				
V_{10}	Serber	≈11	≈27	≈22		^{89}Y, ^{90}Zr	≈40[d]	
V_{10}	Force III	≈12	≈27			^{208}Pb		

[a]See Refs. 8,10-12. [b]See Refs. 13,14. [c]See Refs. 8,10. [d]See Ref. 9. [e]See Sec. VD.

tunately, an accurate determination of the spin dependent V_{10} term could not be obtained from these data. In particular, the (^{3}He,^{3}He') transitions which were restricted to be pure s = 1 were also populated in the (α,α') reaction with approximately the same relative intensity indicating that other mechanisms such as multiple excitation also contribute to the cross sections for these transitions.

Finally, it was shown (see Table XXIV) that the effective interaction obtained in the present analysis is very similar to those used in simple shell-model calculations and those required to fit low-energy nucleon-nucleon scattering data.

ACKNOWLEDGEMENTS

I would like to express my sincere appreciation to all those associated with the 88" cyclotron for their assistance and encouragement during the course of this work. I take particular pleasure in thanking:

Professor Joseph Cerny for suggesting these experiments and for his able guidance and continued interest and encouragement in this work;

Dr. Victor A. Madsen for the use of his DRC program and also for several valuable discussions;

Dr. Dieter Kurath for sending me his coefficients of fractional parentage;

Dr. Sam W. Cosper and Dr. Robert L. McGrath for their assistance with the experimental equipment and for many helpful discussions;

Dr. John C. Hardy for his advice concerning the theoretical aspects of this work;

Dr. Bernard G. Harvey, Dr. David L. Hendrie, Dr. Hans H. Duhm, and Dr. Charles Glashausser for helpful discussions;

Mr. Frederick S. Goulding and Mr. Donald A. Landis for providing the electronic equipment;

Mr. Robert Lothrop for supplying the silicon detectors;

Mr. Creve C. Maples for the use of several of his computer programs and for many interesting and helpful discussions;

Dr. Claude Détraz, Dr. Gilbert W. Butler, Dr. Donald G. Fleming, Mr. Heinz Brunnader, Mr. George W. Goth, Mr. John E. Esterl, and Mr. Gordon J. Wozniak for their invaluable assistance during the long hours of data collection and for many valuable discussions;

Dr. Nolan F. Mangelson, Mr. Chi Chang Lu, Mr. Joel M. Moss, Miss Mary F. Reed, and Mr. Michael S. Zisman for several interesting and helpful discussions;

Mr. Claude Ellsworth for preparing the adenine target;

Mr. John Meneghetti and other members of the machine shop for their technical assistance;

Mr. John Bowen and the cyclotron crew for their cooperation;

My wife, Jacqueline, for her continued encouragement and helpful listening and for proofreading the manuscript.

This work was performed under the auspices of the U. S. Atomic Energy Commission.

References

1. R. M. Haybron and H. McManus, Phys. Rev. 136, B1730 (1964); R. M. Haybron and H. McManus, Phys. Rev. 140, B638 (1965).
2. V. A. Madsen and W. Tobocman, Phys. Rev. 139, B864 (1965); N. K. Glendenning and M. Veneroni, Phys. Letters 14, 228 (1965); N. K. Glendenning, Phys. Letters 21, 549 (1966); A. Faessler, N. K. Glendenning, and A. Plastino, Phys. Rev. 159, 846 (1967).
3. N. K. Glendenning and M. Veneroni, Phys. Rev. 144, 839 (1966).
4. G. R. Satchler, Nucl. Phys. 77, 481 (1966).
5. V. A. Madsen, Nucl. Phys. 80, 177 (1966).
6. W. S. Gray, R. A. Kenefick, J. J. Kraushaar, and G. R. Satchler, Phys. Rev. 142, 735 (1966); M. M. Stautberg and J. J. Kraushaar, Phys. Rev. 151, 969 (1966); M. M. Stautberg, J. J. Kraushaar, and B. W. Ridley, Phys. Rev. 157, 977 (1967); M. M. Stautberg, R. R. Johnson, J. J. Kraushaar, and B. W. Ridley, Nucl. Phys. A104, 67 (1967); R. W. Barnard and G. D. Jones, Nucl. Phys. A106, 497 (1968); ibid A108, 655 (1968); ibid A111, 17 (1968).
7. M. B. Johnson, L. W. Owen, and G. R. Satchler, Phys. Rev. 142, 748 (1966).
8. G. R. Satchler, Nucl. Phys. A95, 1 (1967).
9. W. G. Love and G. R. Satchler, Nucl. Phys. A101, 424 (1967).
10. P. J. Locard, S. M. Austin, and W. Benenson, Phys. Rev. Letters 19, 1141 (1967).
11. C. Wong, J. D. Anderson, J. McClure, B. Pohl, V. A. Madsen, and F. Schmittroth, Phys. Rev. 160, 769 (1967).
12. S. D. Bloom, J. D. Anderson, W. F. Hornyak, and C. Wong, Phys. Rev. Letters 15, 264 (1965); J. D. Anderson, in Isobaric Spin in Nuclear Physics, ed. by J. D. Fox and D. Robson (Academic Press, New York, 1966) p. 530; C. Wong, J. D. Anderson, S. D. Bloom, V. A. Madsen, and F. Schmittroth, Lawrence Radiation Laboratory Report UCRL-70451, 1967 (unpublished).
13. L. F. Hansen, M. L. Stelts, J. G. Vidal, and J. J. Wesolowski, Lawrence Radiation Laboratory Report UCRL-70454, 1967 (unpublished); Bull. Am. Phys. Soc. 12, 534 (1967); L. F. Hansen, M. L. Stelts, and

J. J. Wesolowski, Bull. Am. Phys. Soc. 13, 632 (1968); L. F. Hansen, M. L. Stelts, J. G. Vidal, J. J. Wesolowski, and V. A. Madsen, Phys. Rev. (to be published).

14. J. J. Wesolowski, E. H. Schwarcz, P. G. Roos, and C. A. Ludemann, Phys. Rev. (to be published).

15. H. E. Wegner and W. S. Hall, Phys. Rev. 119, 1654 (1960); A. G. Blair and H. E. Wegner, Phys. Rev. Letters 9, 168 (1962); M. E. Rickey, P. D. Kunz, J. J. Kraushaar, and W. G. Anderson, Phys. Letters 17, 296 (1965); P. F. Donovan and P. D. Parker, Phys. Rev. Letters 14, 147 (1965); R. Sherr, A. G. Blair, and D. D. Armstrong, Phys. Letters 20, 392 (1966); N. Mangelson, M. Reed, C. C. Lu, and F. Ajzenberg-Selove, Phys. Letters 21, 661 (1966); N. Mangelson, F. Ajzenberg-Selove, M. Reed, and C. C. Lu, Nucl. Phys. 88, 137 (1966); P. C. Rogers and H. E. Wegner, Phys. Rev. Letters 17, 148 (1966); W. Whaling, Phys. Rev. 150, 836 (1966); S. F. Eccles, H. F. Lutz, and T. S. Bohn, Lawrence Radiation Laboratory Report UCRL-50001-66-1, 1966 (unpublished), p. 13; L. G. Earwaker, Nucl. Phys. A90, 56 (1967); P. G. Roos, C. A. Ludemann, and J. J. Wesolowski, Phys. Letters 24B, 656 (1967).

16. R. H. Pehl and J. Cerny, Phys. Letters 14, 137 (1965).

17. See the following and references cited therein:
J. Aguilar, W. E. Burcham, J. B. A. England, A. Garcia, P. E. Hodgson, P. V. March, J. S. C. McKee, E. M. Mosinger, and W. T. Toner, Proc. Roy. Soc. (London) A257, 13 (1960); E. R. Flynn and R. H. Bassel, Phys. Rev. Letters 15, 168 (1965); R. J. Griffiths, Nucl. Phys. A102, 329 (1967); E. F. Gibson, J. J. Kraushaar, B. W. Ridley, M. E. Rickey, and R. H. Bassel, Phys. Rev. 155, 1208 (1967).

18. G. C. Ball and J. Cerny, Phys. Rev. 155, 1170 (1967).

19. S. Cohen and D. Kurath, Nucl. Phys. 73, 1 (1965).

20. A. R. Poletti, E. K. Warburton, and D. Kurath, Phys. Rev. 155, 1096 (1967); G. A. Beer, P. Brix, H. G. Clerc, and B. Laube, Phys. Letters 26B, 506 (1968).

21. S. Cohen and D. Kurath, Nucl. Phys. A101, 1 (1967); D. Kurath, (private communication).

22. G. R. Satchler, Nucl. Phys. 55, 1 (1964) and other references given there.

23. B. L. Cohen, and A. G. Rubin, Phys. Rev. 111, 1568 (1958).

24. R. H. Bassel, G. R. Satchler, R. M. Drisko, and E. Rost, Phys. Rev. 128, 2693 (1962); E. Rost, Phys. Rev. 128, 2708 (1962); B. Buck, Phys. Rev. 130, 712 (1963); G. R. Satchler, R. H. Bassel, and R. M. Drisko, Phys. Letters 5, 256 (1963).

25. A. M. Lane, Phys. Rev. Letters 8, 171 (1962); Nucl. Phys. 35, 676 (1962).

26. J. D. Anderson, C. Wong, J. W. McClure, and B. D. Walker, Phys. Rev. 136, B118 (1964); R. M. Drisko, P. G. Roos, and R. H. Bassel, Oak Ridge National Laboratory Report ORNL-4122, 1966 (unpublished), p. 63.

27. R. M. Drisko, R. H. Bassel, and G. R. Satchler, Phys. Letters 2, 318 (1962); G. R. Satchler, R. M. Drisko, and R. H. Bassel, Phys. Rev. 136, B637 (1964).

28. C. Wong, J. D. Anderson, J. W. McClure, and B. Pohl, Phys. Rev. 156, 1266 (1967).

29. A. K. Kerman, H. McManus, and R. M. Thaler, Ann. of Phys. 8, 551 (1959).

30. C. A. Levinson and M. K. Banerjee, Ann. of Phys. 3, 67 (1958); A. Agodi and G. Schiffrer, Nucl. Phys. 50, 337 (1964).

31. T. Une, S. Yamaji, and H. Yoshida, Progr. Theoret. Phys. 35, 1010 (1966).

32. K. A. Amos, V. A. Madsen, and I. E. McCarthy, Nucl. Phys. A94, 103 (1967).

33. Jay Atkinson and V. A. Madsen, Lawrence Radiation Laboratory Report, UCRL-70635, 1967 (unpublished); Bull. Am. Phys. Soc. 13, 631 (1968).

34. J. L. Gammel, R. S. Christian, and R. M. Thaler, Phys. Rev. 105, 311 (1957); J. L. Gammel and R. M. Thaler, Phys. Rev. 107, 291, 1337 (1957); P. S. Signel and R. E. Marshak, Phys. Rev. 109, 1229 (1958); E. K. Lassila, M. H. Hull, H. M. Ruppel, F. A. McDonald, and G. Breit, Phys. Rev. 126, 881 (1962); T. Hamada and I. D. Johnston, Nucl. Phys. 34, 382 (1962).

35. D. G. Fleming, J. Cerny, C. C. Maples, and N. K. Glendenning, Phys. Rev. 166, 1012 (1968).

36. G. W. Butler, J. Cerny, S. W. Cosper, and R. L. McGrath, Phys. Rev. 166, 1096 (1968).

37. F. S. Goulding, Nucl. Instr. Methods 43, 1 (1966).

38. F. S. Goulding, D. A. Landis, J. Cerny, and R. H. Pehl, Nucl. Instr. Methods 31, 1 (1964).

39. Hamilton Watch Co., Metals Division, Lancaster, Pa.

40. A. M. Baldin, V. I. Gol'danskii, and I. L. Rozenthal, Kinematics of Nuclear Reactions, Translated by W. E. Jones, (Pergamon Press, Ltd., New York, 1961), p. 141.

41. R. H. Pehl, Ph.D. Thesis, Lawrence Radiation Laboratory Report UCRL-10993, 1963 (unpublished).

42. C. D. Zafiratos, F. Ajzenberg-Selove, and F. S. Dietrich, Nucl. Phys. 77, 81 (1966).

43. F. Ajzenberg-Selove and T. Lauritsen, Nucl. Phys. (to be published).

44. F. Ajzenberg-Selove and T. Lauritsen, Nucl. Phys. 11, 1 (1959).

45. T. Lauritsen and F. Ajzenberg-Selove, Nuclear Data Sheets, compiled by K. Way et al., (Printing and Publishing Office, National Academy of Sciences- National Research Council, Washington 25, D. C., 1962), sets 5 and 6; F. Ajzenberg-Selove (private communiation).

46. R. E. Segel, S. S. Hanna, and R. G. Allas, Phys. Rev. 139, B818 (1965).

47. I. Talmi and I. Unna, Phys. Rev. Letters 4, 469 (1960); N. Vinh-Mau and G. E. Brown, Nucl. Phys. 29, 89 (1962).

48. D. E. Alburger and D. H. Wilkinson, Phys. Rev. 153, 1061 (1967).

49. G. C. Ball and J. Cerny, Bull. Am. Phys. Soc. 12, 1144 (1967);(to be published).

50. D. Bachelier, M. Bernas, I. Brissaud, P. Radvanyi, and M. Roy, Nucl. Phys. 88, 307 (1966); R. L. Kozub, L. A. Kull, and E. Kashy, Nucl. Phys. A99, 540 (1967); F. Hinterberger, G. Mairle, V. Schmidt-Rohr, P. Turek, and G. J. Wagner, Nucl. Phys. A106, 161 (1968).

51. G. C. Ball and J. Cerny, Phys. Letters 21, 551 (1966).

52. F. C. Barker, Nucl. Phys. 28, 96 (1961); T. Sebe, Progr. Theoret. Phys. (Kyoto) 30, 290 (1963).

53. N. F. Mangelson, Ph.D. Thesis, Lawrence Radiation Laboratory Report UCRL-17732, 1967 (unpublished) and other references listed there.

54. E. K. Warburton and W. T. Pinkston, Phys. Rev. 118, 733 (1960).

55. H. J. Rose, Nucl. Phys. 19, 113 (1960); H. J. Rose, F. Riess, and W. Trost, Nucl. Phys. 52, 481 (1964).

56. W. W. True, Phys. Rev. 130, 1530 (1963).

57. G. W. Phillips, F. C. Young, and J. B. Marion, Phys. Rev. 159, 891 (1967) and references given there.

58. M. Lambert and M. Durand, Phys. Letters 24B, 287 (1967); R. D. Gill, J. S. Lopes, B. C. Robertson, R. A. I. Bell, and H. J. Rose, Nucl. Phys. A106, 678 (1968).

59. E. K. Warburton, P. D. Parker, and P. F. Donovan, Phys. Letters 19, 397 (1965).

60. C. R. Gruhn and E. Kashy, Bull. Am. Phys. Soc. 11, 471 (1966).

61. E. C. Halbert and J. B. French, Phys. Rev. 105, 1563 (1957).

62. B. G. Harvey, J. R. Meriwether, J. Mahoney, A. Bussiere de Nercy, and D. J. Horen, Phys. Rev. 146, 712 (1966).

63. The computer program LORNA was written by Creve Maples, Jr.

64. D. Kurath, Phys. Rev. 101, 216 (1956); F. C. Barker, Nucl. Phys. 45, 467 (1963); A. N. Boyarkina, Adademia Nauk, USSR (English trans.) Physical Series, 28, 255 (1964); E. C. Halbert, Y. E. Kim, and T. T. S. Kuo, Phys. Letters 20, 657 (1966); F. C. Barker, Nucl. Phys. 83, 418 (1966).

65. W. R. Gibbs, V. A. Madsen, J. A. Miller, W. Tobocman, E. C. Cox, and L. Mowry, NASA Technical Note, NASA TN D-2170, 1964.

66. A modified version of the computer program SEEK (M. A. Melkanoff, J. Raynal, and T. Sawada, SEEK, Department of Physics, University of California, Los Angeles, Report No. 66-10, January 1966) was used in this analysis.

67. G. R. Satchler, Nucl. Phys. A100, 497 (1967).

68. E. B. Carter, G. E. Mitchell, and R. H. Davis, Phys. Rev. 133, B1421 (1964); E. M. Kellogg and R. W. Zurmühle, Phys. Rev. 152, 890 (1966).

69. D. J. Baugh, G. J. B. Pyle, P. M. Rolph, and S. M. Scarrott, Nucl. Phys. A95, 115 (1967).

70. E. F. Gibson, B. W. Ridley, J. J. Kraushaar, M. E. Rickey, and R. H. Bassel, Phys. Rev. 155, 1194 (1967).

71. When the coefficients of fractional parentage obtained by CK are used, the quantity γ in Eq. (17) represents the energy eigenvalue of the parent state. In addition, the phase factor $(-)^{j_1+j_2}$ must be included in the expression, Eq. (16), for $\mathcal{S}$ since the coupling order implied by Eq. (17) is $[j_1 \times J'']^{J_i}$ (V. A. Madsen, private communication) whereas the coupling order used by CK is $[J'' \times j_1]^{J_i}$ (see Ref. 21).

72. W. M. Visscher and R. A. Ferrell, Phys. Rev. 107, 781 (1957).

73. D. E. Alburger, A. Gallmann, J. B. Nelson, J. T. Sample, and E. K. Warburton, Phys. Rev. 148, 1050 (1966).

74. K. P. Lieb and R. Hartmann, Z. Physik 200, 432 (1967).

75. F. G. Perey, in Proceedings of the Conference on Direct Interactions and Nuclear Reaction Mechanisms, Padua, 1962, ed. by E. Clementel and C. Villi (Gordon and Breach Science Publishers, Inc., New York, 1963) p. 125; N. Austern, Phys. Rev. 137, B752 (1965).

76. F. G. Perey and D. S. Saxon, Phys. Letters 10, 107 (1964).

77. R. H. Bassel, Phys. Rev. 149, 791 (1966); R. Stock, R. Bock, P. David, H. H. Duhm, and T. Tamura, Nucl. Phys. A104, 136 (1967); R. H. Bassel, (to be published).

78. D. G. Fleming and J. Cerny, (unpublished data).

79. A(JSLT)=(0000) amplitude is allowed for the 8.86 MeV, 1/2- level in ^{13}C if CK wave functions are used. However, nuclear structure factor calculations predict that this amplitude is approximately equal to zero.

80. E. L. Petersen, I. Slaus, J. W. Verba, R. F. Carlson, and J. Reginald Richardson, Nucl. Phys. A102, 145 (1967).

81. G. C. Ball and J. Cerny, (unpublished data).

82. W. W. Eidson and J. G. Cramer, Jr., Phys. Rev. Letters 9, 497 (1962).

83. T. Tamura, Nucl. Phys. 73, 241 (1965); J. S. Vincent, E. T. Boschitz, and J. R. Priest, Phys. Letters 25B, 81 (1967).

84. G. R. Bishop, M. Bernheim, and P. Kossanyi-Demay, Nucl. Phys. 54, 353 (1964).

85. The use of Eq. (8) for α-particles involves a further approximation since this expression was derived specifically for mass three projectiles.

86. G. R. Satchler, Nucl. Phys. A100, 481 (1967).

87. V. Gillet and N. Vinh-Mau, Nucl. Phys. 54, 321 (1964).

88. R. S. Christian and E. W. Hart, Phys. Rev. 77, 441 (1950).

89. L. Rosenfeld, Nuclear Forces (North-Holland Publishing Co., Amsterdam, 1948) p. 234.

90. R. A. Ferrell and W. M. Visscher, Phys. Rev. 102, 450 (1956).

91. M. A. Preston, Physics of the Nucleus (Addison-Wesley Publishing Co., 1962) p. 34.

92. M. J. Kearsley, Nucl. Phys. 4, 157 (1957).

93. M. H. L. Pryce, Proc. Phys. Soc. (London) A65, 773 (1952).

94. T. Lauritsen and F. Ajzenberg-Selove, Nucl. Phys. 78, 1 (1966).

95. J. D. Anderson, C. Wong, and V. A. Madsen, Lawrence Radiation Laboratory Report UCRL-50197, 1967 (unpublished).

96. L. F. Chase, Jr., R. E. McDonald, W. W. True, and E. K. Warburton, Phys. Rev. 166, 997 (1968); J. W. Olness and E. K. Warburton, Phys. Rev. 166, 1004 (1968).

97. R. G. Thomas, Phys. Rev. 81, 148 (1951); Phys. Rev. 88, 1109 (1952); J. B. Ehrman, Phys. Rev. 81, 412 (1951).

98. C. C. Maples and J. Cerny, (unpublished data).